Copy 334
RM L54H18

NACA

RESEARCH MEMORANDUM

AN INVESTIGATION OF THE EFFECTS OF A GEOMETRIC TWIST ON THE AERODYNAMIC LOADING CHARACTERISTICS OF A 45° SWEPTBACK WING-BODY CONFIGURATION AT TRANSONIC SPEEDS

By Claude V. Williams

Langley Aeronautical Laboratory
Langley Field, Va.

NATIONAL ADVISORY COMMITTEE FOR AERONAUTICS

WASHINGTON

October 12, 1954

NATIONAL ADVISORY COMMITTEE FOR AERONAUTICS

RESEARCH MEMORANDUM

AN INVESTIGATION OF THE EFFECTS OF A GEOMETRIC TWIST ON THE AERODYNAMIC LOADING CHARACTERISTICS OF A 45° SWEPTBACK WING-BODY CONFIGURATION AT TRANSONIC SPEEDS

By Claude V. Williams

SUMMARY

An investigation was made in the Langley 8-foot transonic tunnel of the pressure distribution on a wing-body configuration having a twisted 45° sweptback wing with aspect ratio 4, taper ratio 0.6, and NACA 65A006 airfoil sections parallel to the plane of symmetry. The body had a curved forebody profile and an afterbody which was cylindrical from the region of the leading edge of the wing-body juncture rearward to the base. Data were obtained at Mach numbers of 0.60 to 1.13. The test Reynolds number varied from 1.7×10^6 to 2.1×10^6. In order to indicate the effect of a wing twist on the loading and associated characteristics, the results of this investigation are compared with similar data previously obtained for a plane or untwisted 45° sweptback wing in combination with the same body.

The comparison indicated that the twisted-wing configuration must be at higher angles of attack than the plane-wing configuration for the same normal-force coefficient. This increased angle of attack caused the body of the twisted-wing configuration to carry a larger percentage of the total load than the body of the plane-wing configuration. Also, as a result of the increased angle of attack, the loads over the inboard sections of the twisted wing were increased, and the loads over the outboard sections were decreased, relative to the loading on the plane wing. The center of pressure of the twisted wing moved forward and inboard of the location for the plane wing without significantly altering the wing torsional characteristics. As might be expected, the wing bending-moment coefficients for the twisted wing were less than those for the plane wing. The twisted wing had more positive pitching-moment coefficients than the plane wing, but wing twist appeared to have little effect on the longitudinal stability characteristics of the wing-body combination.

INTRODUCTION

The evaluation of changes in spanwise loading which result from twisting due to aeroelastic bending is one of the structural design considerations resulting from the current use of thin sweptback wings on transonic-airplane configurations. In general, the changes in loading must be determined by experimental investigations, since regions of separated and mixed flows over the wings at transonic speeds seriously hamper accurate theoretical calculation of the necessary loading parameters. Such an investigation has been conducted to obtain the pressure distribution for a geometrically twisted, thin, 45° sweptback wing in the Langley 8-foot transonic tunnel. The twist of this wing is considered to be a typical variation and does not represent the twist of any particular type of wing structural system. The model was tested at Mach numbers of 0.60 to 1.13 and at angles of attack of 0° to 20°. The Reynolds number of the investigation varied from approximately 1.7×10^6 to 2.1×10^6 based on the wing mean aerodynamic chord.

The results of a previous load investigation of an untwisted or plane wing of similar plan form in combination with the same body have been reported in reference 1. These untwisted or plane-wing data and the twisted-wing data of the present investigation are compared in order to indicate the effects of a wing twist on the loading and pitching-moment characteristics of the wing-body combination. A very brief comparison of these configurations has previously been presented in reference 2. Several load investigations of the plane wing mounted on a body different from that of the present investigation have been conducted, and the results of these tests are presented in references 3, 4, and 5. The data of reference 1 evaluate the wing-body interference effect of these two different body shapes.

SYMBOLS

a chordwise distance from wing 0.25-chord line to wing chordwise center of pressure

b wing span

$b_e/2$ wing semispan outboard of wing-body juncture

c local chord measured parallel to body center line

c' wing mean aerodynamic chord

$\bar{c}$ wing average chord, S/b

D body diameter at any longitudinal station

L body length

M Mach number

P pressure coefficient, $\frac{p - p_o}{q_o}$

p local static pressure

p_o stream static pressure

q_o stream dynamic pressure, $\rho V^2/2$

R body radius at any station

S wing area (includes area blanketed by body)

V stream velocity

x_B distance measured from body nose along body center line (positive rearward)

x_W distance measured from wing leading edge along any chord line (positive rearward)

y spanwise distance measured from body center line

y_e spanwise distance measured from wing-body juncture line

α_p angle of attack of body center line of plane wing-body configuration

α_t angle of attack of body center line of twisted wing-body configuration

θ wing twist angle measured between local chord line and body center line (angles below body center line negative)

Λ sweep angle of wing 0.25-chord line

ρ stream density

Wing Coefficients

C_B wing bending-moment coefficient about wing-body juncture line, $\frac{4}{b\left(b - d_{max}\right)} \int_{R_{max}}^{b/2} \frac{c_{n_W} c}{\bar{c}} \left(y - R_{max}\right) dy$

C_{m_W} wing pitching-moment coefficient about 0.25-mean-aerodynamic-chord line, $\frac{2}{b} \int_{R_{max}}^{b/2} c_{m_{c'/4}} \frac{c^2}{\bar{c}c'} dy$

$c_{m_{c/4}}$ wing section pitching-moment coefficient about 0.25-chord line, $\frac{1}{c^2} \int_0^c \left(P_L - P_U\right)\left(\frac{c}{4} - x_W\right) dx_W$

$c_{m_{c'/4}}$ wing section pitching-moment coefficient about 0.25-mean-aerodynamic-chord line, $c_{m_{c/4}} + \frac{c_{n_W}}{c}\left(x_{c'/4} - x_{c/4}\right)$ where $\left(x_{c'/4} - x_{c/4}\right)$ is chordwise distance from 0.25-mean-aerodynamic-chord line to 0.25-local-chord line (x positive rearward)

C_{N_W} wing normal-force coefficient (perpendicular to body center line; c_{n_W} uncorrected for twist angle θ), $\frac{2}{b} \int_{R_{max}}^{b/2} \frac{c_{n_W} c}{\bar{c}} dy$

c_{n_W} wing section normal-force coefficient (normal to local chord lines), $\frac{1}{c} \int_0^c \left(P_L - P_U\right) dx_W$

C_T wing twisting-moment coefficient about 0.25-chord line, $-\cos \Lambda \frac{a}{c'} C_{N_W}$

$\left(\frac{x_{cp}}{c'}\right)_W$ wing chordwise center of pressure, $0.25 - \frac{C_{m_W}}{C_{N_W}}$

$\frac{y_{e_{cp}}}{b_e/2}$ spanwise center of pressure in terms of semispan of wing outboard of body, C_B/C_{N_W}

Body Coefficients

C_{m_B} body pitching-moment coefficient about 0.25-mean-aerodynamic-chord line and based on wing area S,

$$\frac{D_{max}}{Sc'}\int_0^L c_{n_B}\frac{D}{D_{max}}\left(x_{c'/4} - x_B\right)dx_B,$$ where $\left(x_{c'/4} - x_B\right)$ is distance from intersection of 0.25 wing mean aerodynamic chord and body center line to any transverse section

C_{N_B} body normal-force coefficient based on wing area S,

$$\frac{D_{max}}{S}\int_0^L c_{n_B}\frac{D}{D_{max}}\,dx_B$$

c_{n_B} body transverse-section normal-force coefficient,

$$\frac{1}{R}\int_0^R \left(P_L - P_U\right)dy$$

Wing-Body Coefficients

C_m total pitching-moment coefficient, $C_{m_W} + C_{m_B}$

C_N total normal-force coefficient, $C_{N_W} + C_{N_B}$

$\frac{x_{cp}}{c'}$ longitudinal center of pressure, $0.25 - \frac{C_m}{C_N}$

Subscripts:

L lower surface

max maximum

U upper surface

APPARATUS AND METHODS

Tunnel

The investigation was conducted in the Langley 8-foot transonic tunnel. This facility has a dodecagonal slotted test section in which the Mach number can be continuously varied through the speed range up to a Mach number of approximately 1.14. Detailed discussions of the design and calibration of this tunnel are given in references 6 and 7, respectively.

Model

Dimensional details of the sting-mounted model are shown in figure 1. Photographs of the model installed in the tunnel are shown in figure 2. The steel body had the same dimensions as that of body D of the force investigation reported in reference 8. The force data for the body alone are included in reference 8. Pressure measurements on the body alone are presented in reference 9. Ordinates of the body nose are presented in table I. The afterbody of the model was cylindrical rearward from the 20-inch station (fig. 1).

The steel wing of the model had 45° sweepback of the 0.25-chord line, aspect ratio 4, taper ratio 0.6, and NACA 65A006 airfoil sections parallel to the vertical plane of symmetry. The wing sections were twisted about the wing 0.25-chord line in planes parallel to the vertical plane of symmetry to produce the spanwise twist variation shown in figure 3. The wing had the same plan form and airfoil section and was mounted in the midwing position at the same longitudinal location on the body as the wing of reference 1. Both wings had 0° dihedral and plan-form areas of 1 square foot. The body covered 16.9 percent of the wing area.

Throughout this report, the untwisted wing used in the investigation of reference 1 is referred to as the plane wing, whereas the wing of the present investigation is identified as the twisted wing.

Model Instrumentation

Static pressures were measured at 156 body orifices and 115 wing orifices located as shown in figures 4 and 5.

The angle of attack was obtained from an electrical indicator located in the movable portion of the tunnel sting-support system rearward of the model and was corrected by means of calibration of the sting deflection between the model and the measuring unit.

Tests and Accuracy

The model was tested at stream Mach numbers of 0.60, 0.80, 0.85, 0.90, 0.95, 0.98, 1.00, 1.03, 1.08, 1.10, and 1.13. The maximum random error in measuring stream Mach number is believed to be about 0.003. Mach number deviations in the region of the model generally increase with

Mach number but ordinarily do not exceed approximately 0.006 at stream Mach numbers up to 1.13 (ref. 7). The model was subject to the effects of wall-reflected shock disturbances at Mach numbers greater than 1.0. It is believed that these effects were small, and no corrections for these shock reflections have been applied to the data.

The repeatability of measurement of the pressure coefficients is believed to be ±0.006. At each Mach number, the model was tested at nominal angles of attack of 0°, 4°, 8°, 12°, and 20°. A consideration of the factors involved indicates that the accuracy of the corrected angle-of-attack measurements presented was approximately ±0.1°. The Reynolds number during the investigation varied from approximately 1.7×10^6 to 2.1×10^6 when based on the wing mean aerodynamic chord of 6.125 inches.

RESULTS AND DISCUSSION

Basic Pressure Measurements

General comments.- The basic wing and body pressure-coefficient distributions are presented in figures 6 and 7, respectively. In these figures, the data are arranged on facing pages at constant Mach numbers.

In figure 6, the wing pressure-coefficient distributions are presented for five spanwise stations at nominal angles of attack of 0°, 4°, 8°, 12°, and 20°. Corrected angle-of-attack values are given for each condition. Comparisons of the data for the two wing configurations have been made at Mach numbers of 0.60, 0.95, 1.00 and 1.13 in figures 6(a), 6(e), 6(g), and 6(k), respectively. In these figures, plain symbols signify data for the twisted wing and flagged symbols data for the plane wing. In an effort to avoid confusion, the plane-wing-configuration data are unfaired.

The basic pressure-coefficient distributions for the six meridians around the body are presented in figure 7 at nominal angles of attack of 0°, 4°, 8°, 12°, and 20°. Comparisons of the two configurations at Mach numbers of 0.60, 0.95, 1.00, and 1.13 are made in figures 7(a), 7(e), 7(g), and 7(k), respectively. In these figures, the faired curves indicate data for the twisted wing, and the circles indicate data for the plane-wing configuration.

Wing section characteristics.- The variations with angle of attack of the wing-section pressure-coefficient distributions are presented in figure 6. As would be expected, these data indicate that the flow at low angles of attack was essentially unseparated; hence, the pressure-coefficient distributions for the wing sections were primarily governed by the local angles of attack. This is shown throughout the Mach number range by the data presented for angles of attack of 0° and 4°, and at subsonic speeds by the data at an angle of attack of 8°. These data indicate that the pressure-coefficient distributions for the twisted and plane wings were essentially the same over the inboard wing sections where the local angles of attack were similar. Over the outboard regions of the wing, however, where the local angles of attack of the twisted wing were lower than those of the plane wing, considerable differences in the pressure-coefficient distributions existed, primarily at the leading-edge regions of the wings.

At an angle of attack of 8° at Mach numbers of 0.95 and 1.00 (figs. 6(e) and 6(g)), the negative pressure-coefficient distributions over the outboard trailing-edge regions of the upper surface of the twisted wing indicate that the flow was essentially unseparated, in contrast to considerable separation noted for the similar region of the plane wing. These pressure-distribution characteristics indicating separation on the plane wing resulted from a shock wave which formed at the trailing edge of the wing-body juncture and extended laterally across the span. Because of the lower section angle of attack of the twisted wing, and hence lower induced flow, the shock was somewhat weaker on the twisted wing than on the plane wing and, therefore, caused less shock-induced separation to occur on the twisted wing, resulting in the relatively smaller lift loads shown at the trailing edge of the twisted wing.

At subsonic speeds at an angle of attack of 12°, the flow over the upper surfaces of both wings consisted primarily of a vortex which originated at the leading edge of the wing-body juncture and extended outward and rearward across the span. This vortex is common to thin sweptback wings. Considerable flow separation associated with the vortex existed over the upper surface of most of the span of both wings as evidenced by the flat upper-surface pressure-coefficient distributions. The pressure-coefficient distributions indicate, however, that the separation over the twisted wing was somewhat less severe than that which existed over the plane wing. At the higher test Mach numbers, the effect of this vortex was gradually reduced because of the more efficient turning of the flow in the supersonic region at the leading edge of the wing.

At an angle of attack of 20°, severe separation occurred over the upper surface of both wings, and this phenomenon completely obliterated any effect of geometric twist. Therefore, the pressure-coefficient distributions for both wings were essentially the same at an angle of attack of 20° throughout the Mach number range investigated.

Body characteristics.- In general, the basic pressure measurements for the body of the twisted wing-body configuration, presented in figure 7, show the usual pressure-coefficient peaks associated with the influence of the flow field of the wing on the body pressures. Throughout the Mach number range an increase in angle of attack caused the peaks to increase and also to spread longitudinally along the body. As would be expected, the pressure-coefficient peaks were greatest for the meridians nearest the wing and decreased in level around the body.

The comparisons at nearly constant angles of attack of the pressure-coefficient distributions over the bodies of the two configurations indicate that the body pressure coefficients in the region of the twisted wing-body juncture were always slightly less negative over the upper body meridians and slightly less positive over the lower body meridians than in the similar region of the plane wing-body configuration. The pressure coefficients over the extremities of the body of both configurations were identical.

Loading Characteristics

General comments.- In table II is presented a compilation of the section normal-force and pitching-moment coefficients (taken about the 25-percent-local-chord location) for the twisted wing at all the Mach numbers and angles of attack presented in this paper. The same information for the plane wing is presented in table III. These data have been included in this paper as an aid for correlating and checking of various load-distribution computational methods.

The loading data presented in this paper were obtained by conventional graphical-mechanical integration procedures. In the analysis figures, the data are compared at several total wing-body normal-force coefficients, with the values of the various parameters presented having been obtained from cross plots.

Wing spanwise load distributions.- The effect of a geometric wing twist on the spanwise variation of the section normal-loading coefficient $\frac{c_{n_W}c}{\bar{c}}$ at total normal-force coefficients of 0, 0.2, 0.4, 0.6, and 0.8 are presented in figure 8 for all Mach numbers of the investigation. Also included in this figure are accessory plots of C_{N_W} against C_N and α against C_N. Throughout the test Mach number range, the variations of angle of attack with normal-force coefficient indicate that in the approximately linear normal-force-coefficient range the twisted-wing configuration must be at a higher angle of attack (referred to the body center line) than the plane-wing configuration in order to obtain a given total normal-force coefficient. At this condition the local angles of attack of the inboard sections of the twisted wing were higher and the local angles of attack of the outboard sections lower than the corresponding sections of the plane wing. In general, these wing-section angle-of-attack differences resulted in the loads over the inboard sections of the twisted wing being higher and in the loads over the outboard sections being lower than the loads over the plane wing at all total normal-force coefficients through 0.6.

The largest differences in value of the section normal-loading coefficient $\frac{c_{n_W} c}{\bar{c}}$ for the two wings occurred over the outboard regions of the wings at a normal-force coefficient of 0.6 in the Mach number range from 0.60 to 0.95 (figs. 8(a) to 8(e)). These differences in value resulted from varying degrees of separation associated with the difference in angle of attack of the configurations. At a normal-force coefficient of 0.6 the inboard sections of the twisted wing were operating in the angle-of-attack range where the vortex-type flow occurred. This vortex caused the flow over the outboard sections of the twisted wing to separate to a greater degree than that over the outboard sections of the plane wing. This greater separation occurred even though the section angles of attack for the outboard portions of the twisted wing were approximately the same or less than the corresponding sections of the plane wing.

At a normal-force coefficient of 0.8 at subsonic Mach numbers the spanwise distributions of loading indicate that the flow over the wings was severely separated over the outboard regions. This separation is associated with the leading-edge vortex-type flow mentioned previously. Increase in Mach number at this normal-force coefficient caused the loadings over the tips to increase because of a reduction in the strength of the separation.

The plots of wing normal-force coefficient against total normal-force coefficient included in figure 8 show that throughout the Mach number range the variations were essentially the same, and the curves essentially differed only in value.

Wing bending characteristics.- The data in figure 9 show the location of the lateral centers of pressure for the twisted and plane wings, expressed in terms of the semispan of the wings outboard of the body. These data, compared at constant total normal-force coefficients, indicate that the center of pressure of the twisted wing was always inboard of that of the plane wing which resulted in beneficial reductions in the wing bending-moment coefficients for the twisted wing (fig. 10).

A comparison of the variations with normal-force coefficient of the wing bending-moment coefficients for the twisted and plane wings is presented in figure 11. These data indicate that throughout the Mach number range an increase in normal-force coefficient, in general, resulted in an increase in bending-moment coefficient. This condition occurred even though the lateral center of pressure at high normal-force coefficients moved inboard from the location at somewhat lower normal-force coefficients (fig. 9).

Wing twisting-moment characteristics.- The curves of figure 12 show that wing twist had little effect on the torsional or twisting moments about the 0.25-percent-chord line of the wing. This small effect occurred because the center of pressure for the twisted wing was always inboard and ahead of that for the plane wing (figs. 9 and 13) which, in effect, caused the center of pressure to move approximately parallel to the wing 0.25-percent-chord line.

Percent total load carried by body.- The data presented in figure 14 show that at a constant normal-force coefficient the body of the twisted-wing configuration carried more of the total load than the body of the plane-wing configuration throughout the Mach number range. For example, at $C_N = 0.4$ and $M = 1.00$, the load was 17 percent of the total load for twisted wing and 15 percent of the total load for plane wing. The larger percentage of load carried by the body for the twisted-wing configuration may be attributed to the fact that at a constant total normal-force coefficient the body and inboard wing sections operated at a higher angle of attack than the plane wing-body configuration, hence, had somewhat higher induced loads.

Pitching-Moment Characteristics

Variations with normal-force coefficient.- A comparison of the variations with normal-force coefficient of the pitching-moment coefficients for the bodies, the wings, and the wing-body configurations is presented in figure 15 for Mach numbers of 0.60, 0.95, 1.00, and 1.13. These curves indicate that at all Mach numbers the twisted wing had more positive values of pitching-moment coefficient than did the plane wing. Little effect of twist was noted on the variations with normal-force coefficient.

The more positive total pitching-moment coefficients for the twisted wing-body configuration resulted from the addition of the twist effects on both the body and the wings. The more positive values for the body occurred because the twisted-wing configuration operated at a higher angle of attack than the plane wing-body configuration for the same total normal-force coefficient. The curves of figure 7 show that one of the effects of increasing the angle of attack was to cause peaks in the pressure-coefficient curves in the region of the wing-body juncture. These pressure peaks increased the loading over the forward portions of the body, ahead of the 0.25-mean-aerodynamic-chord location (approximately 68 percent of the body length), which resulted in a positive increase in the value of the pitching moment for the body with an increase in angle of attack.

The more positive values of pitching-moment coefficient for the twisted wing C_{m_W} resulted from the fact that the load over the twisted wing was inboard of the load for the plane wing at a constant normal-force coefficient, which generally on a sweptback wing results in more positive pitching moments about the same 0.25-mean-aerodynamic-chord location.

Variations with Mach number.- In figure 16 is presented a comparison of the variation with Mach number of the pitching-moment coefficients for the bodies, the wings, and the wing-body configurations at constant total normal-force coefficients. These data indicate that the twisted wing had essentially the same variations of pitching moment with Mach number as the plane wing.

Longitudinal center of pressure.- A comparison of the longitudinal center-of-pressure variations with Mach number for the twisted and plane wing-body configurations is presented in figure 17. These data indicate that throughout the Mach number range the center-of-pressure location of the twisted-wing configuration was always ahead of that for the plane-wing configuration by an amount varying from approximately 15 percent of the mean aerodynamic chord at a normal-force coefficient of 0.2 to 2 to 5 percent at a normal-force coefficient of 0.8.

CONCLUSIONS

The results of an investigation of a twisted sweptback wing have been compared with those obtained from tests of a similar untwisted wing and the following conclusions are made:

1. At constant normal-force coefficients through 0.6, the loads over the inboard sections of the twisted wing were higher and over the outboard sections lower than the loads over the corresponding regions of the plane wing. At a normal-force coefficient of 0.8 at subsonic speeds, severe separation occurred over the outboard regions of both wings. Increase in Mach number reduced the separation and therefore increased the loadings over the tips of both wings.

2. Throughout the speed range, the bending-moment coefficients at constant normal-force coefficients for the twisted wing were less than those for the plane wing. Increase in normal-force coefficient in general resulted in increased wing-bending-moment coefficients for both wings throughout the Mach number range of this test. This occurred even though the lateral center of pressure moved outboard and then inboard with increase in normal-force coefficient.

3. The center of pressure of the twisted wing was forward and inboard of that for the plane wing at constant normal-force coefficients. This change in location of the center of pressure did not affect the overall torsional characteristics about the 25-percent-chord line but had a decided influence in decreasing the wing bending-moment coefficient of the twisted wing.

4. At low angles of attack the flow over both wings was primarily governed by the local wing angles of attack. At 20° angle of attack, severe separation over the upper surfaces of the wings obliterated any effects of geometric twist.

5. The twisted wing had somewhat lower pressure-coefficient peaks over the body in the region of the wing-body juncture. The pressures measured over the extremities of the body of both configurations were identical.

6. The twisted wing-body configuration had more positive values of pitching-moment coefficient than did the plane-wing-body configuration, although the variation with normal-force coefficient and Mach number for both configurations was essentially the same.

7. At a constant normal-force coefficient, the body of the twisted-wing configuration carried a greater percentage of the total load than did the body of the plane-wing configuration.

Langley Aeronautical Laboratory,
National Advisory Committee for Aeronautics,
Langley Field, Va., August 3, 1954.

REFERENCES

1. Loving, Donald L.: The Effect of a Change in Body Shape on the Loading of a 45° Sweptback Wing-Body Combination at Transonic Speeds. NACA RM L54B09, 1954.

2. Williams, Claude V., and Kuhn, Richard E.: A Study of Aerodynamic Loads on Sweptback Wings at Transonic Speeds. NACA RM L53E08b, 1953.

3. Loving, Donald L., and Estabrooks, Bruce B.: Transonic-Wing Investigation in the Langley 8-Foot High-Speed Tunnel at High Subsonic Mach Numbers and at a Mach Number of 1.2. Analysis of Pressure Distribution of Wing-Fuselage Configuration Having a Wing of 45° Sweepback, Aspect Ratio 4, Taper Ratio 0.6, and NACA 65A006 Airfoil Section. NACA RM L51F07, 1951.

4. Loving, Donald L., and Williams, Claude V.: Basic Pressure Measurements on a Fuselage and a 45° Sweptback Wing-Fuselage Combination at Transonic Speeds in the Slotted Test Section of the Langley 8-Foot High-Speed Tunnel. NACA RM L51F05, 1951.

5. Loving, Donald L., and Williams, Claude V.: Aerodynamic Loading Characteristics of a Wing-Fuselage Combination Having a Wing of 45° Sweepback Measured in the Langley 8-Foot Transonic Tunnel. NACA RM L52B27, 1952.

6. Wright, Ray H., and Ritchie, Virgil S.: Characteristics of a Transonic Test Section With Various Slot Shapes in the Langley 8-Foot High-Speed Tunnel. NACA RM L51H10, 1951.

7. Ritchie, Virgil S., and Pearson, Albin O.: Calibration of the Slotted Test Section of the Langley 8-Foot Transonic Tunnel and Preliminary Experimental Investigation of Boundary-Reflected Disturbances. NACA RM L51K14, 1952.

8. Loving, Donald L., and Wornom, Dewey E.: Transonic Wind-Tunnel Investigation of the Interference Between a 45° Sweptback Wing and a Systematic Series of Four Bodies. NACA RM L52J01, 1952.

9. Robinson, Harold L.: Pressures and Associated Aerodynamic and Load Characteristics for Two Bodies of Revolution at Transonic Speeds. NACA RM L53L28a, 1954.

TABLE I

ORDINATES OF BODY NOSE

x_B, in.	R, in.
0	0
.200	.092
.300	.119
.500	.171
1.000	.289
2.000	.482
3.000	.645
4.000	.788
6.000	1.037
8.000	1.236
10.000	1.386
12.000	1.496
14.000	1.573
16.000	1.625
18.000	1.657
20.000	1.667
L.E. radius: 0.0005	

TABLE II

SECTION COEFFICIENTS FOR TWISTED WING

M	α_t, deg	$\frac{y}{b/2} = 0.20$		$\frac{y}{b/2} = 0.40$		$\frac{y}{b/2} = 0.60$		$\frac{y}{b/2} = 0.80$		$\frac{y}{b/2} = 0.95$	
		c_{n_W}	$c_{m_{c/4}}$	c_{n_W}	$c_{m_{c/4}}$	c_{n_W}	$c_{m_{c/4}}$	c_{n_W}	$c_{m_{c/4}}$	c_{n_W}	$c_{m_{c/4}}$
0.60	0	-0.053	-0.007	-0.087	-0.003	-0.133	-0.001	-0.159	-0.001	-0.103	-0.011
	3.9	.192	-.005	.159	.001	.128	.001	.071	.006	.051	.003
	7.9	.449	-.001	.427	-.012	.377	-.009	.274	.003	.172	.014
	11.9	.703	-.001	.803	-.033	.484	-.014	.388	-.033	.397	-.053
	20.0	1.302	-.125	1.099	-.174	.763	-.103	.475	-.044	.305	-.026
.80	-.1	-.060	.007	-.103	.005	-.137	-.003	-.165	-.004	-.112	-.014
	4.0	.209	-.007	.179	0	.154	0	.092	.006	.059	.006
	7.9	.487	-.019	.443	-.015	.401	-.009	.301	.006	.201	.009
	11.9	.762	-.019	.871	-.055	.614	-.077	.396	-.034	.236	-.019
	20.0	1.161	-.186	.974	-.152	.714	-.097	.508	-.053	.309	-.025
.85	-.1	-.061	.007	-.108	.005	-.144	-.004	-.171	-.006	-.112	-.015
	3.9	.210	-.009	.188	0	.161	.001	.094	.007	.056	.008
	7.9	.505	-.026	.478	-.003	.417	-.006	.312	.004	.196	.005
	11.9	.781	-.033	.903	-.078	.716	-.097	.412	-.033	.152	-.003
	20.0	1.159	-.194	.970	-.157	.738	-.099	.524	-.052	.301	-.018
.90	-.1	-.058	.009	-.116	.009	-.148	-.005	-.179	-.008	-.124	-.019
	3.9	.225	-.028	.202	.001	.165	.003	.105	.009	.063	.008
	7.9	.525	-.047	.519	-.006	.477	.029	.390	.038	.281	.021
	11.9	.803	-.071	.930	-.098	.757	-.086	.418	-.035	.153	0
	20.0	1.204	-.186	.992	-.166	.767	-.112	.548	-.057	.314	-.018
.95	-.1	-.063	.013	-.122	.015	-.166	-.002	-.198	-.013	-.139	-.026
	4.0	.236	-.023	.226	-.012	.187	.001	.125	.013	.065	.010
	7.9	.518	-.057	.536	-.030	.543	-.015	.464	.032	.315	.028
	11.9	.774	-.091	.923	-.125	.726	-.022	.471	-.029	.351	-.016
	20.0	1.255	-.172	1.081	-.188	.841	-.128	.611	-.067	.339	-.011
.98	-.1	-.056	.013	-.115	.015	-.172	.011	-.212	-.004	-.151	-.032
	3.9	.221	-.020	.210	-.016	.190	-.015	.141	.001	.076	.013
	7.9	.496	-.058	.536	-.032	.528	-.029	.503	-.003	.359	.023
	11.6	.757	-.092	.894	-.131	.786	-.041	.678	-.023	.498	-.029
	20.1	1.234	-.150	1.219	-.207	.925	-.154	.708	-.090	.413	-.025
1.00	-.1	-.057	.012	-.099	.011	-.169	.013	-.225	.008	-.161	-.028
	4.0	.216	-.021	.205	-.016	.183	-.014	.153	-.010	.068	.011
	7.9	.494	-.058	.518	-.033	.523	-.030	.501	-.012	.380	.013
	11.6	.727	-.086	.838	-.116	.779	-.044	.770	-.057	.577	-.029
	20.1	1.265	-.187	1.356	-.242	1.006	-.170	.714	-.100	.443	-.037
1.03	-.1	-.050	.012	-.096	.013	-.151	.009	-.217	.011	-.155	-.023
	3.9	.216	-.020	.208	-.015	.188	-.018	.152	-.013	.077	.010
	7.9	.492	-.058	.513	-.035	.528	-.034	.501	-.013	.386	-.003
	11.5	.717	-.083	.814	-.114	.762	-.046	.754	-.059	.568	-.028
	20.1	1.223	-.183	1.401	-.283	1.116	-.192	.768	-.118	.476	-.059
1.08	-.1	-.056	.019	-.103	.013	-.163	.013	-.231	.014	-.172	-.016
	3.9	.217	-.021	.201	-.012	.178	-.016	.127	-.011	.075	.006
	7.9	.467	-.056	.477	-.031	.501	-.035	.487	-.030	.379	-.011
	11.5	.689	-.089	.732	-.101	.759	-.065	.776	-.091	.554	-.034
	20.0	1.196	-.183	1.370	-.280	1.128	-.189	.761	-.111	.442	-.058
1.10	-.1	-.019	.013	-.081	.014	-.142	.015	-.225	.022	-.171	-.006
	3.9	.220	-.019	.200	-.011	.188	-.016	.149	-.021	.090	-.002
	7.9	.452	-.052	.470	-.036	.498	-.038	.487	-.036	.395	-.022
	11.5	.667	-.085	.669	-.064	.785	-.086	.769	-.099	.538	-.032
	20.0	1.181	-.177	1.312	-.257	1.106	-.187	.748	-.112	.439	-.061
1.13	-.1	-.041	.008	-.081	.007	-.126	.005	-.207	-.017	-.161	-.006
	3.9	.218	-.023	.194	-.017	.175	-.020	.126	-.019	.096	-.009
	7.9	.449	-.052	.466	-.036	.486	-.038	.481	-.052	.394	-.033
	11.5	.646	-.086	.680	-.062	.771	-.095	.746	-.106	.543	-.042
	20.0	1.127	-.174	1.297	-.267	1.072	-.173	.792	-.120	.455	-.061

TABLE III

SECTION COEFFICIENTS FOR PLANE WING

M	α_p, deg	$\frac{y}{b/2} = 0.20$		$\frac{y}{b/2} = 0.40$		$\frac{y}{b/2} = 0.60$		$\frac{y}{b/2} = 0.80$		$\frac{y}{b/2} = 0.95$	
		c_{n_W}	$c_{m_{c/4}}$	c_{n_W}	$c_{m_{c/4}}$	c_{n_W}	$c_{m_{c/4}}$	c_{n_W}	$c_{m_{c/4}}$	c_{n_W}	$c_{m_{c/4}}$
0.60	4.0	0.239	-0.012	0.256	-0.005	0.252	0.001	0.223	0.007	0.164	0.004
	8.0	.538	-.013	.553	0	.570	-.024	.450	-.011	.316	-.007
	12.0	.807	-.008	.986	-.052	.834	-.134	.459	-.056	.242	-.021
	20.0	1.237	-.199	1.088	-.173	.785	-.114	.554	-.069	.390	-.049
.95	4.0	.296	-.042	.340	-.025	.349	-.001	.316	.035	.217	.031
	8.0	.592	-.078	.661	-.043	.692	-.021	.727	-.056	.457	-.039
	12.0	.866	-.104	1.059	-.152	.796	-.106	.511	-.049	.236	-.008
	20.0	1.276	-.197	1.132	-.202	.892	-.147	.701	-.095	.431	-.037
1.00	4.0	.268	-.037	.305	-.028	.341	-.022	.359	-.005	.237	.026
	8.0	.543	-.073	.620	-.043	.667	-.042	.761	-.073	.621	-.063
	12.0	.808	-.103	1.014	-.154	.885	-.099	.849	-.098	.451	-.028
	20.0	1.300	-.177	1.386	-.251	1.023	-.182	.772	-.122	.514	-.050
1.13	4.0	.258	-.039	.292	-.026	.320	-.027	.328	-.020	.252	.009
	8.0	.497	-.067	.563	-.047	.628	-.064	.683	-.093	.501	-.032
	12.0	.712	-.099	.803	-.090	.894	-.128	.812	-.099	.595	-.052
	20.0	1.218	-.181	1.352	-.277	1.088	-.190	.808	-.131	.521	-.071

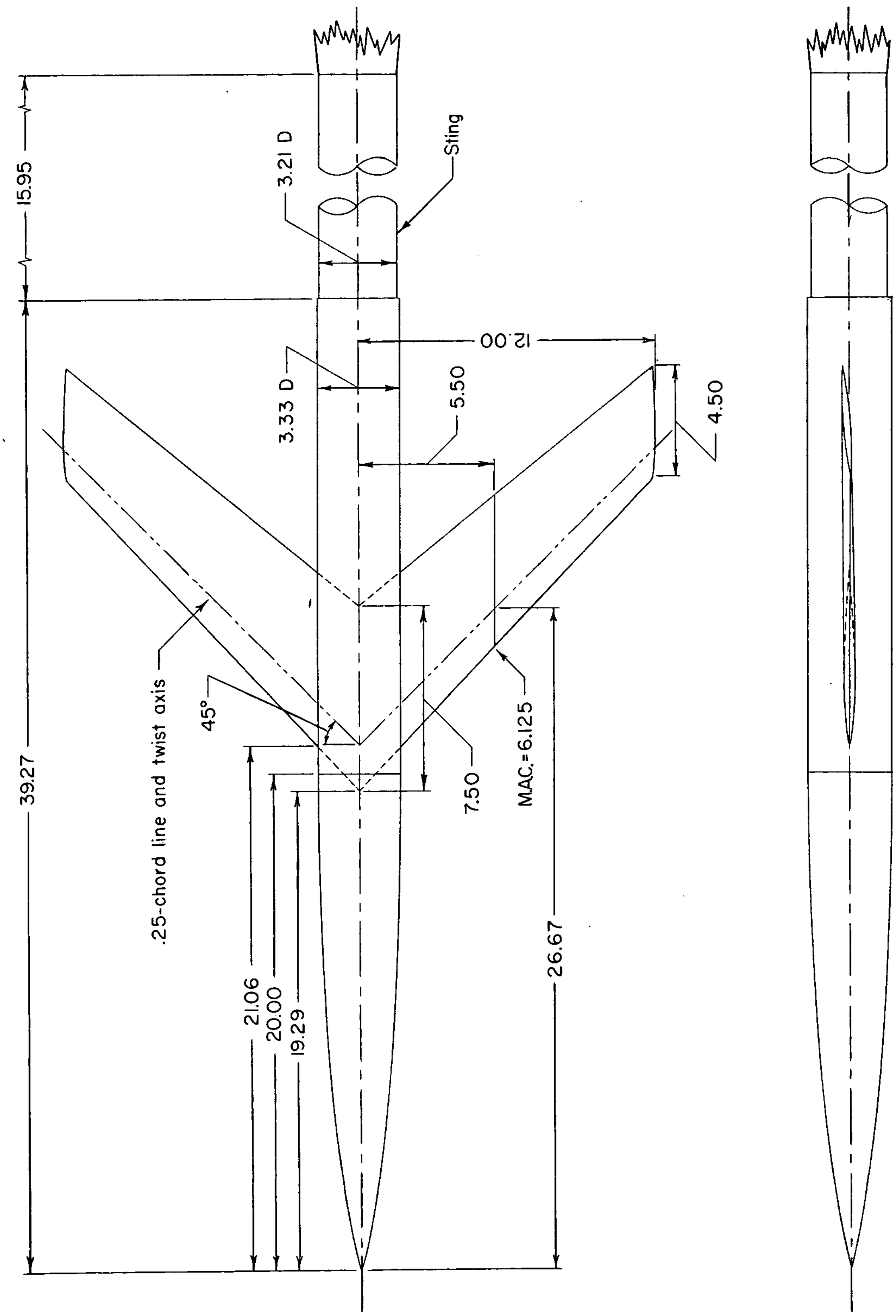

Figure 1.- Details of the wing-body configuration. All dimensions are in inches.

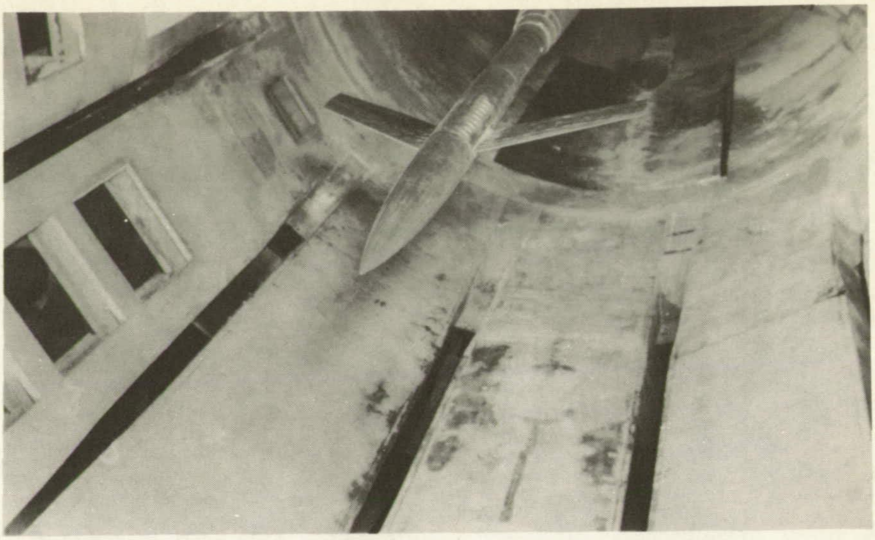

L-79100

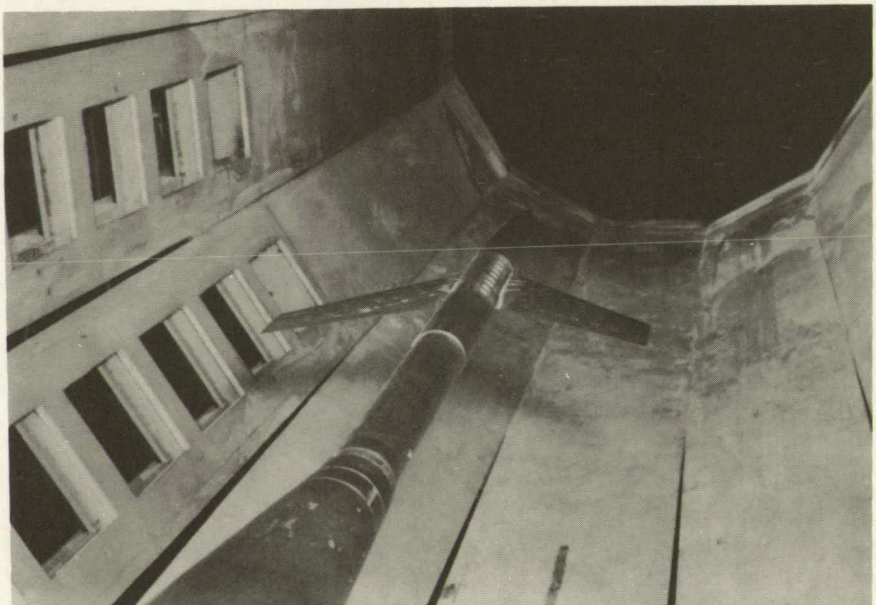

L-79101

Figure 2.- Views of the model installed in the Langley 8-foot transonic tunnel.

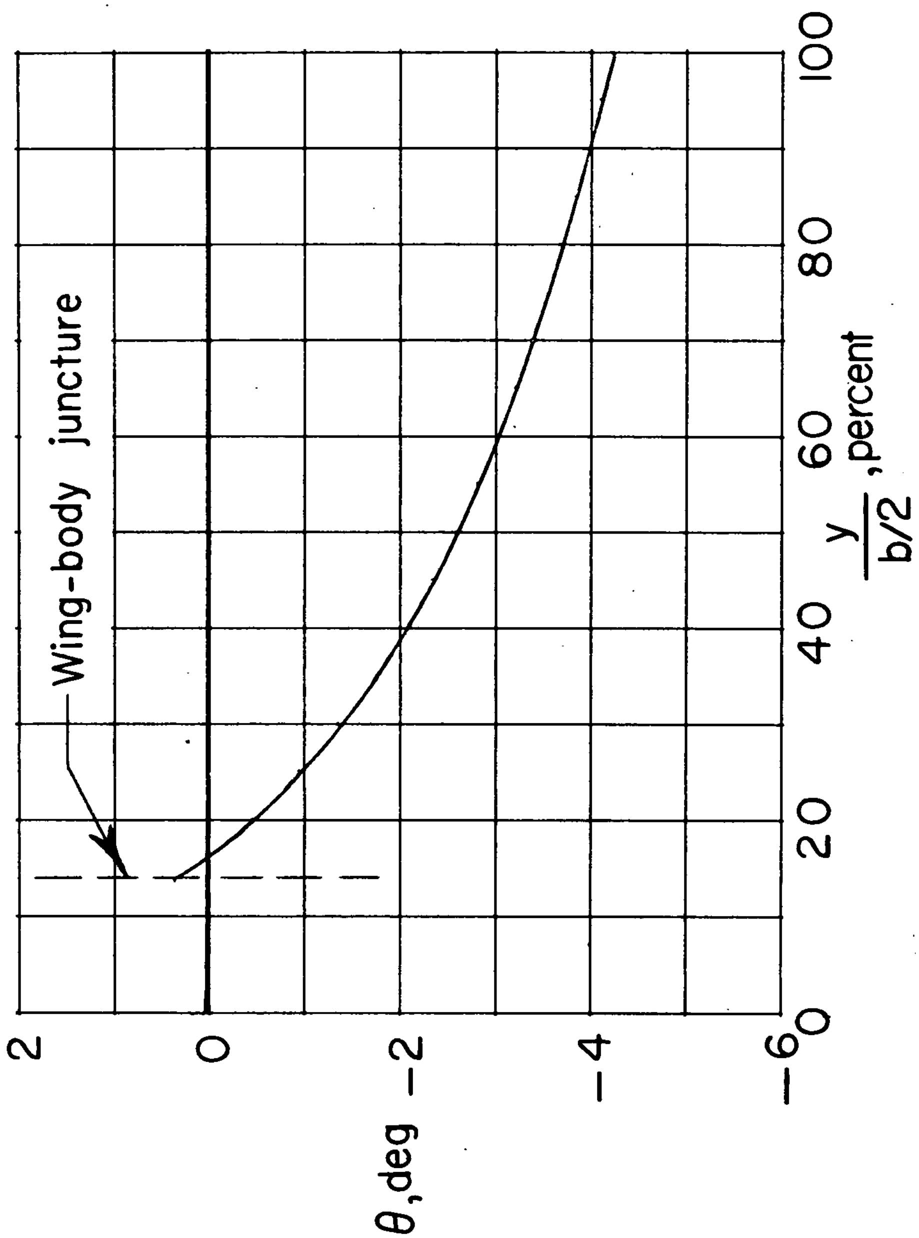

Figure 3.- Spanwise variation of wing twist.

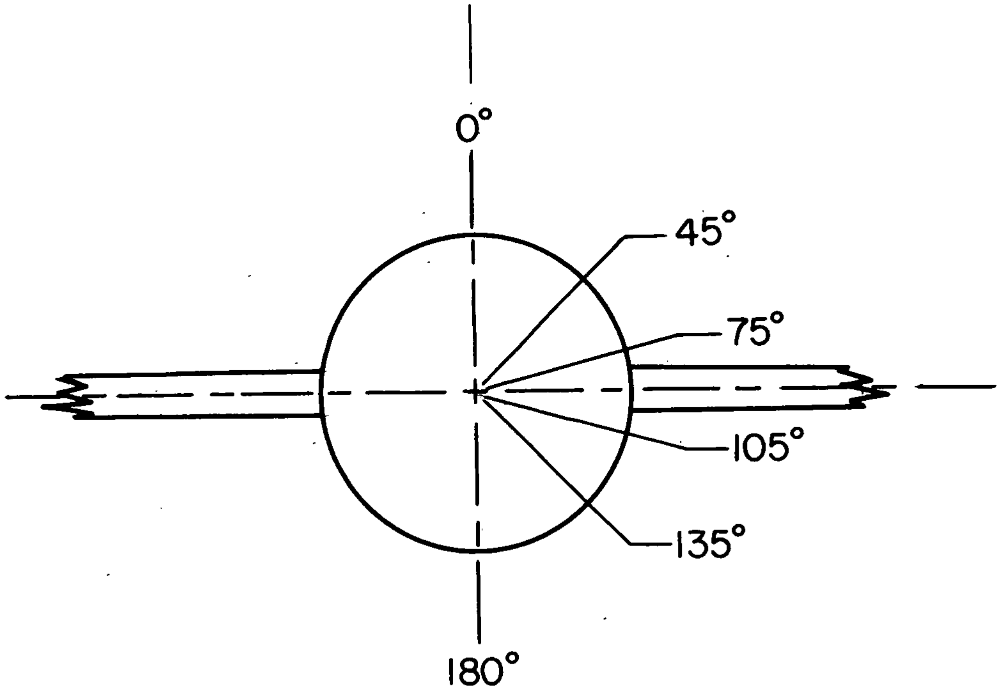

View looking downstream

Longitudinal location of body pressure orifices, $\frac{x_B}{L}$, percent											
0^{a} meridian		45^{o} meridian		75^{o} meridian		105^{o} meridian		135^{o} meridian		180^{o} meridian	
1.3	61.5	6.4	56.4	6.4	61.5	6.4	61.5	6.4	61.5	6.4	56.4
3.8	64.1	11.5	61.5	11.5	64.1	11.5	64.1	11.5	64.1	11.5	61.5
6.4	66.6	16.6	66.6	16.6	66.6	16.6	66.6	16.6	66.6	16.6	66.6
8.9	69.2	21.6	71.7	21.6	69.2	21.6	69.2	21.6	69.2	21.6	71.7
11.5	71.7	26.7	76.8	26.7	71.7	26.7	71.7	26.7	71.7	26.7	76.8
14.0	74.3	31.8	81.9	31.8	74.3	31.8	74.3	31.8	74.3	31.8	81.9
16.6	76.8	36.9	87.0	36.9	76.8	36.9	76.8	36.9	76.8	36.9	87.0
21.6	79.4	42.0	92.1	42.0	79.4	42.0	79.4	42.0	79.4	42.0	92.1
26.7	81.9	46.2	97.1	46.2	81.9	46.2	81.9	46.2	81.9	46.2	97.1
31.8	84.5	51.4	99.7	51.4	87.0	51.4	87.0	51.4	87.0	51.4	99.7
36.9	87.0			53.9	92.1	53.9	92.1	53.9	92.1		
42.0	89.5			56.4	47.1	56.4	97.1	56.4	97.1		
43.7	92.1			59.0	99.7	59.0	99.7	59.0	99.7		
46.2	94.6										
48.8	97.1										
51.4	97.8										
53.9	98.4										
56.4	99.1										
59.0	99.7										

Figure 4.- Body-pressure orifice locations.

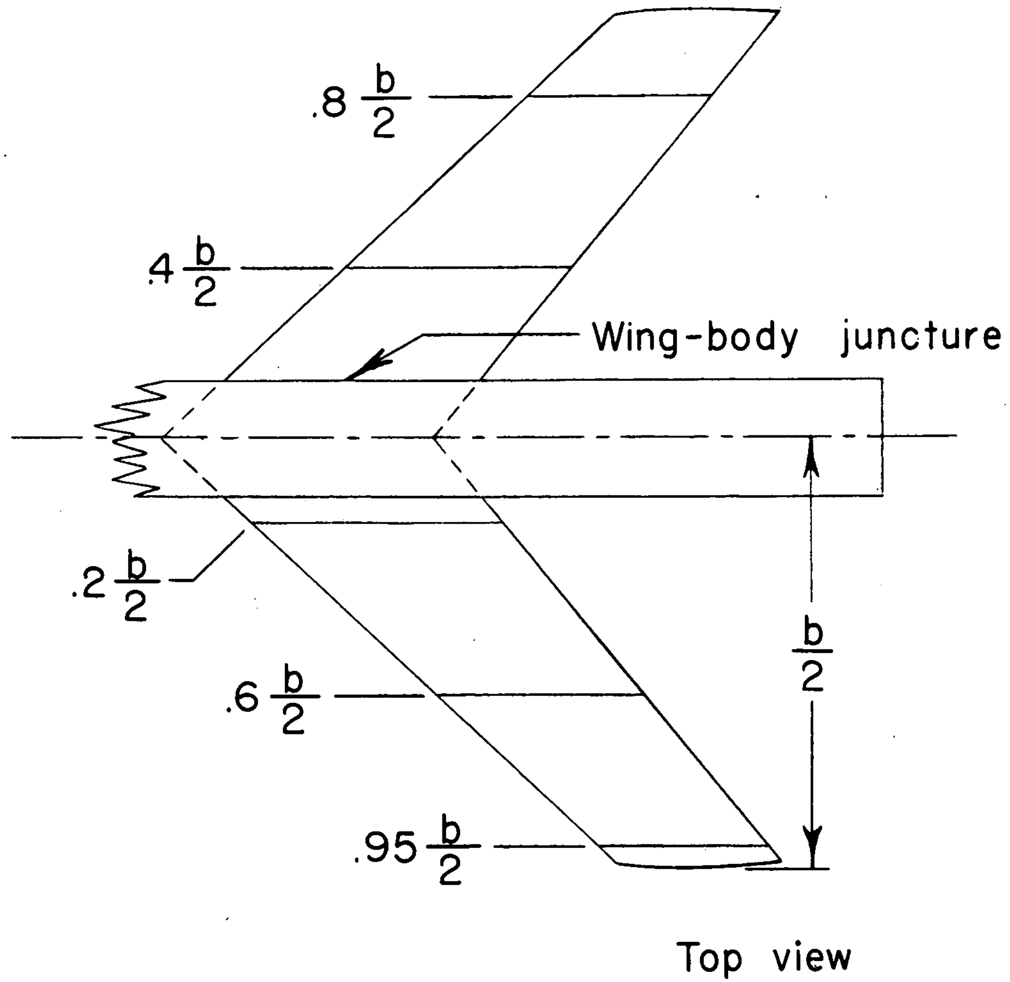

Wing section orifice locations, $\frac{x_W}{c}$, percent	
Upper surface	Lower surface
0	- -
2.5	2.5
7.5	7.5
15.0	15.0
25.0	25.0
35.0	35.0
45.0	45.0
55.0	55.0
65.0	65.0
75.0	75.0
85.0	85.0
90.0	90.0

Figure 5.- Wing-pressure orifice locations.

(a) M = 0.60.

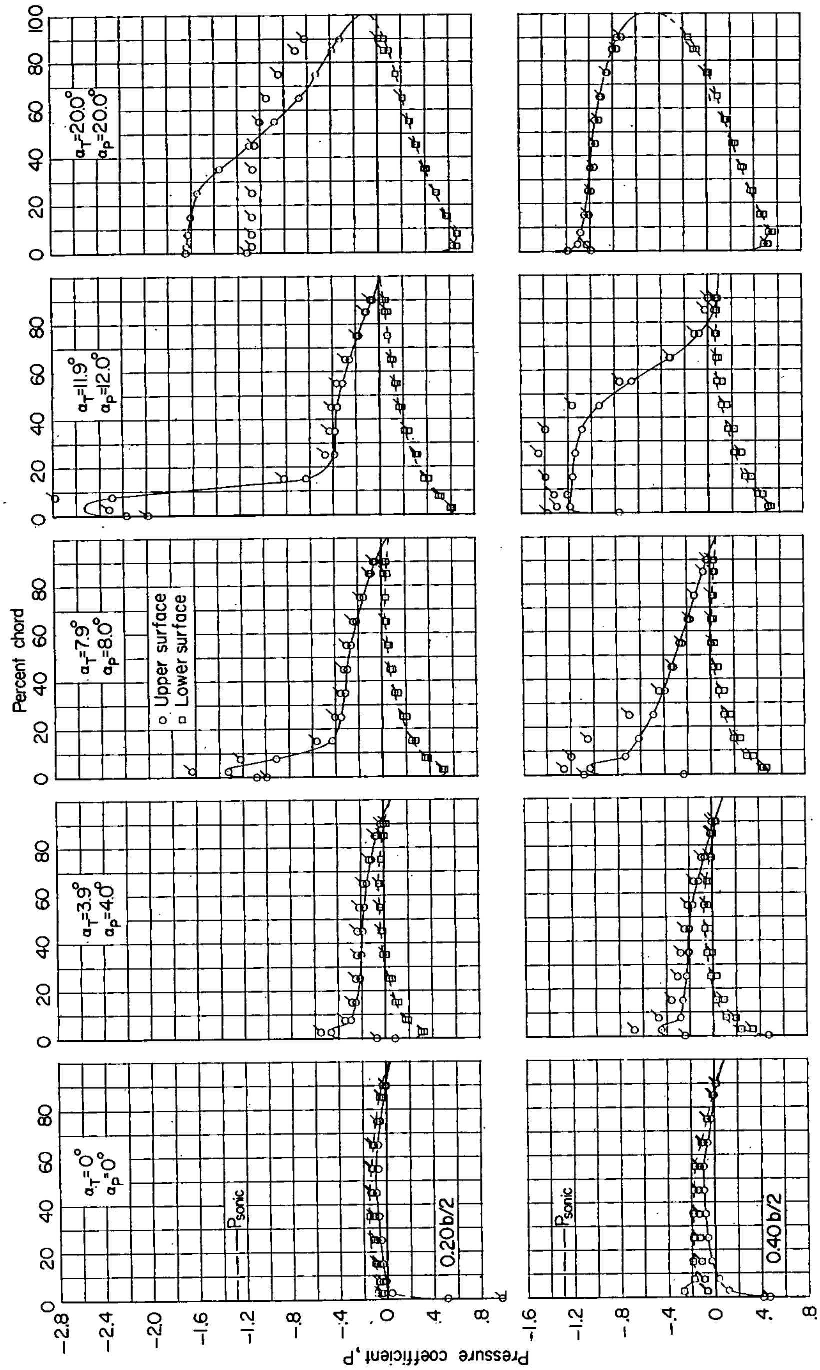
$\alpha_T=0^\circ$ $\alpha_p=0^\circ$
$\alpha_T=3.9^\circ$ $\alpha_p=4.0^\circ$
$\alpha_T=7.9^\circ$ $\alpha_p=8.0^\circ$
$\alpha_T=11.9^\circ$ $\alpha_p=12.0^\circ$
$\alpha_T=20.0^\circ$ $\alpha_p=20.0^\circ$
○ Upper surface
□ Lower surface
Percent chord
P_{sonic}
0.20b/2
0.40b/2
Pressure coefficient, P

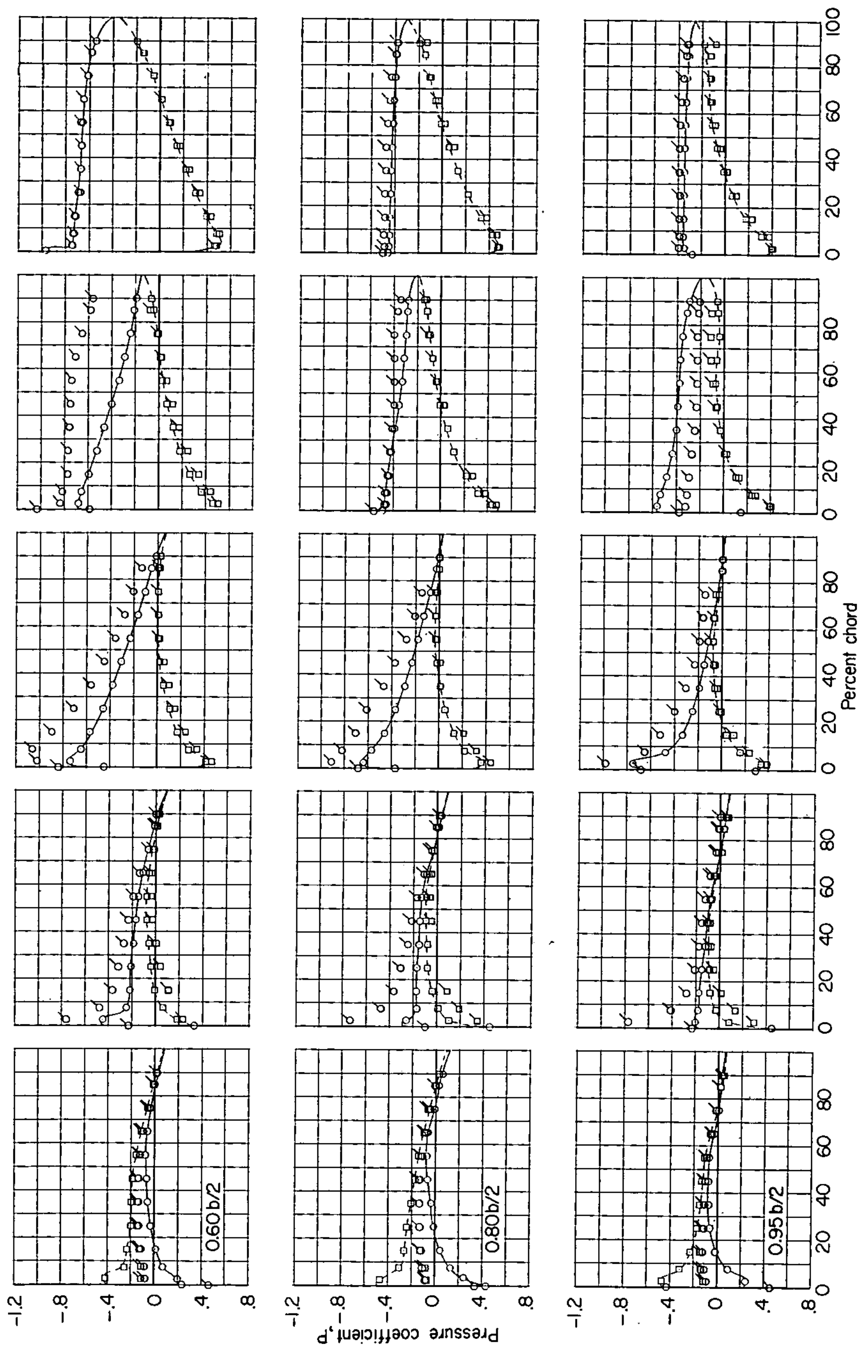

(a) M = 0.60. Concluded.

Figure 6.- Basic pressure measurements for the twisted and plane wings. Flags indicate plane-wing data.

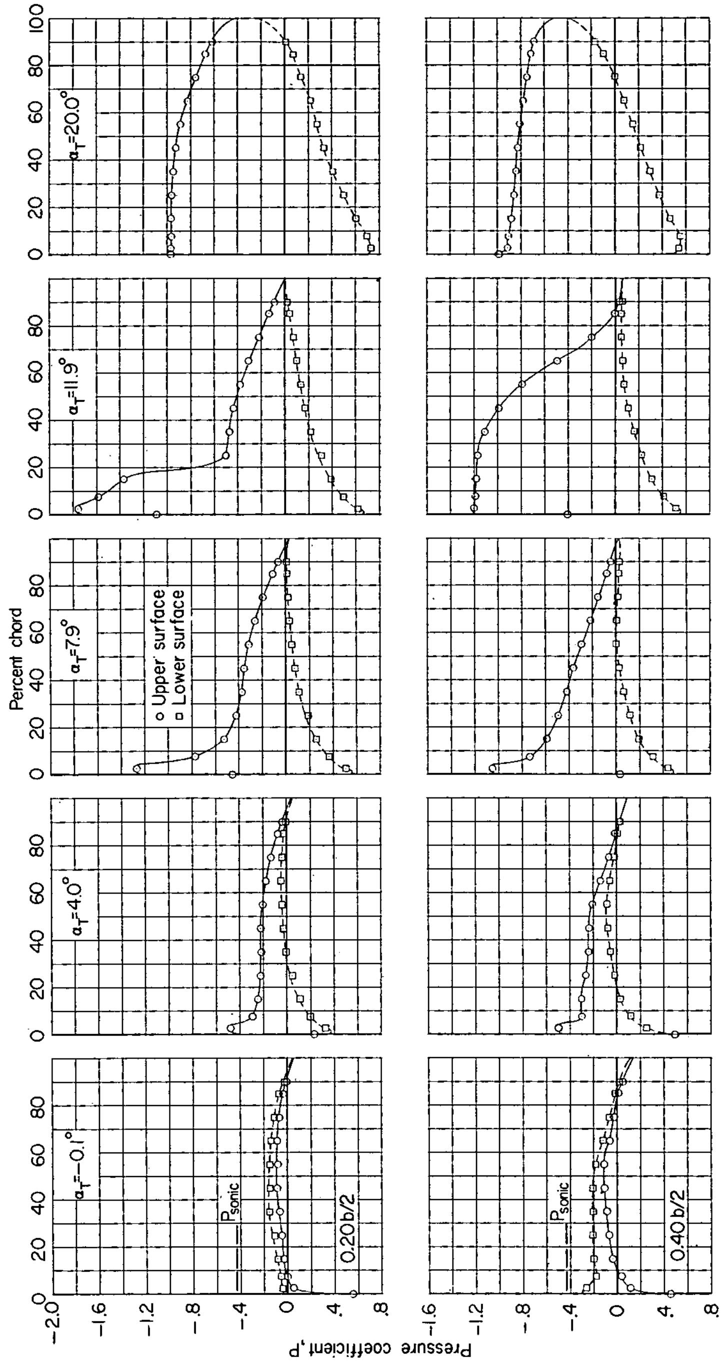

α_T=20.0°
α_T=11.9°
α_T=7.9°
α_T=4.0°
α_T=-0.1°
Percent chord
o Upper surface
□ Lower surface
P_{sonic}
0.20b/2
0.40b/2
Pressure coefficient, P

(b). M = 0.80.

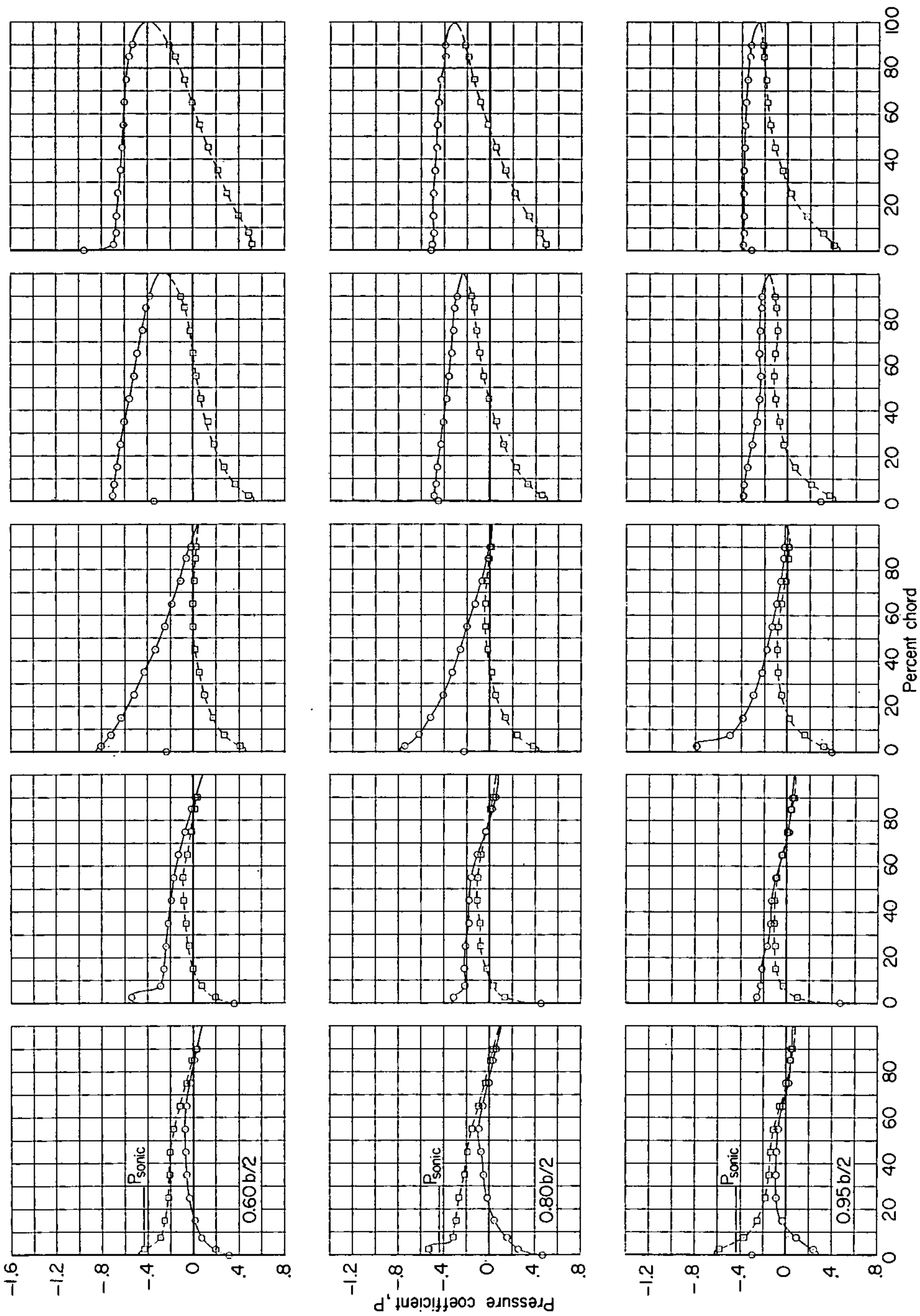

(b) M = 0.80. Concluded.

Figure 6.- Continued.

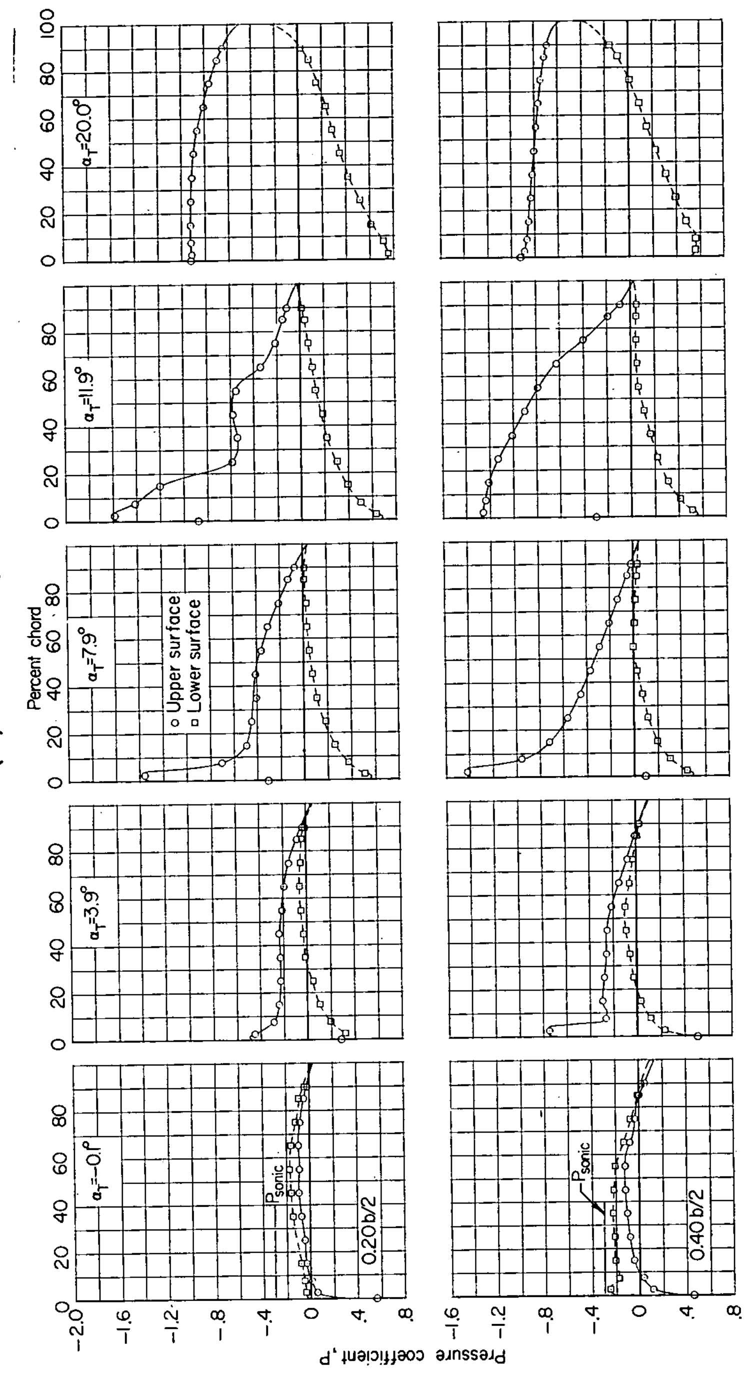

α_T=20.0°
α_T=11.9°
α_T=7.9°
α_T=3.9°
α_T=-0.1°
Percent chord
○ Upper surface
□ Lower surface
P_{sonic}
0.20b/2
0.40b/2
Pressure coefficient, P

(c) M = 0.85.

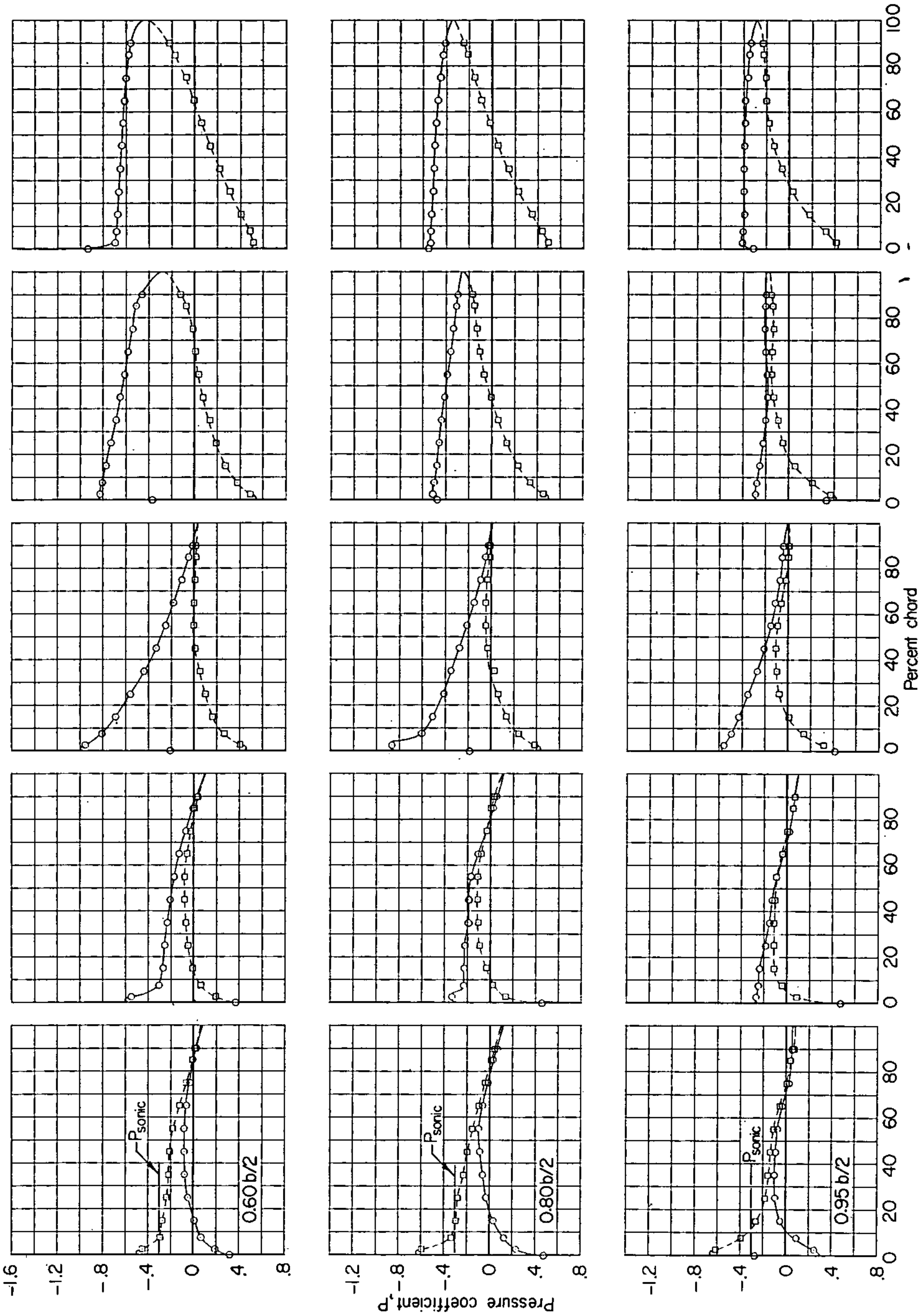

(c) M = 0.85. Concluded.

Figure 6.- Continued.

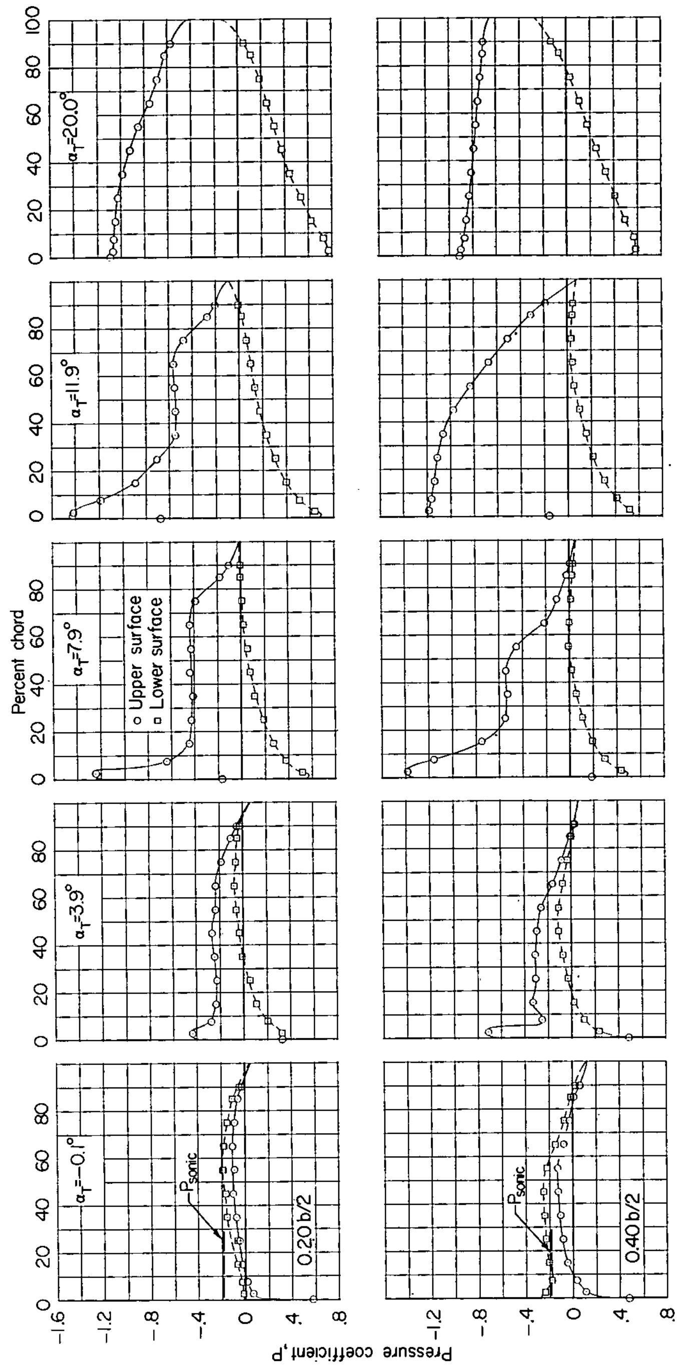
αT=20.0°
αT=11.9°
αT=7.9°
αT=3.9°
αT=-0.1°
Percent chord
○ Upper surface
□ Lower surface
Psonic
0.20 b/2
0.40 b/2
Pressure coefficient, P

(d) M = 0.90.

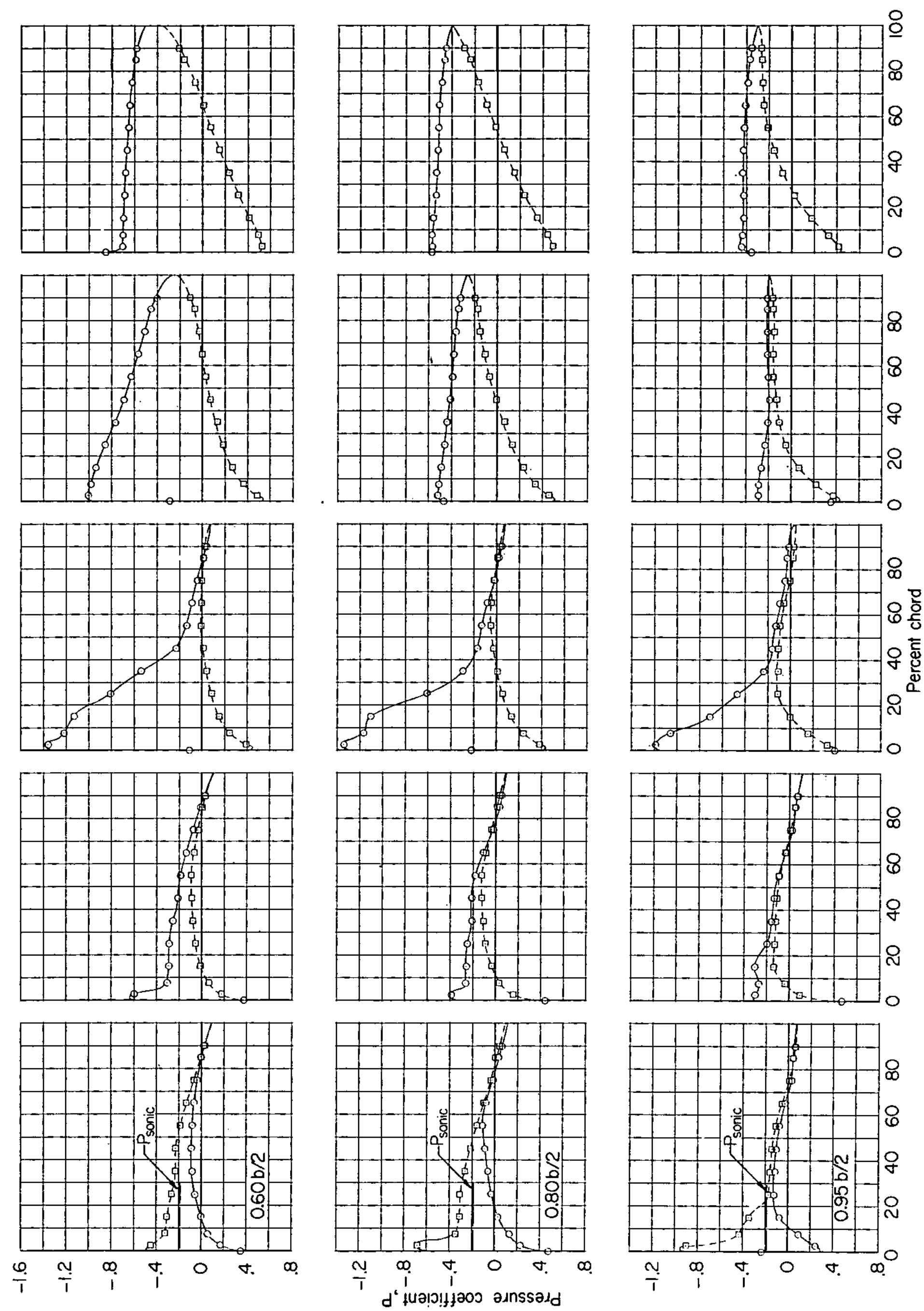

(d) M = 0.90. Concluded.

Figure 6.- Continued.

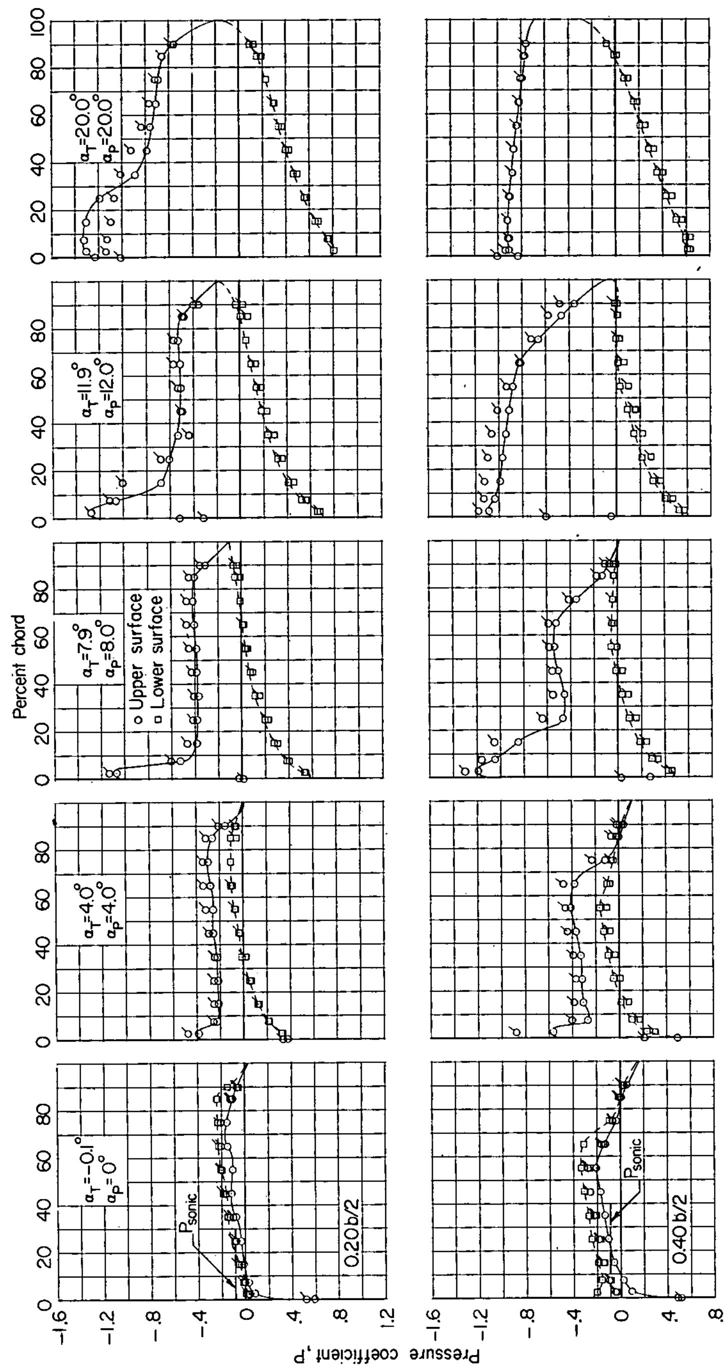

α_T=20.0°
α_p=20.0°
α_T=11.9°
α_p=12.0°
α_T=7.9°
α_p=8.0°
○ Upper surface
□ Lower surface
α_T=4.0°
α_p=4.0°
α_T=-0.1°
α_p=0°
P_{sonic}
0.20b/2
0.40b/2
Percent chord
Pressure coefficient, P

(e) M = 0.95.

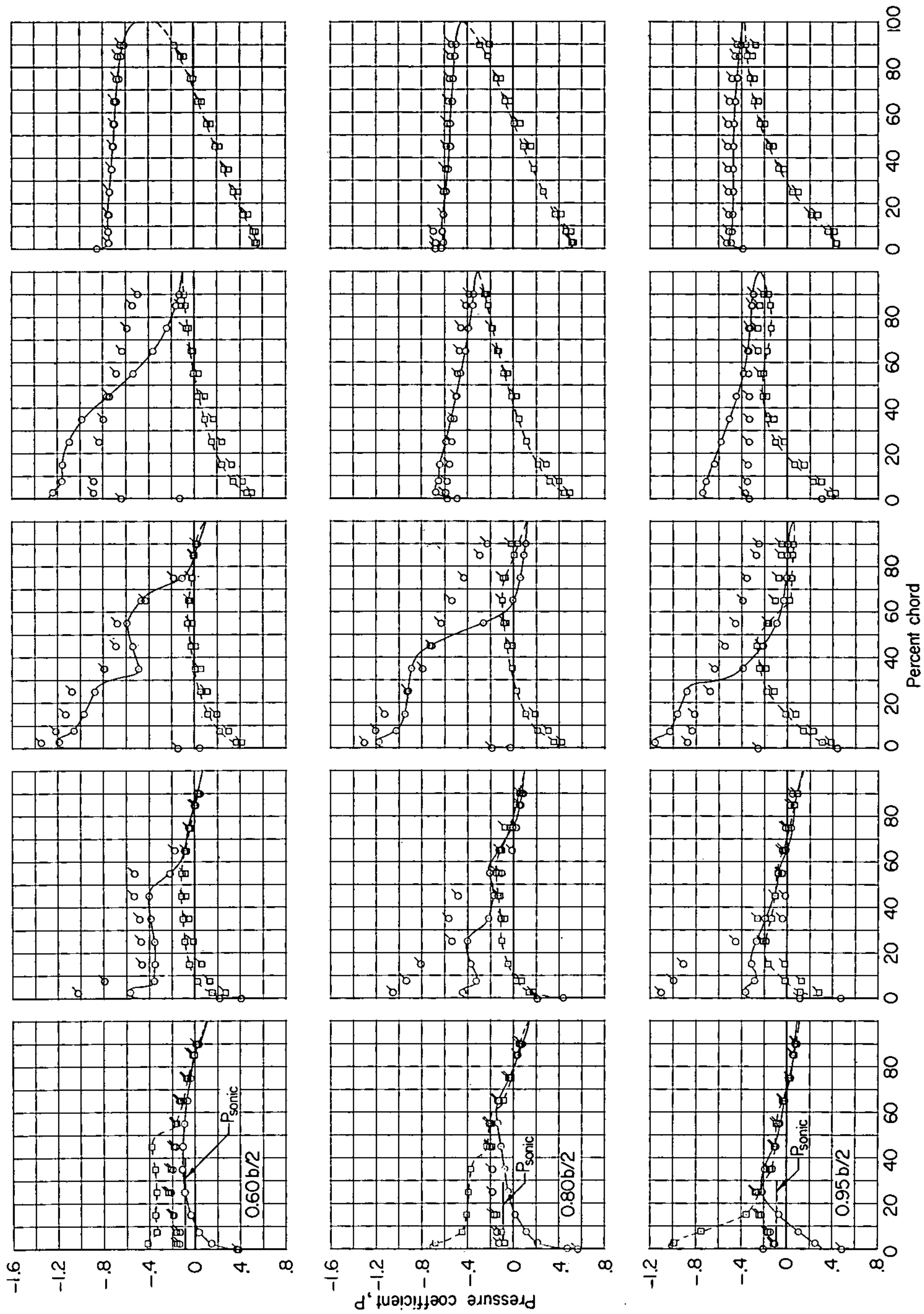

(e) M = 0.95. Concluded.

Figure 6.- Continued.

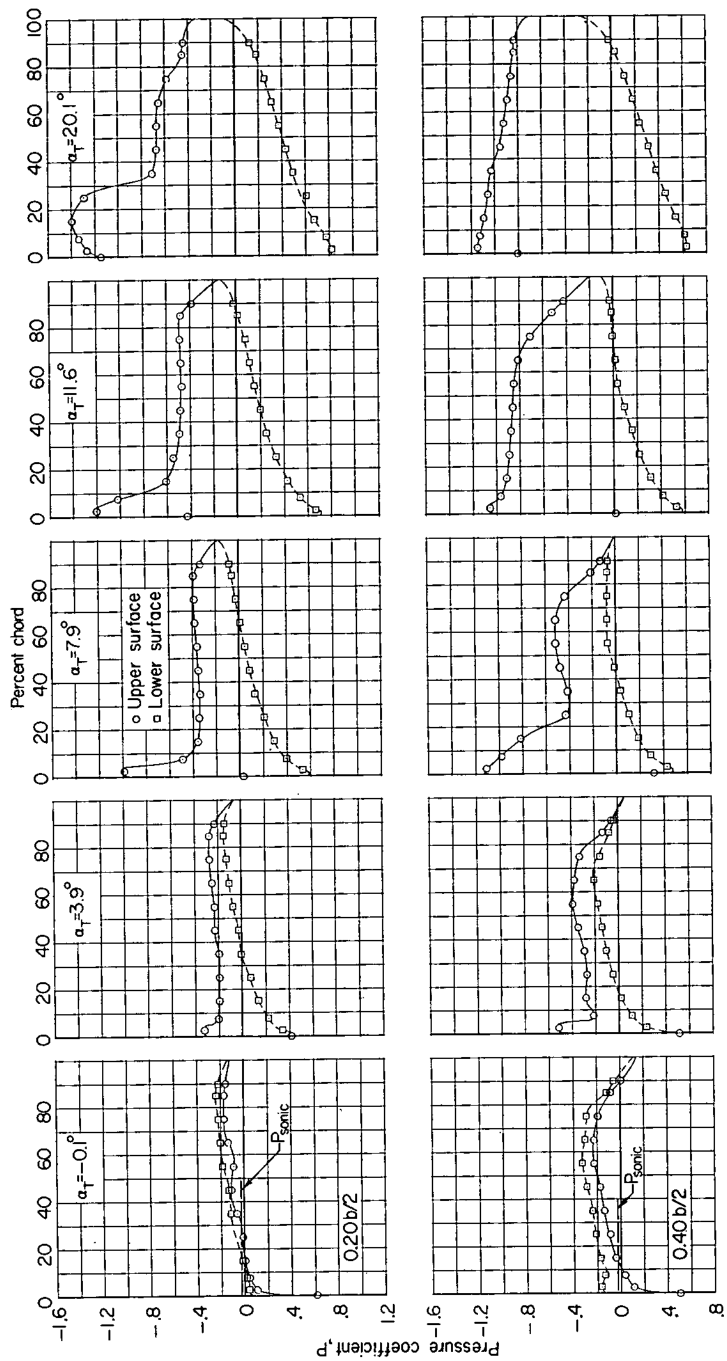

α_T=20.1°
α_T=11.6°
α_T=7.9°
α_T=3.9°
α_T=-0.1°
o Upper surface
□ Lower surface
Percent chord
P_{sonic}
0.20b/2
0.40b/2
Pressure coefficient, P

(f) M = 0.98.

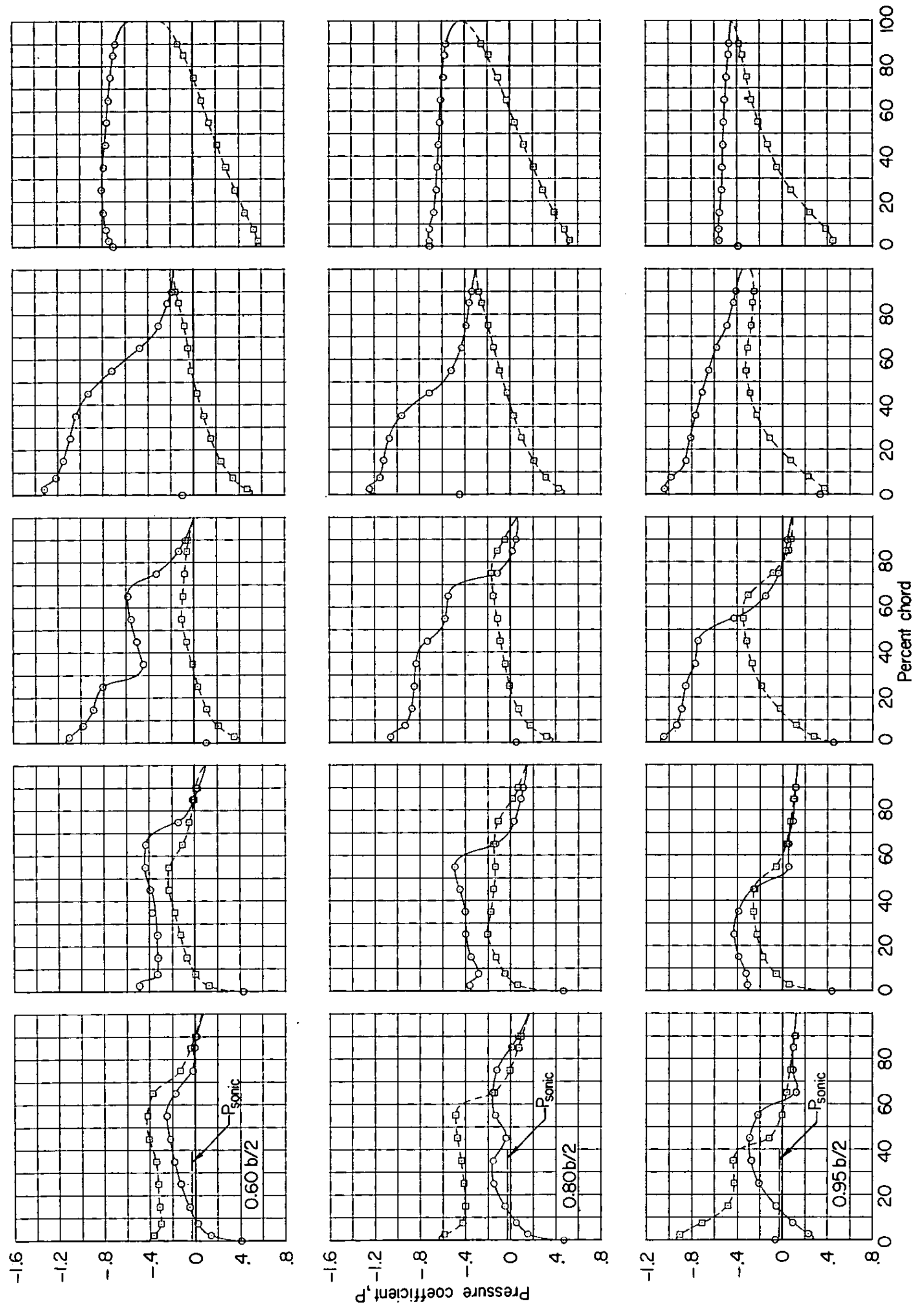

(f) M = 0.98. Concluded.

Figure 6.- Continued.

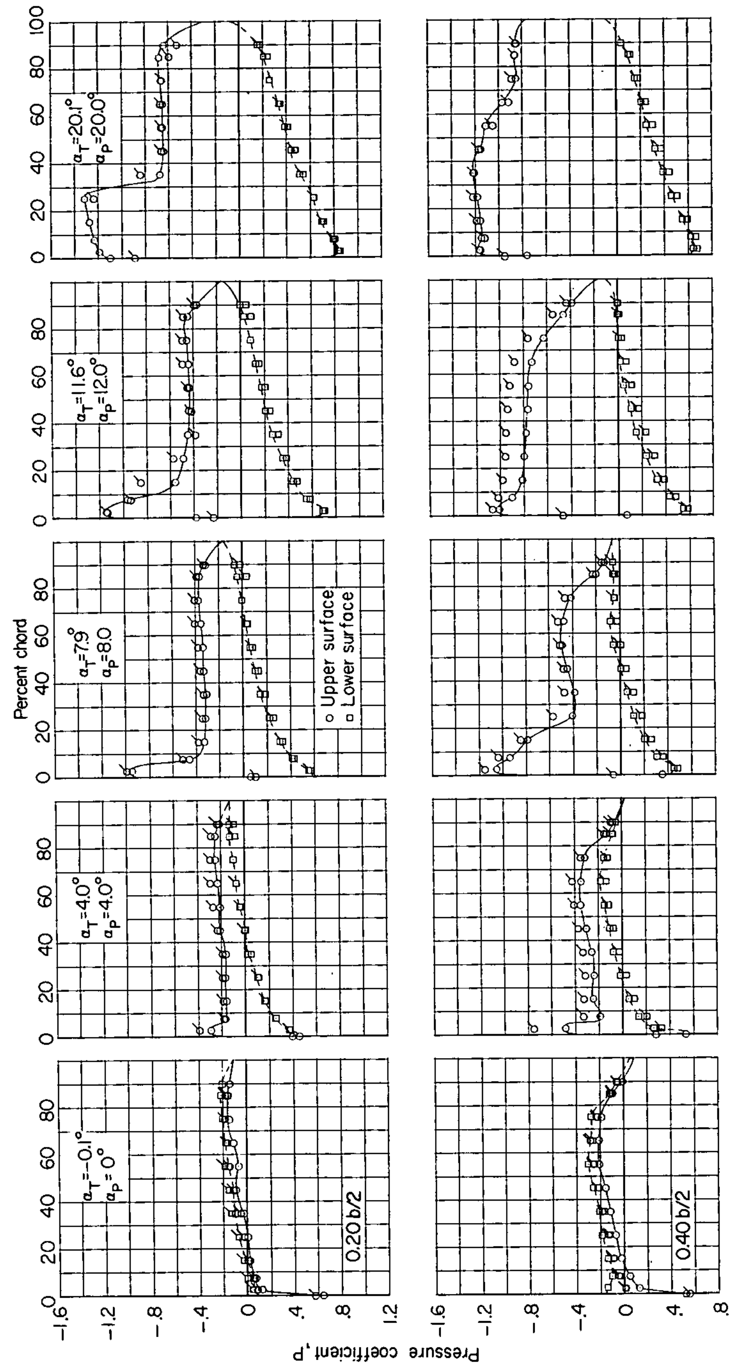

Percent chord
Pressure coefficient, P
α_T=-0.1° α_p=0°
α_T=4.0° α_p=4.0°
α_T=7.9° α_p=8.0
α_T=11.6° α_p=12.0°
α_T=20.1° α_p=20.0°
○ Upper surface
□ Lower surface
0.20b/2
0.40b/2

(g) M = 1.00.

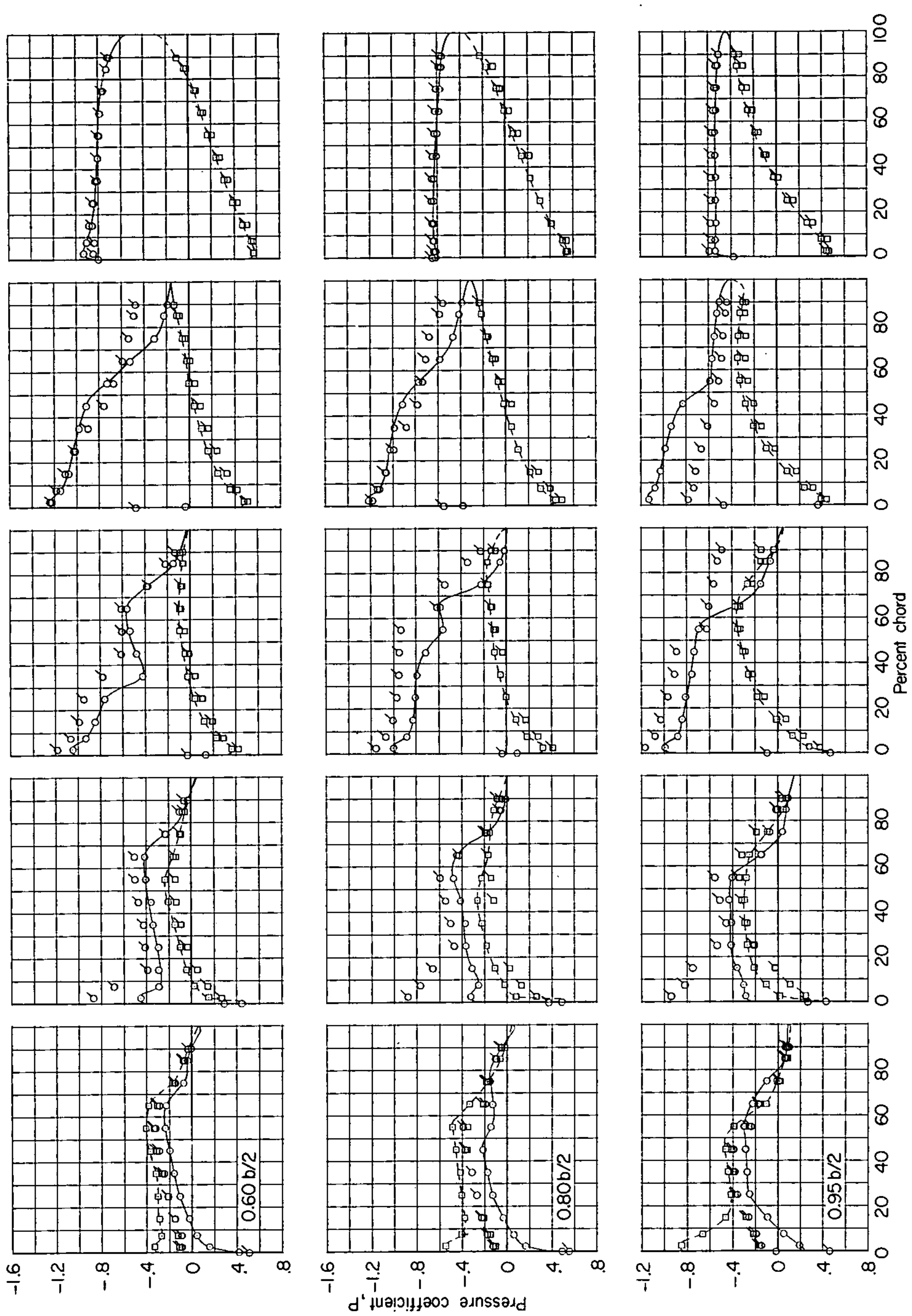

(g) M = 1.00. Concluded.

Figure 6.- Continued.

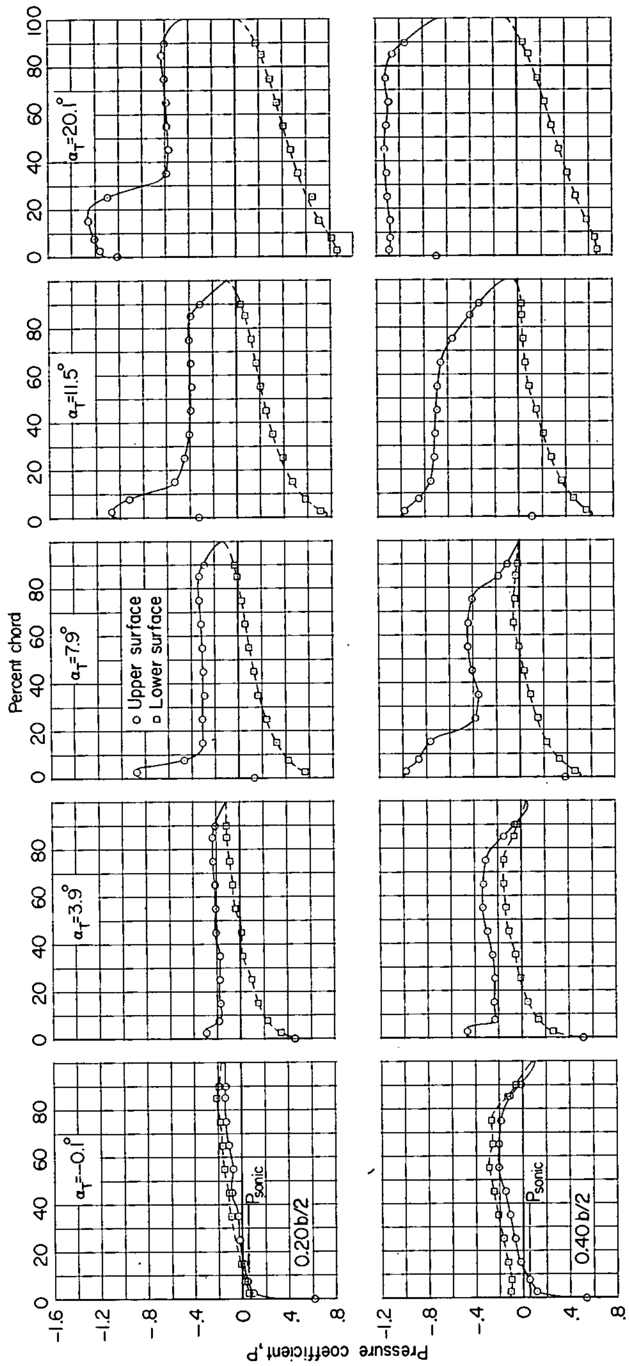
α_T=20.1°
α_T=11.5°
α_T=7.9°
α_T=3.9°
α_T=-0.1°
o Upper surface
□ Lower surface
Percent chord
P_{sonic}
0.20b/2
0.40b/2
Pressure coefficient, P

(h) M = 1.03.

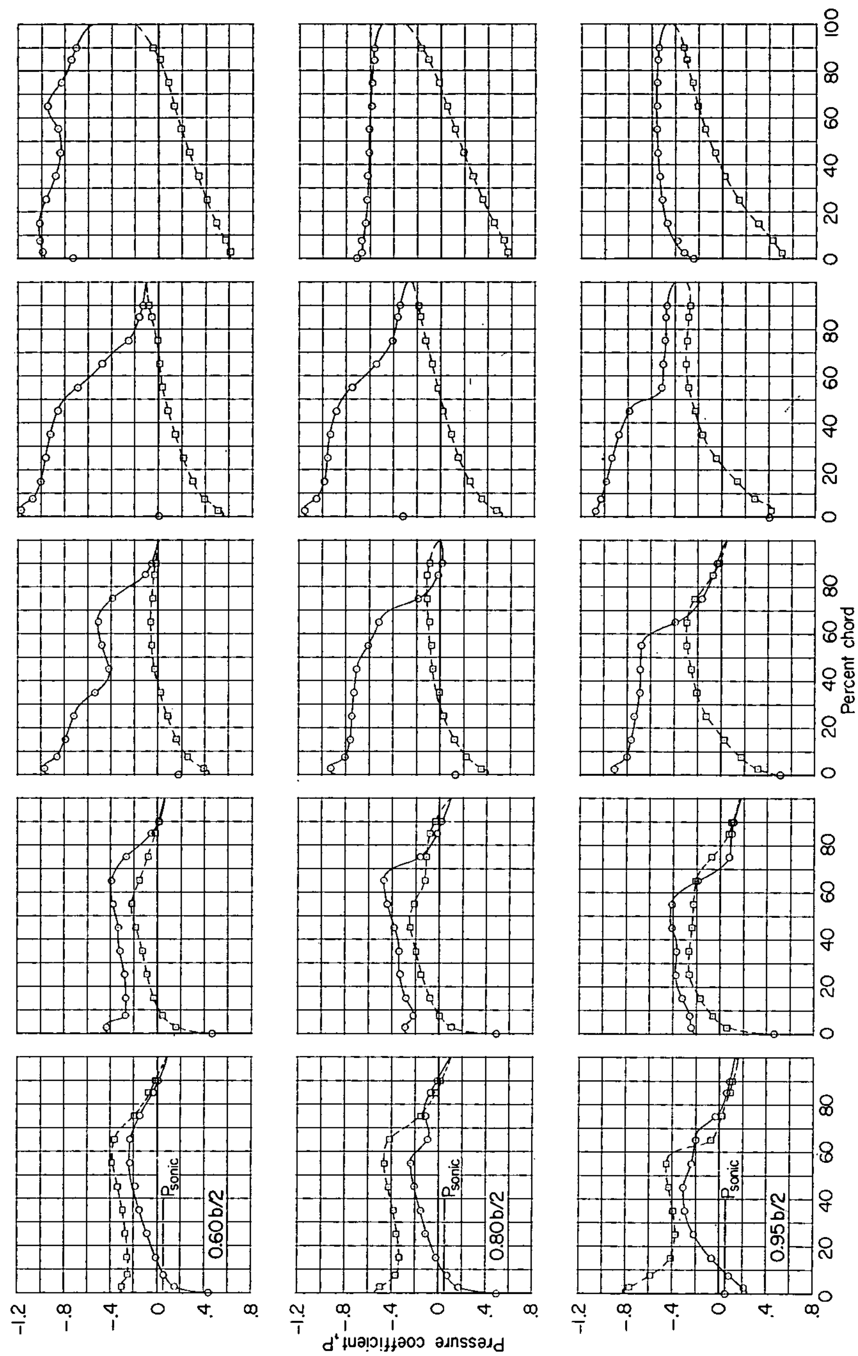

(h) M = 1.03. Concluded.

Figure 6.- Continued.

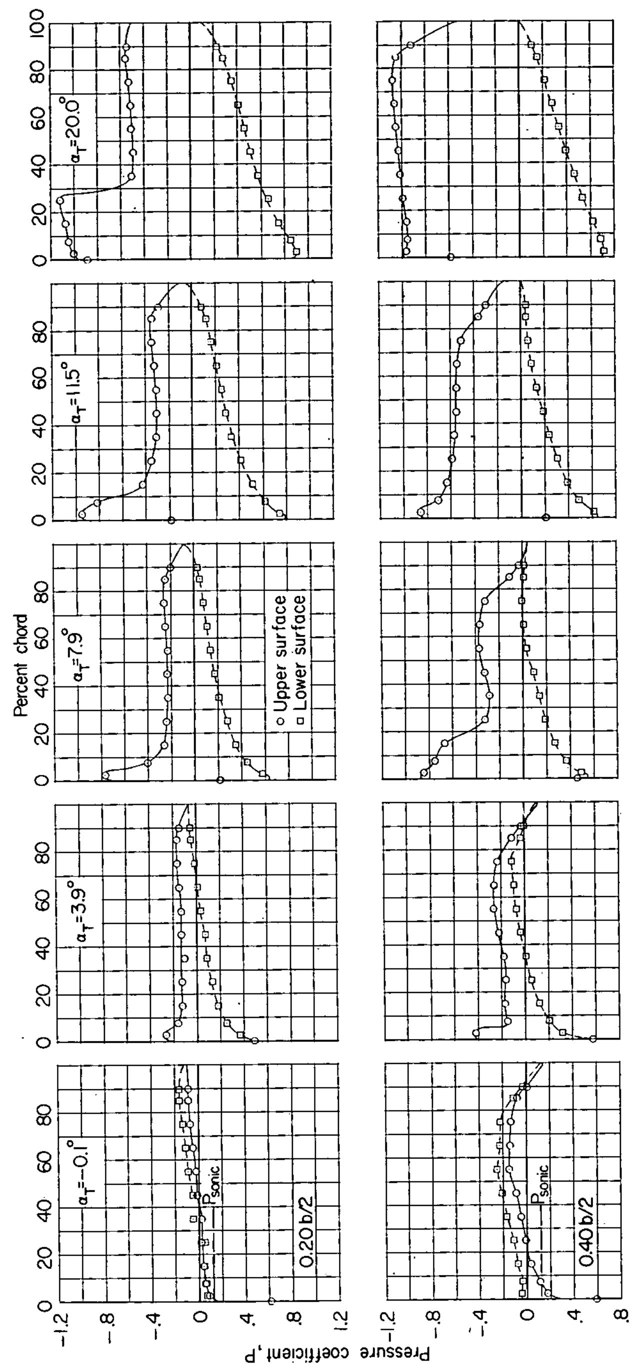

α_T=-0.1°
α_T=3.9°
α_T=7.9°
α_T=11.5°
α_T=20.0°
Percent chord
○ Upper surface
□ Lower surface
P_sonic
0.20b/2
0.40b/2
Pressure coefficient, P

(1) M = 1.08.

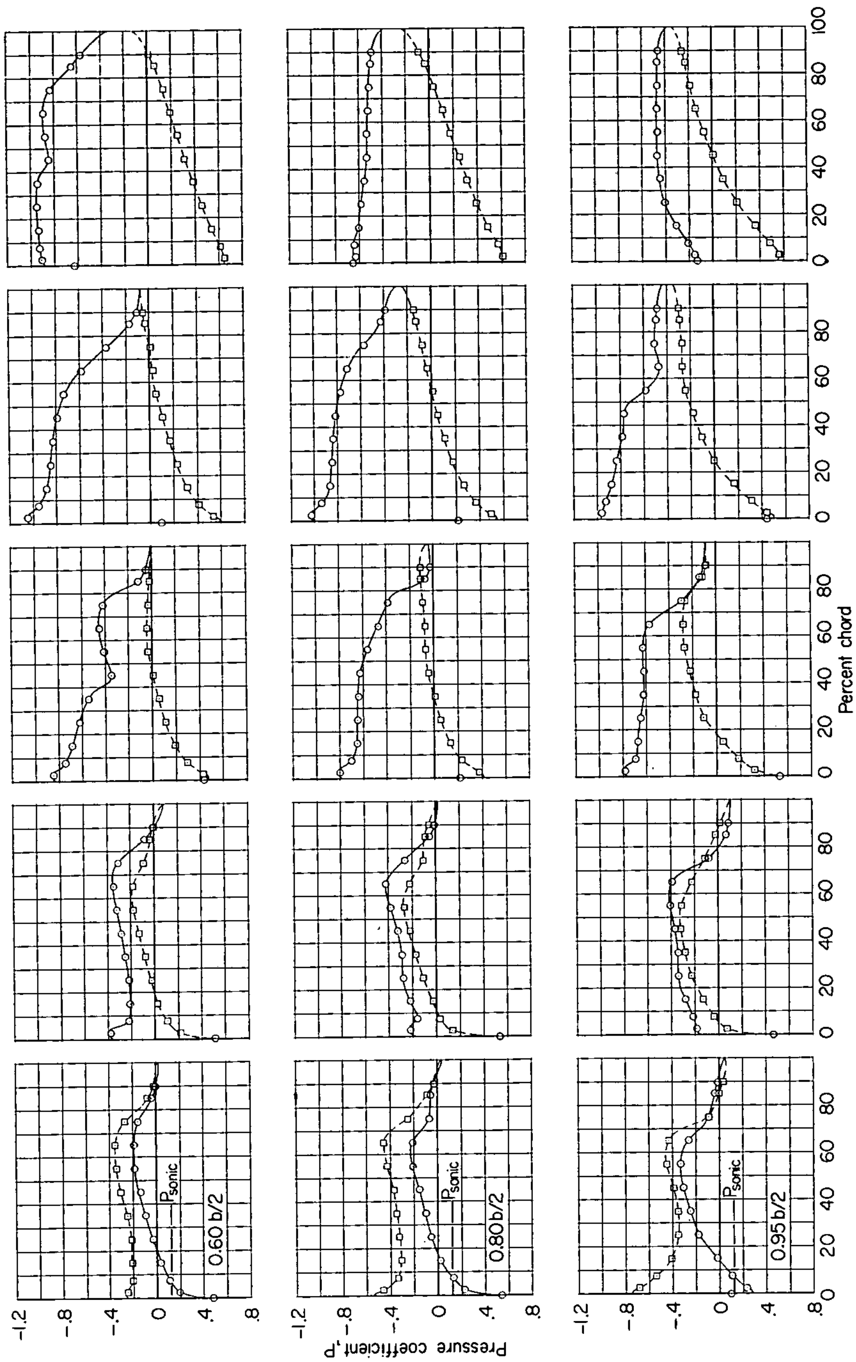

(i) M = 1.08. Concluded.

Figure 6.- Continued.

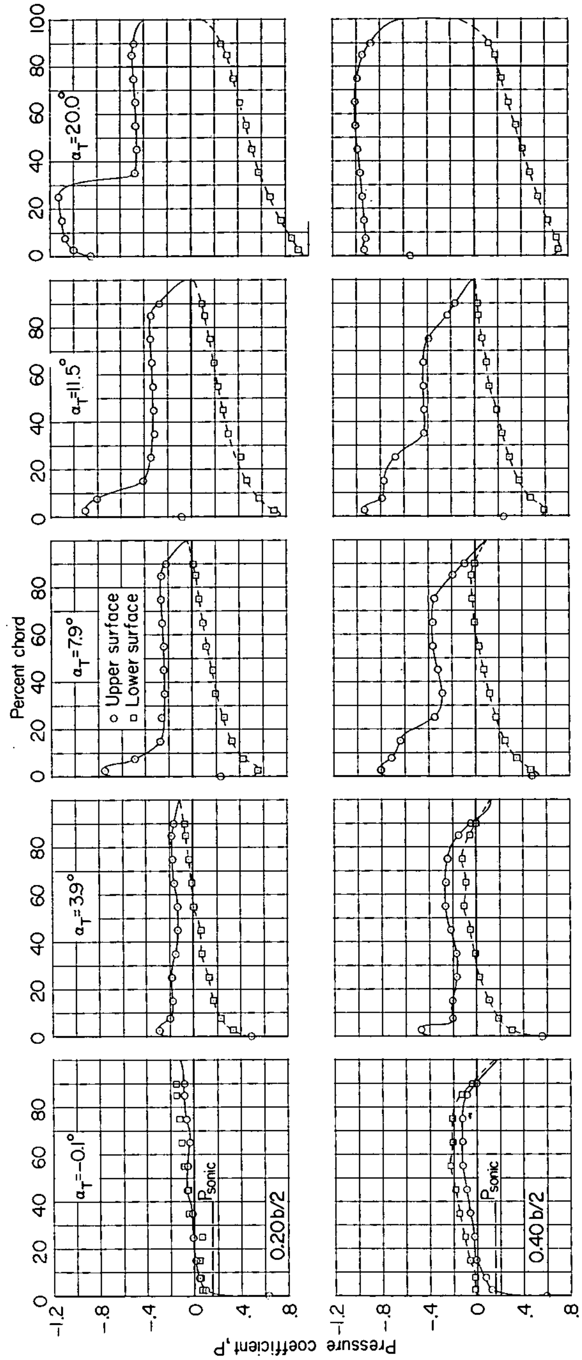
αT=-0.1°
αT=3.9°
αT=7.9°
αT=11.5°
αT=20.0°
Percent chord
○ Upper surface
□ Lower surface
Psonic
0.20b/2
0.40 b/2
Pressure coefficient, P

(J) M = 1.10.

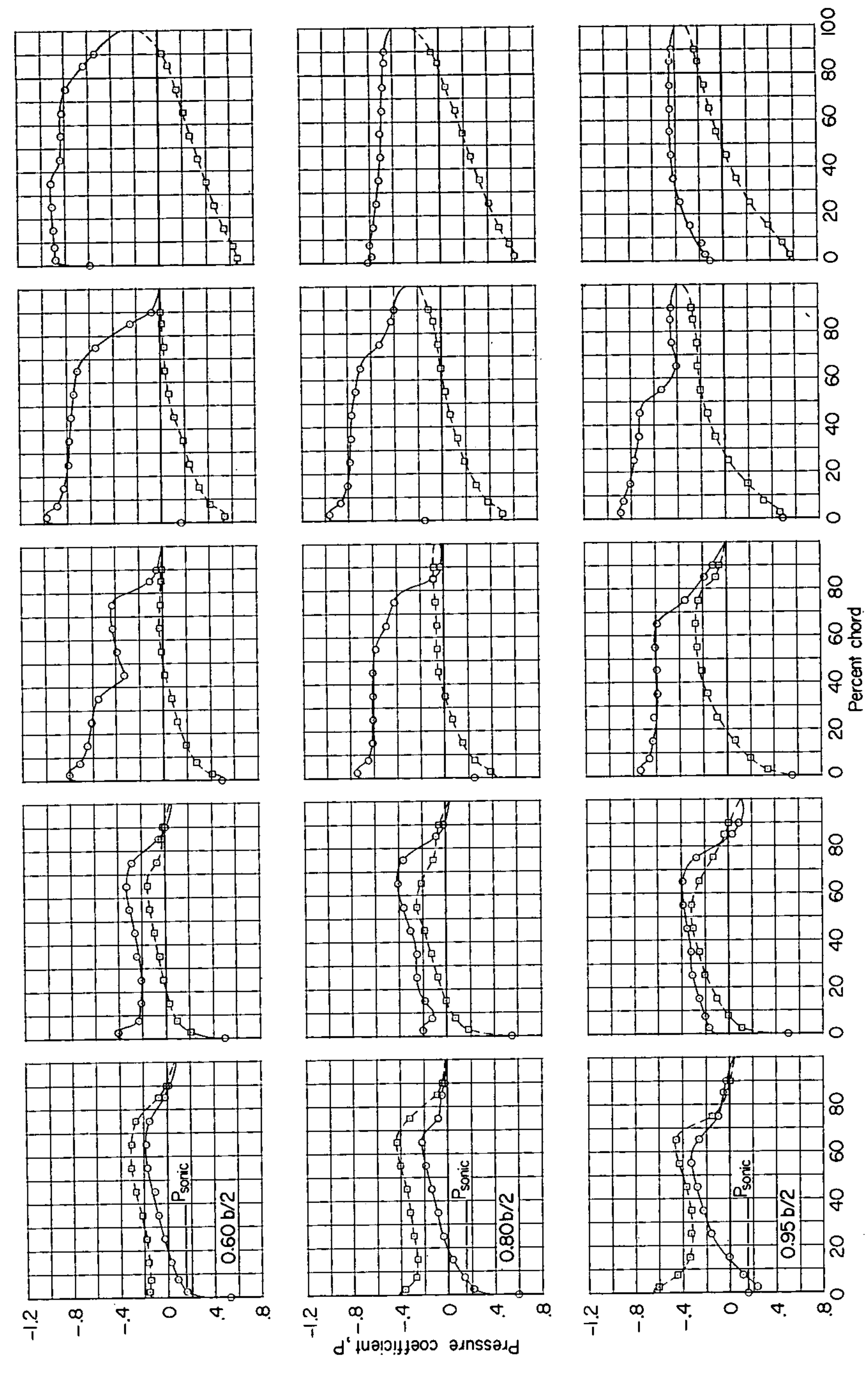

(j) M = 1.10. Concluded.

Figure 6.- Continued.

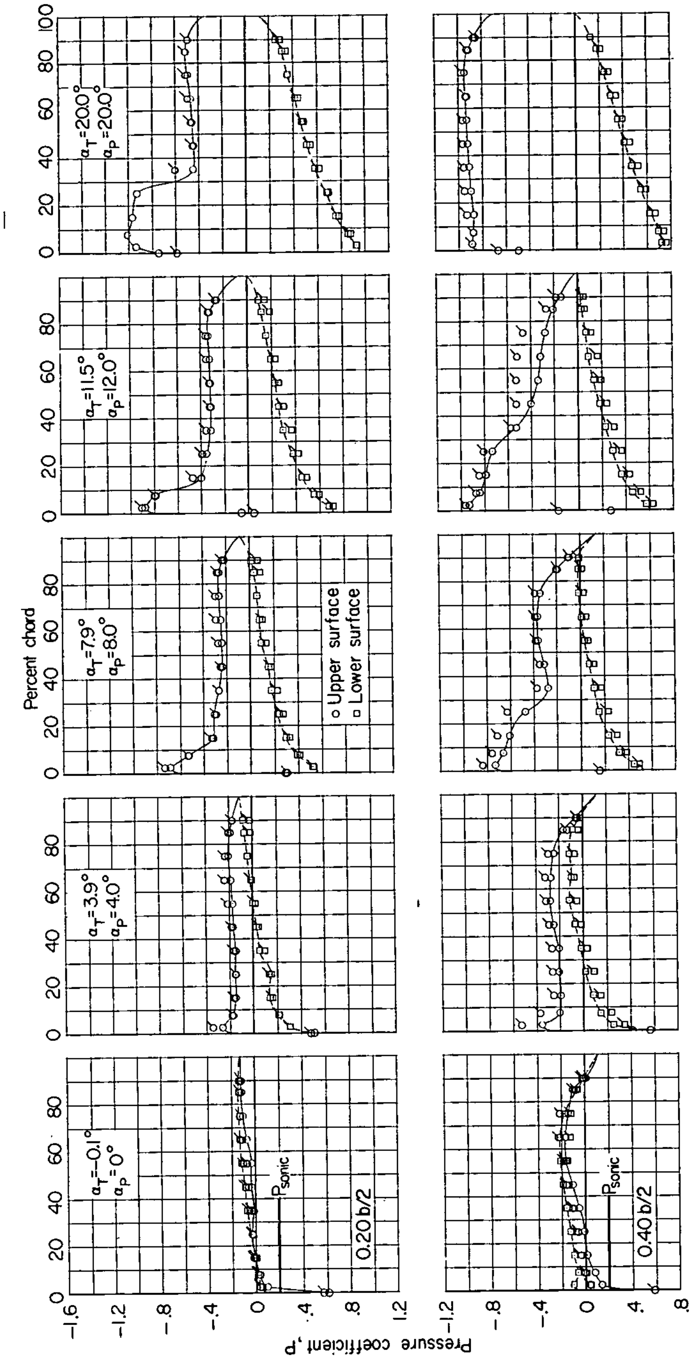
$\alpha_T = -0.1°$
$\alpha_p = 0°$
$\alpha_T = 3.9°$
$\alpha_p = 4.0°$
$\alpha_T = 7.9°$
$\alpha_p = 8.0°$
$\alpha_T = 11.5°$
$\alpha_p = 12.0°$
$\alpha_T = 20.0°$
$\alpha_p = 20.0°$
Percent chord
○ Upper surface
□ Lower surface
P_{sonic}
0.20 b/2
0.40 b/2
Pressure coefficient, P

(k) M = 1.13.

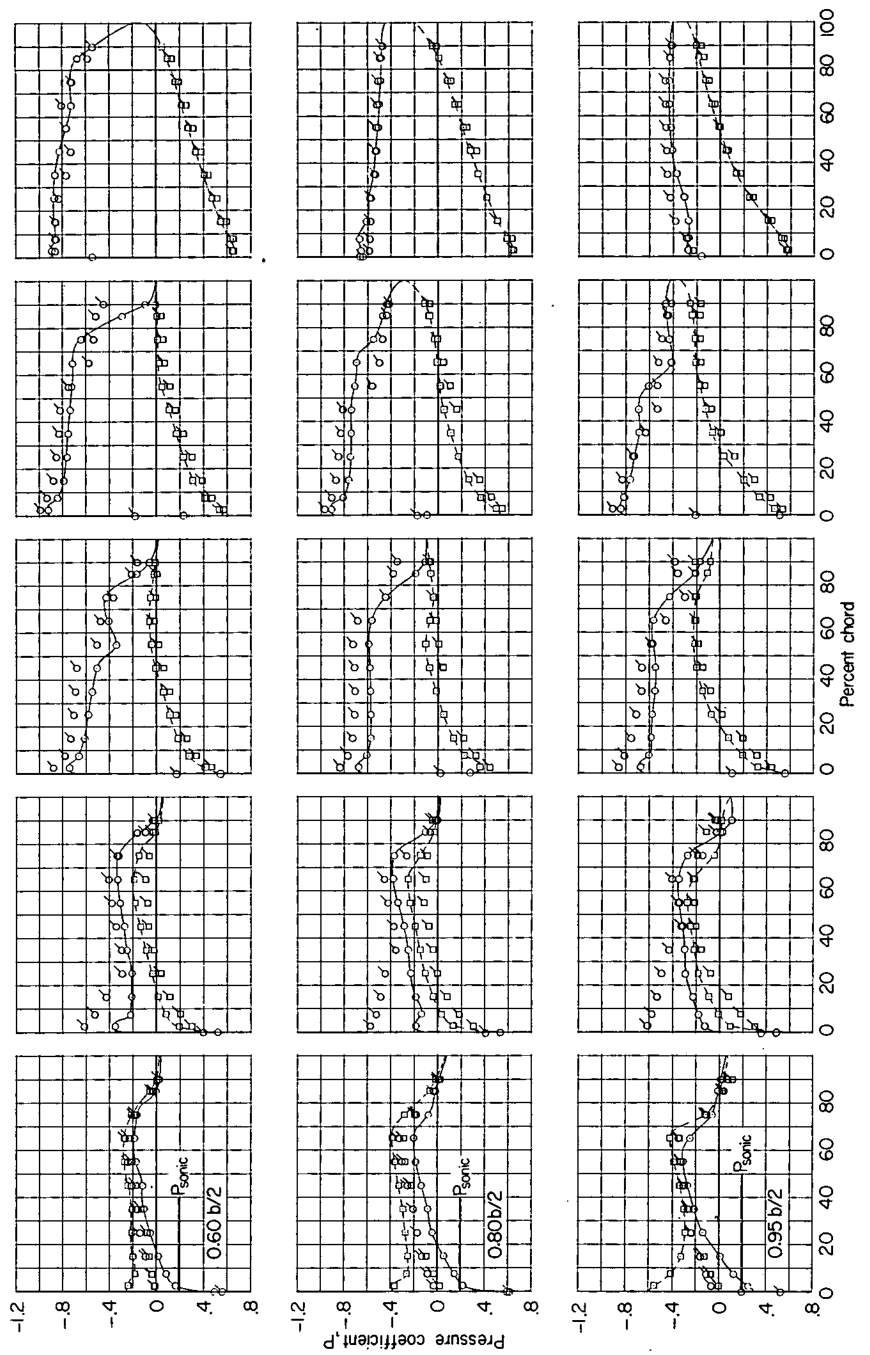

(k) M = 1.13. Concluded.

Figure 6.- Concluded.

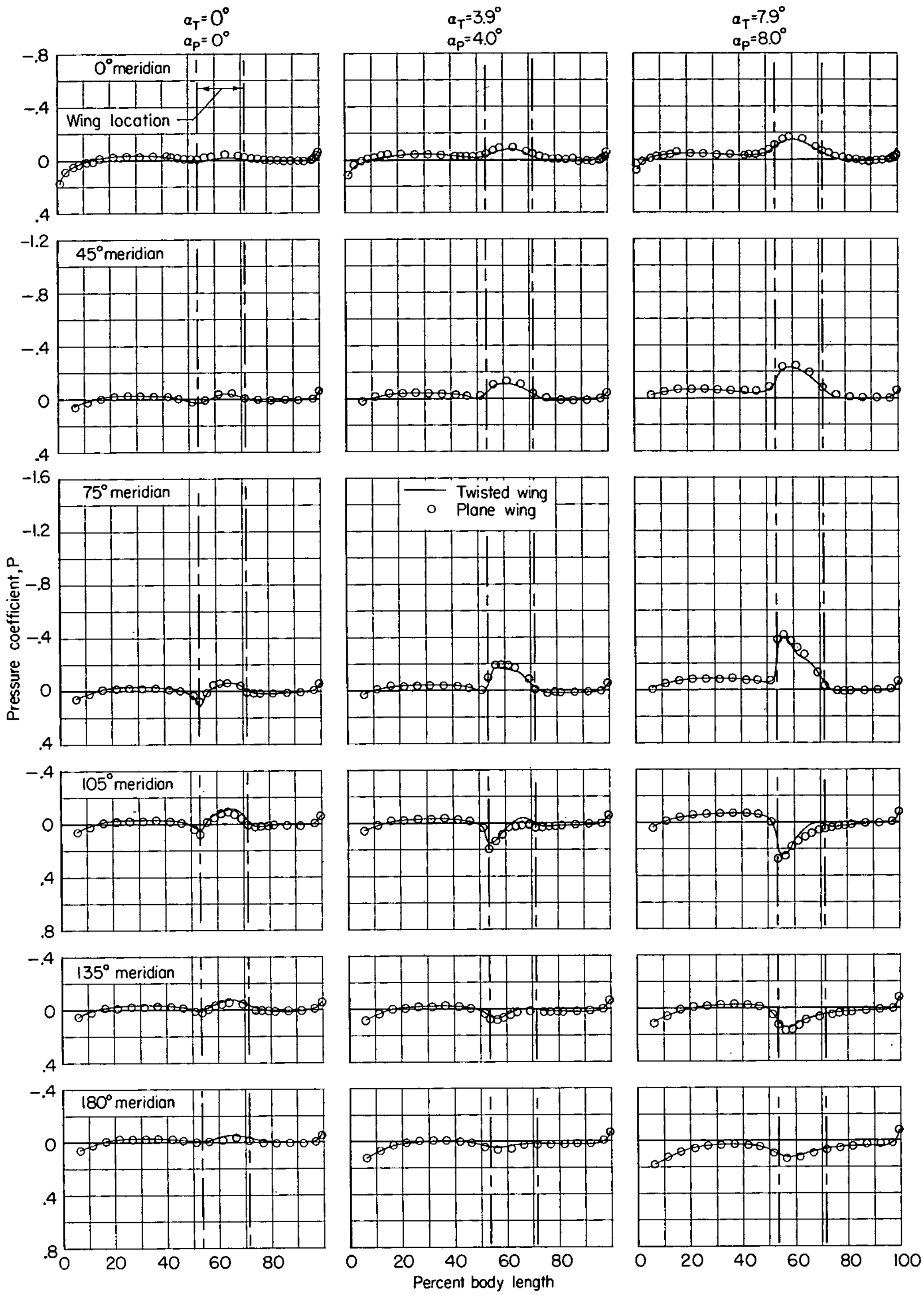

(a) M = 0.60.

Figure 7.- Basic pressure measurements for the body with twisted and plane wings. (The circles indicate data points for body with plane wing.)

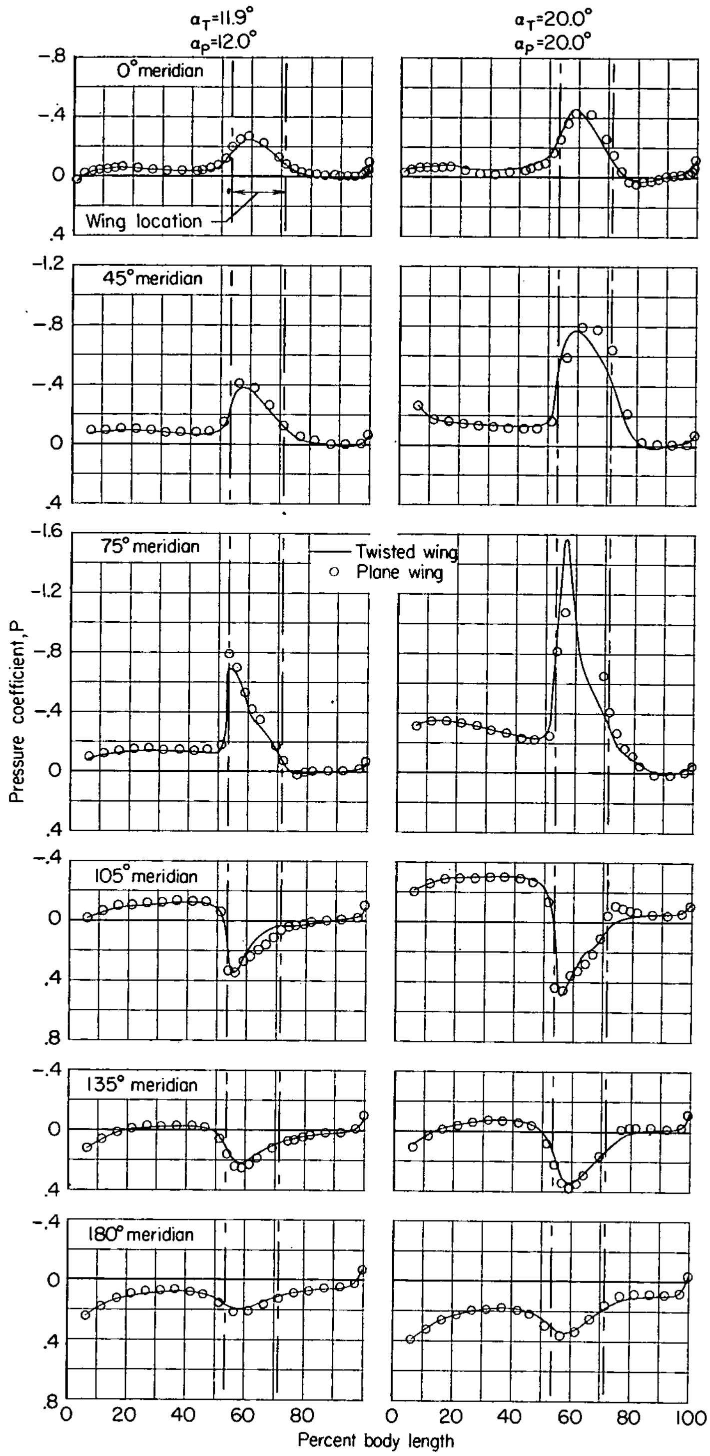

(a) M = 0.60. Concluded.

Figure 7.- Continued.

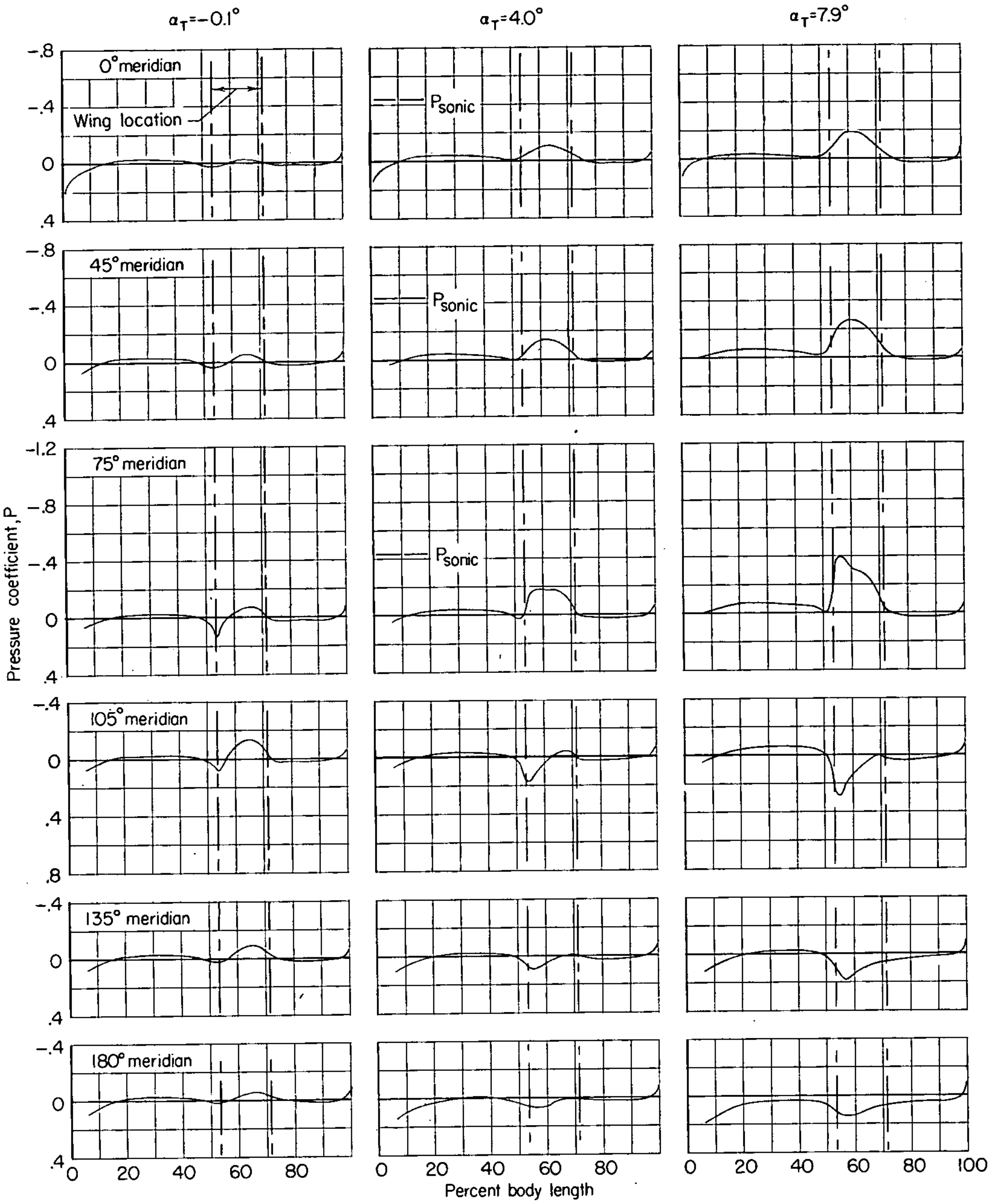

(b) M = 0.80.

Figure 7.- Continued.

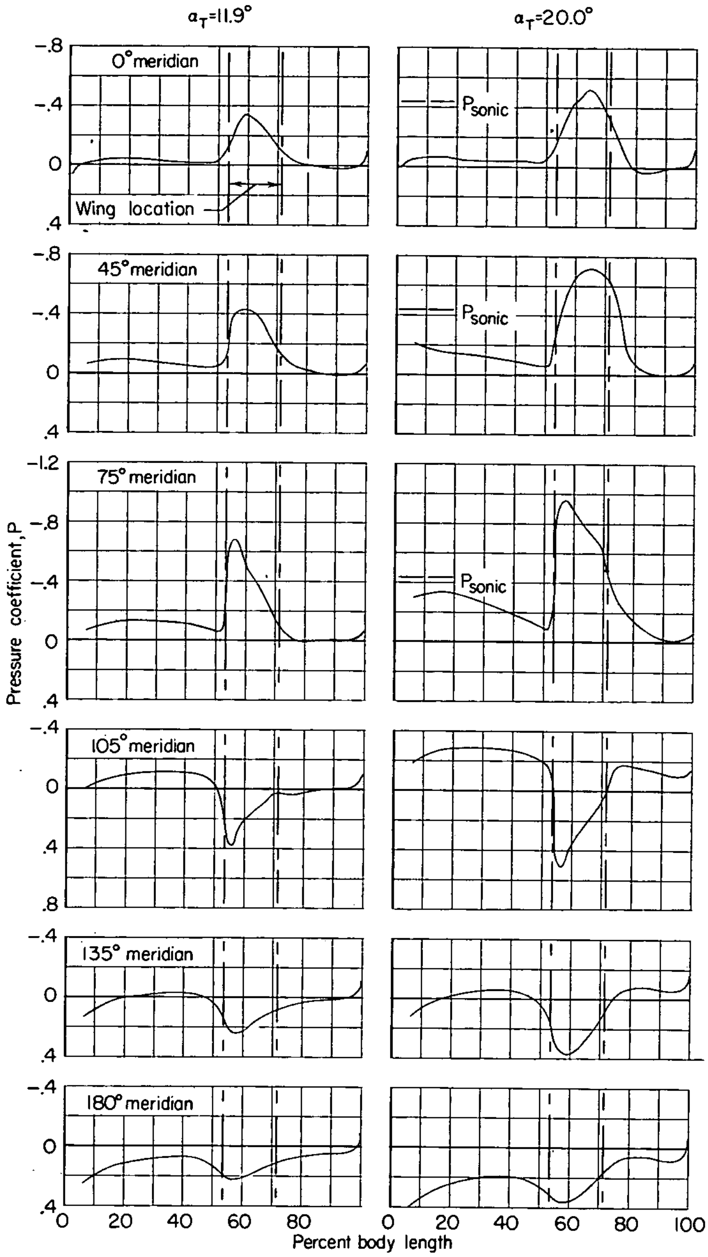

(b) M = 0.80. Concluded.

Figure 7.- Continued.

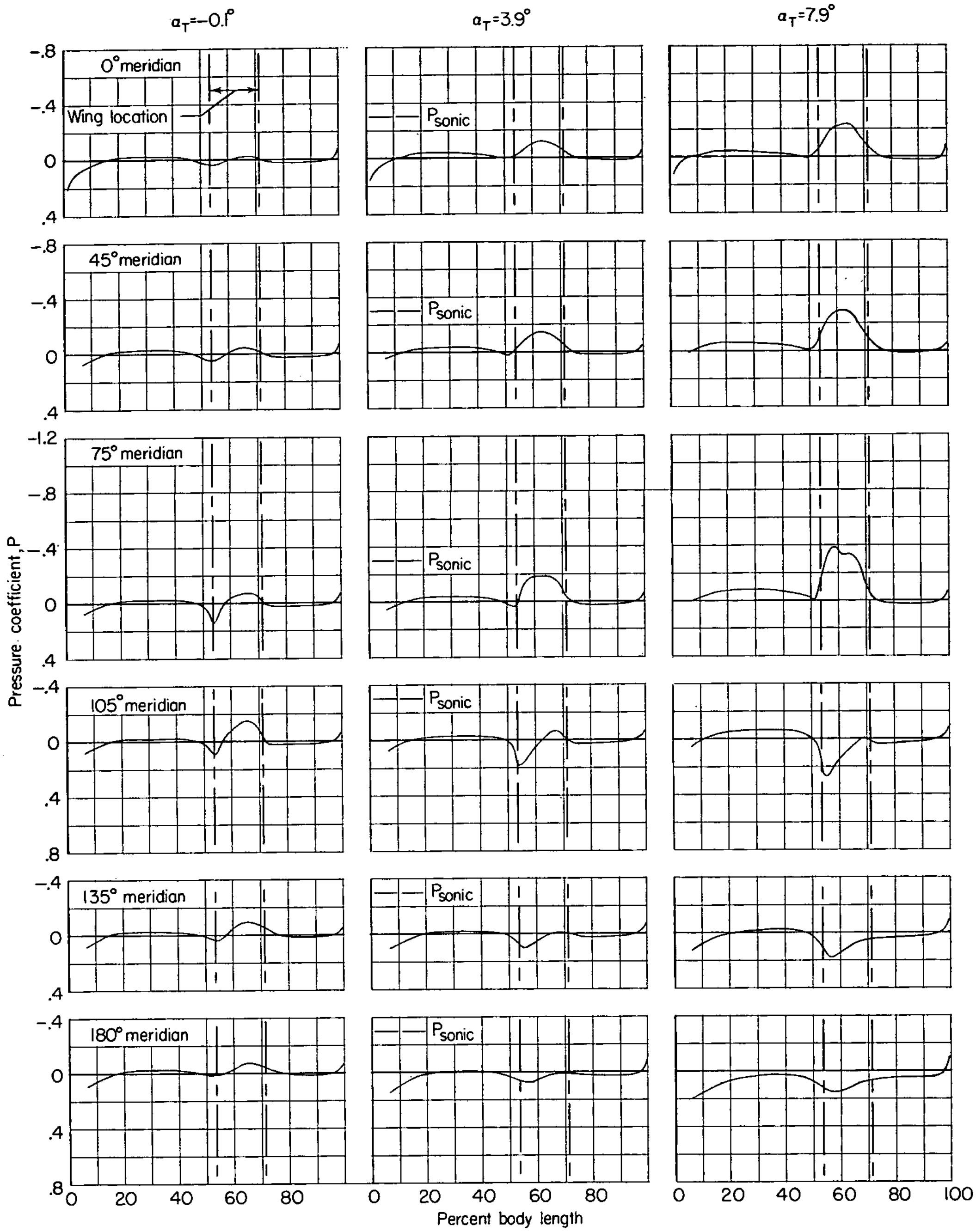

(c) M = 0.85.

Figure 7.- Continued.

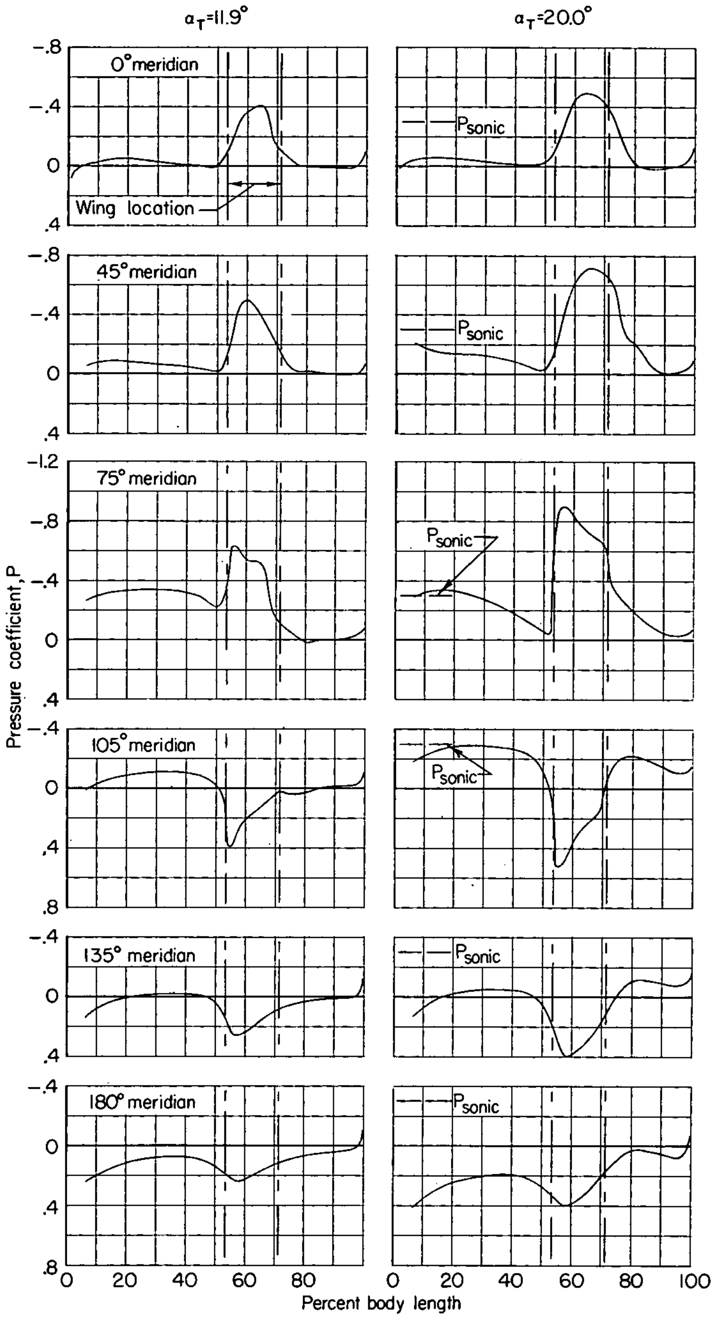

(c) M = 0.85. Concluded.

Figure 7.- Continued.

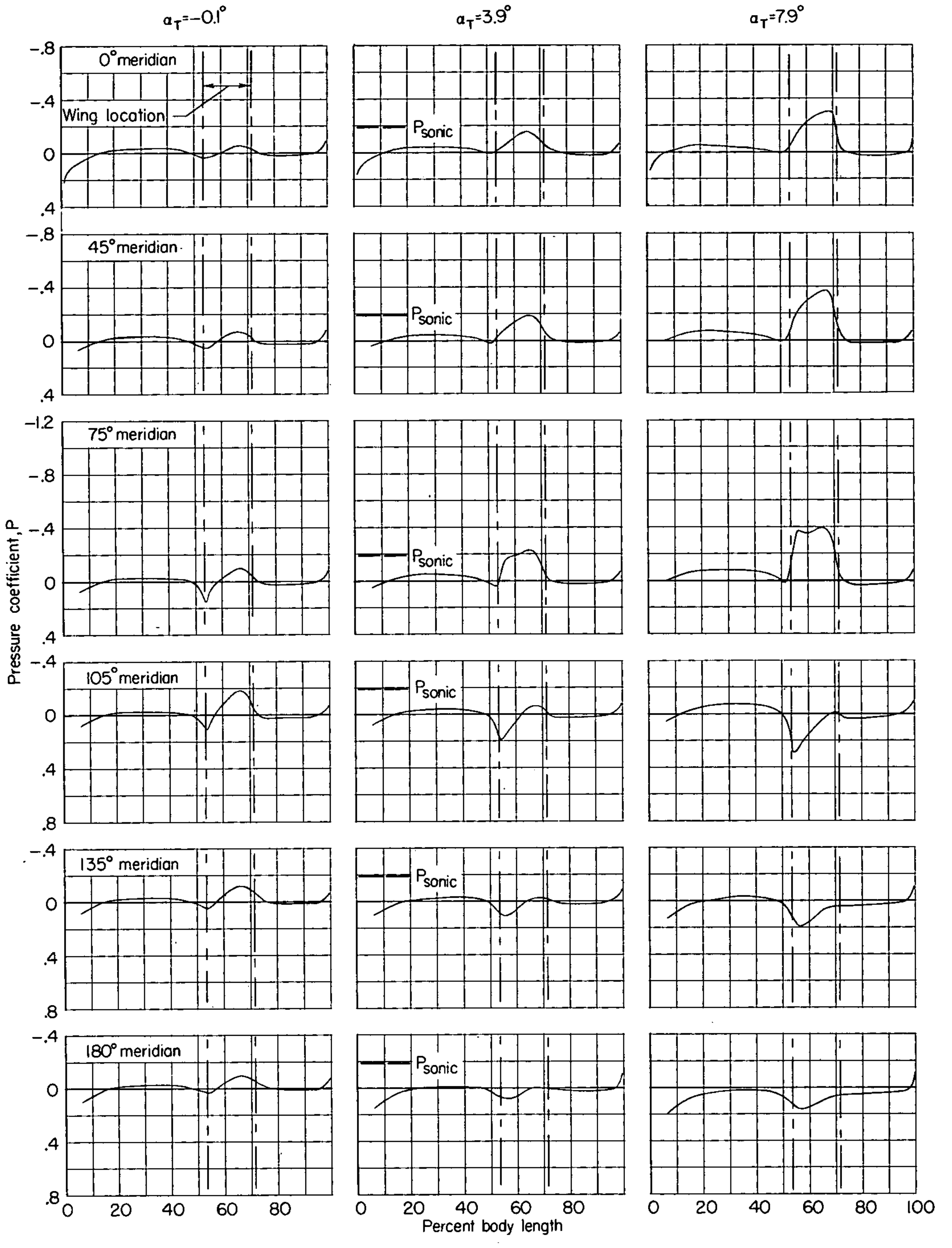

(d) M = 0.90.

Figure 7.- Continued.

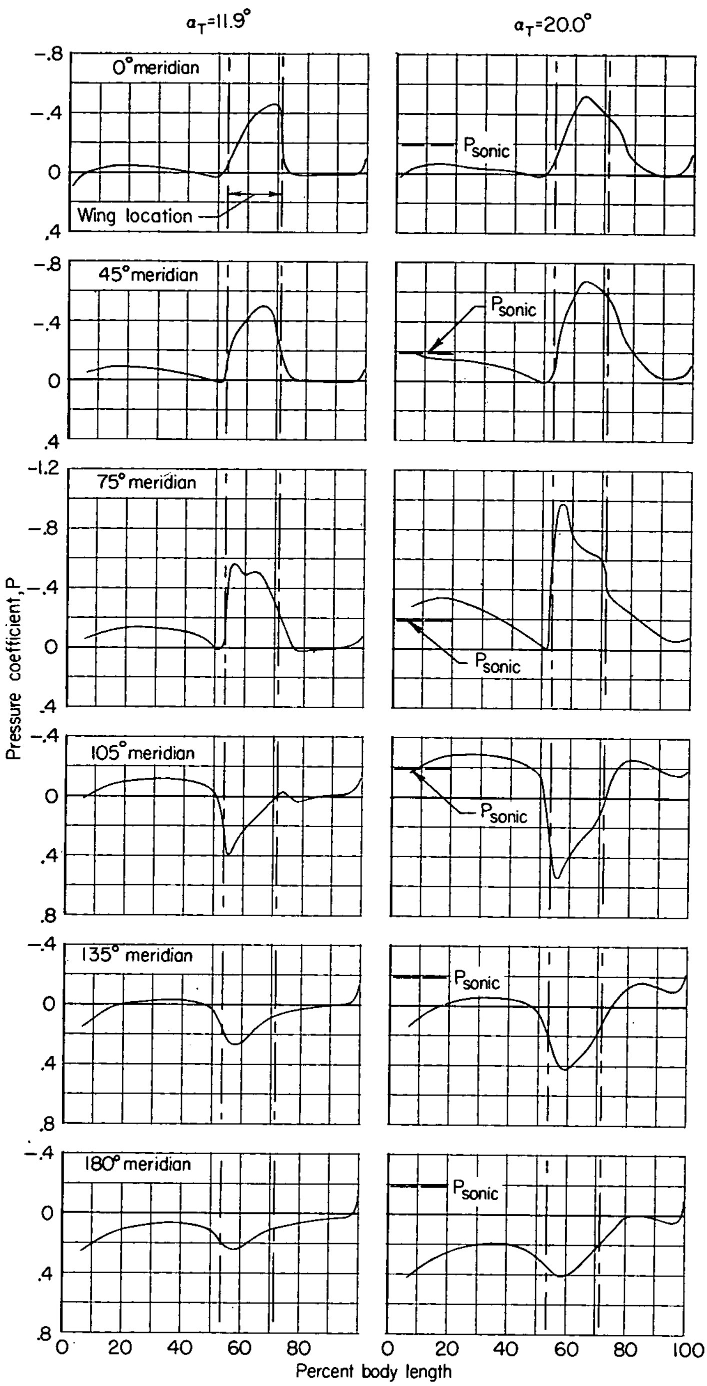

(d) M = 0.90. Concluded.

Figure 7.- Continued.

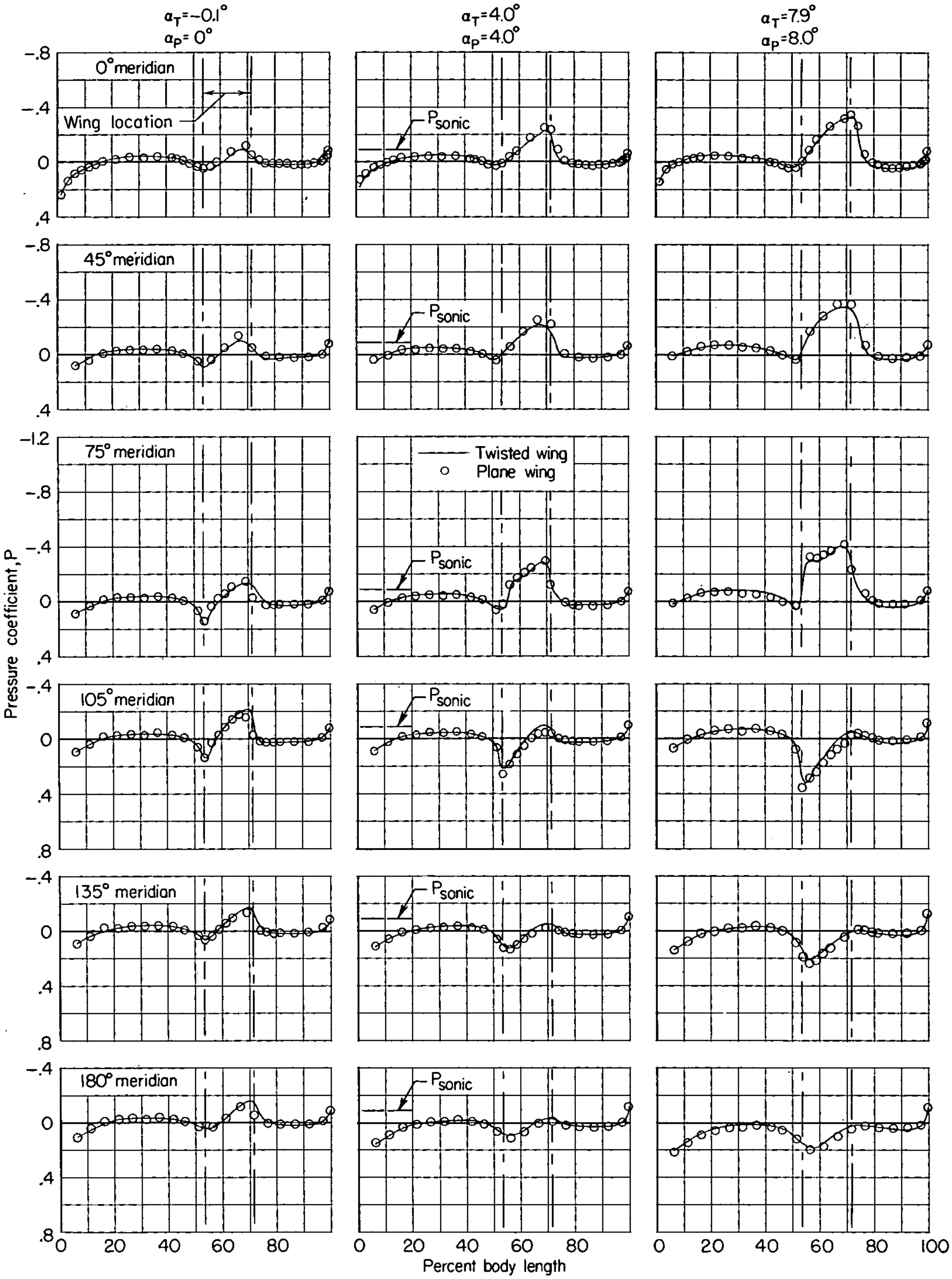

(e) M = 0.95.

Figure 7.- Continued.

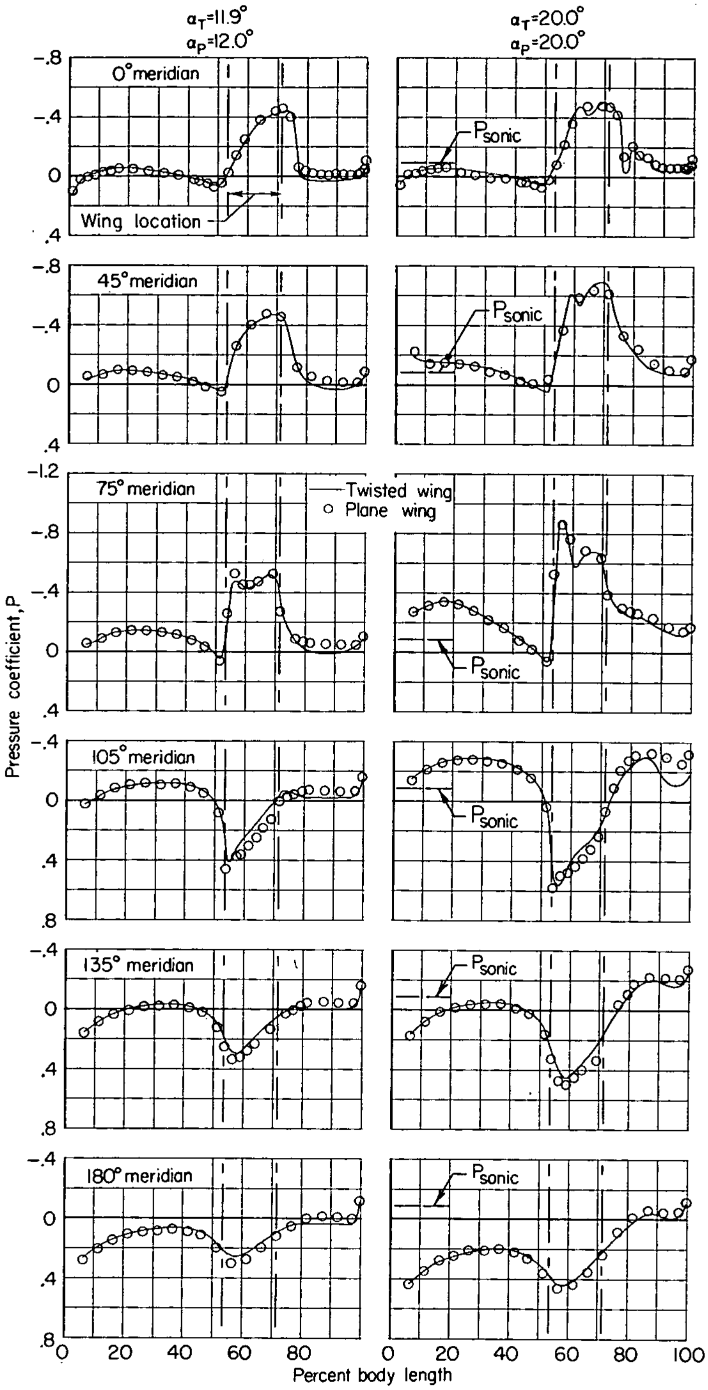

(e) M = 0.95. Concluded.

Figure 7.- Continued.

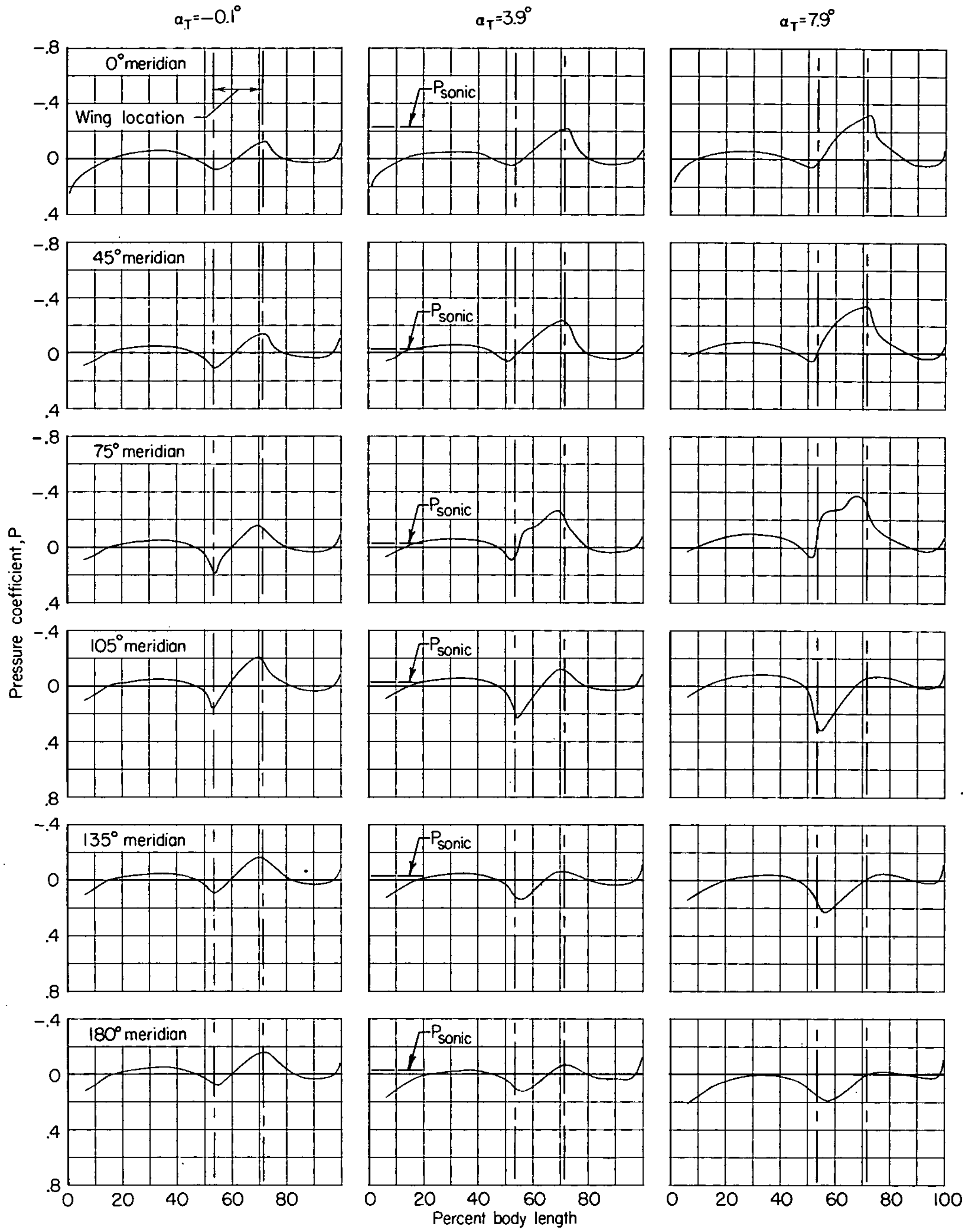

(f) M = 0.98.

Figure 7.- Continued.

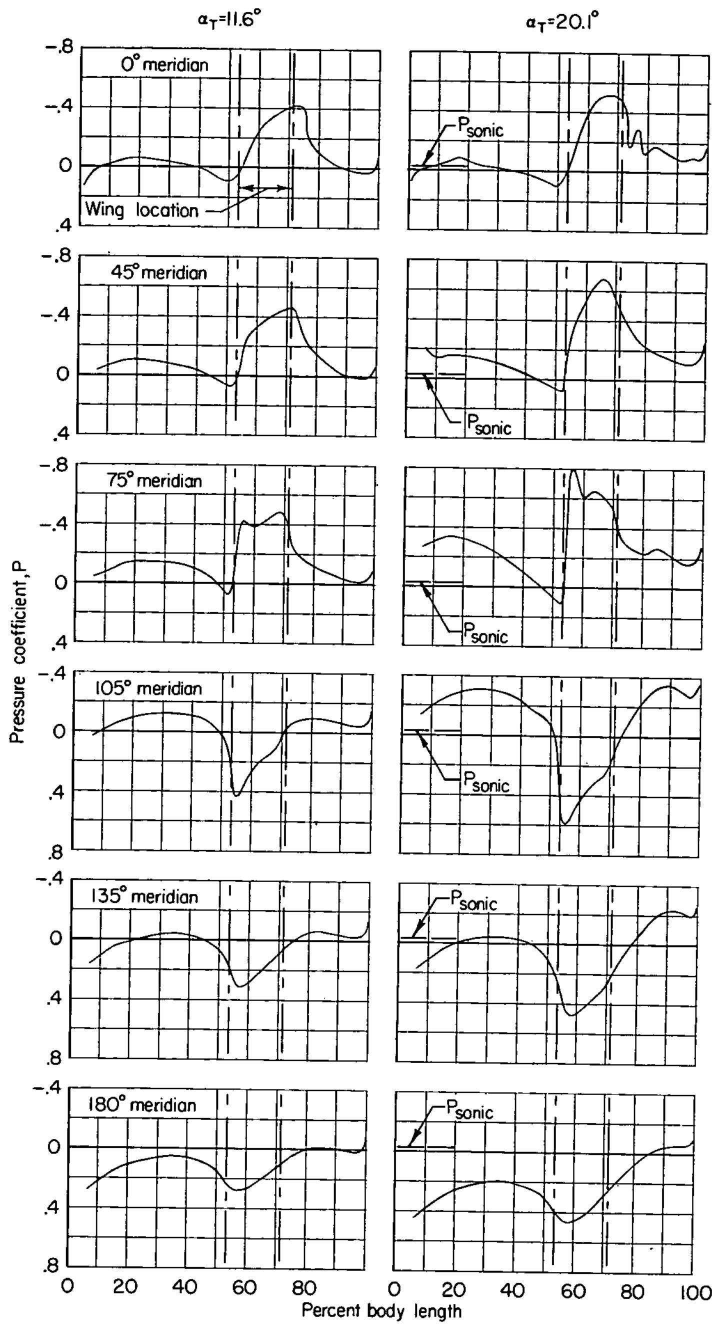

(f) M = 0.98. Concluded.

Figure 7.- Continued.

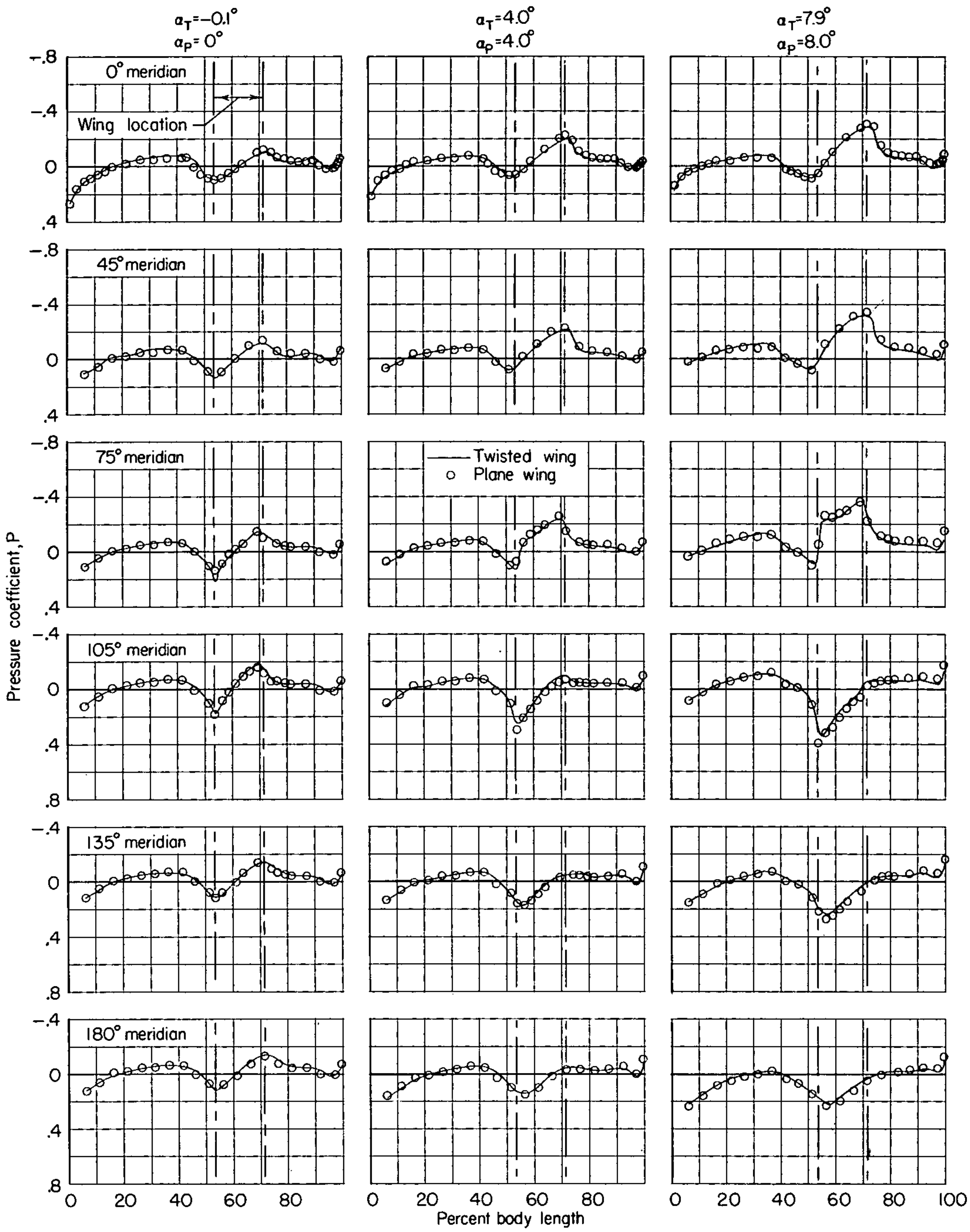

(g) M = 1.00.

Figure 7.- Continued.

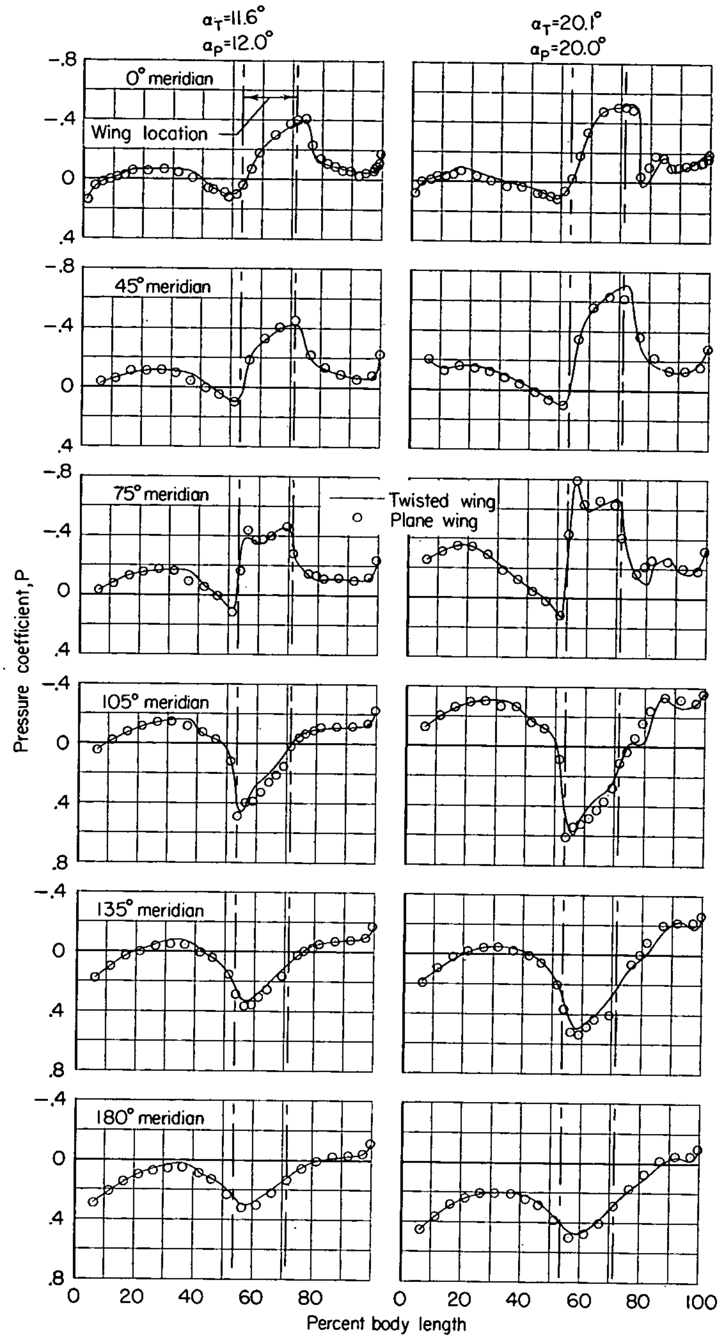

(g) M = 1.00. Concluded.

Figure 7.- Continued.

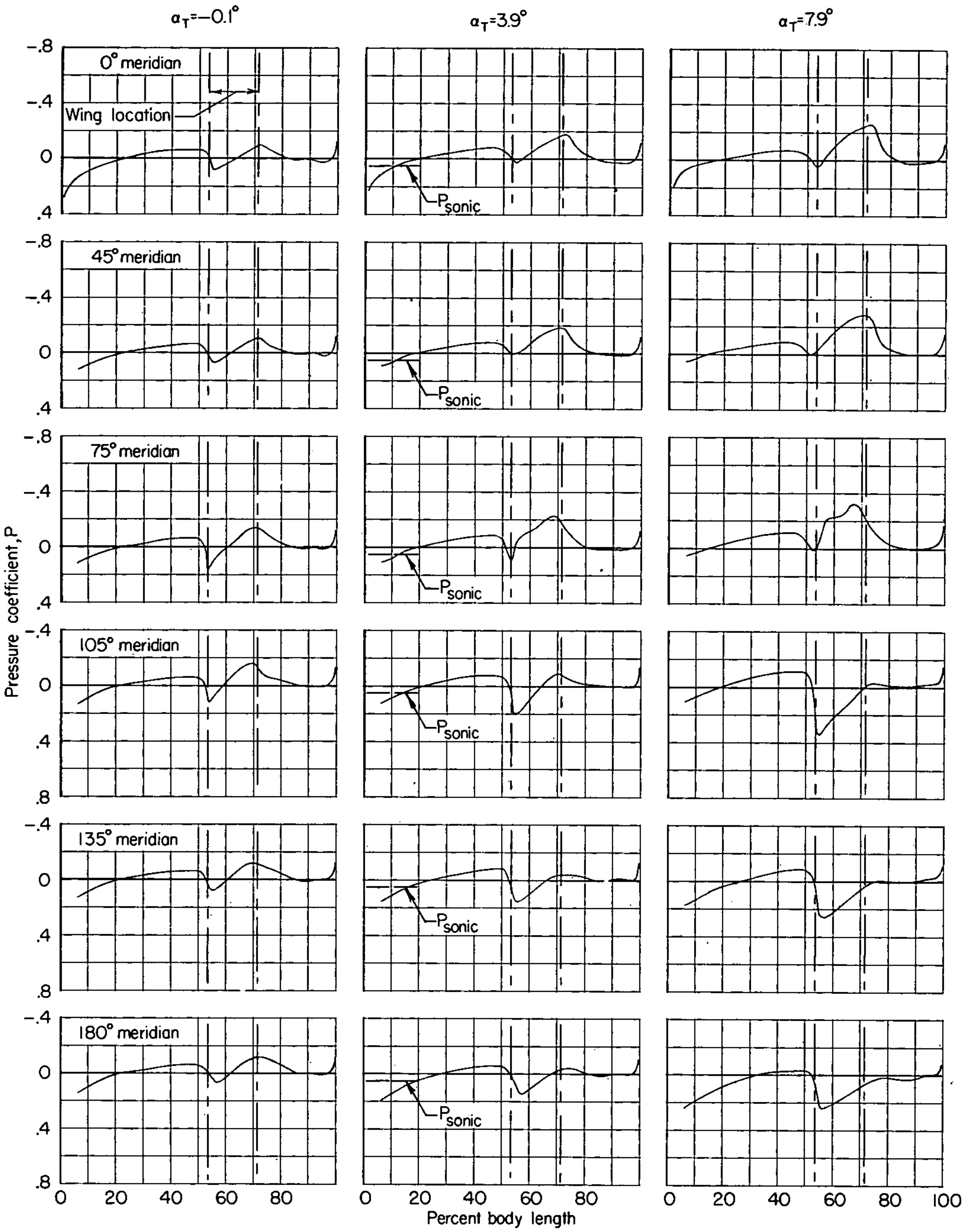

(h) M = 1.03.

Figure 7.- Continued.

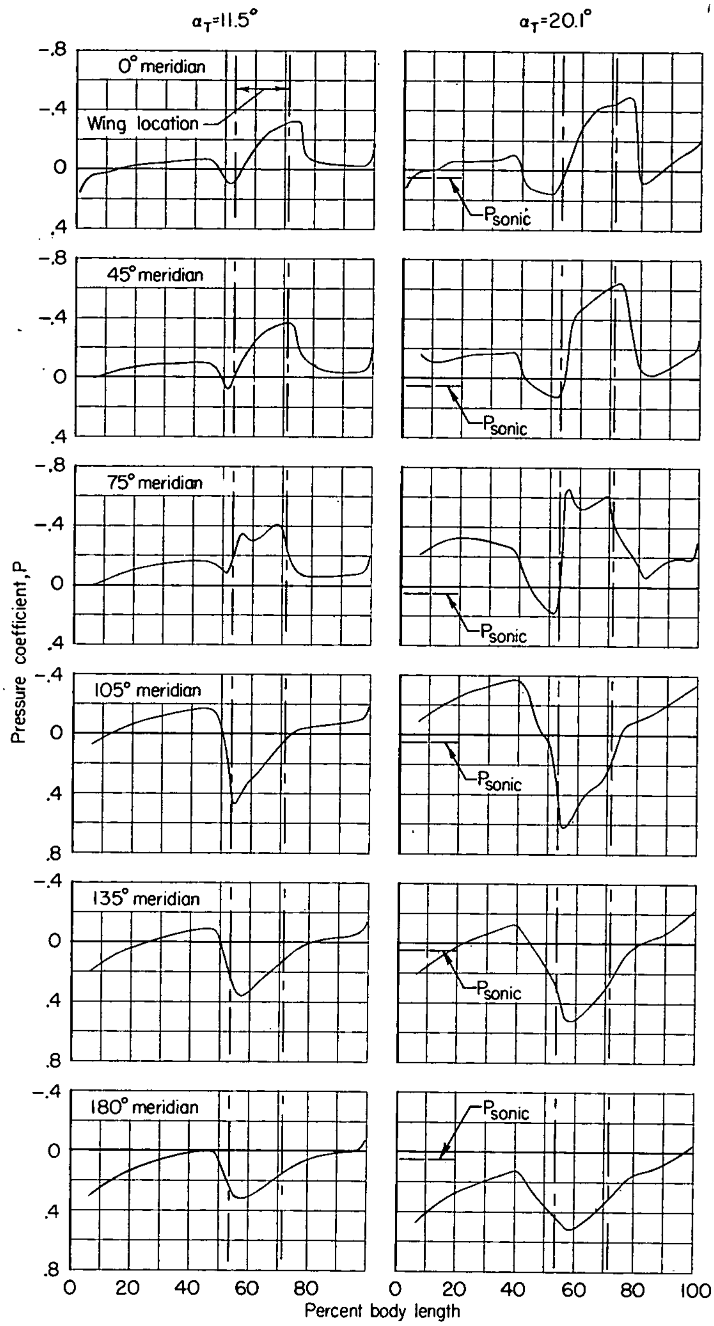

(h) M = 1.03. Concluded.

Figure 7.- Continued.

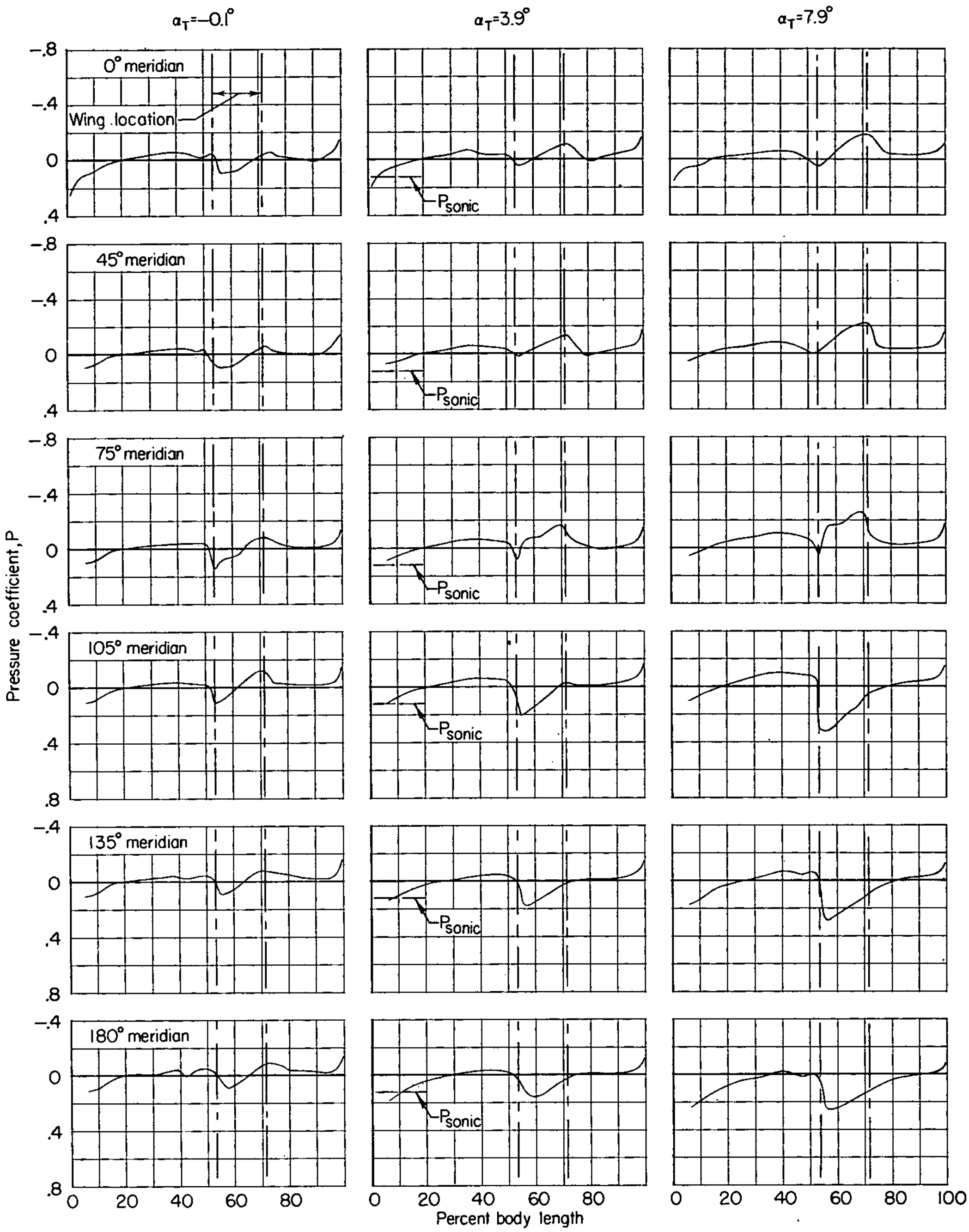

(i) M = 1.08.

Figure 7.- Continued.

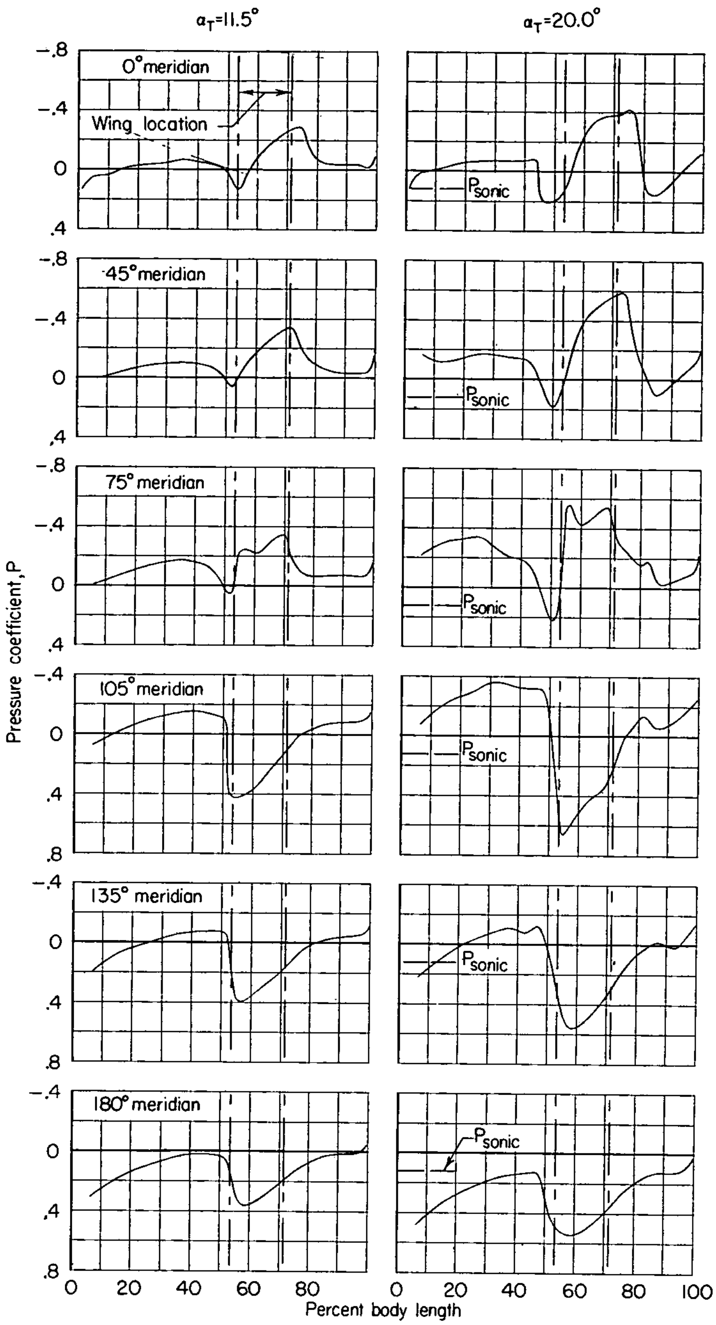

(i) M = 1.08. Concluded.

Figure 7.- Continued.

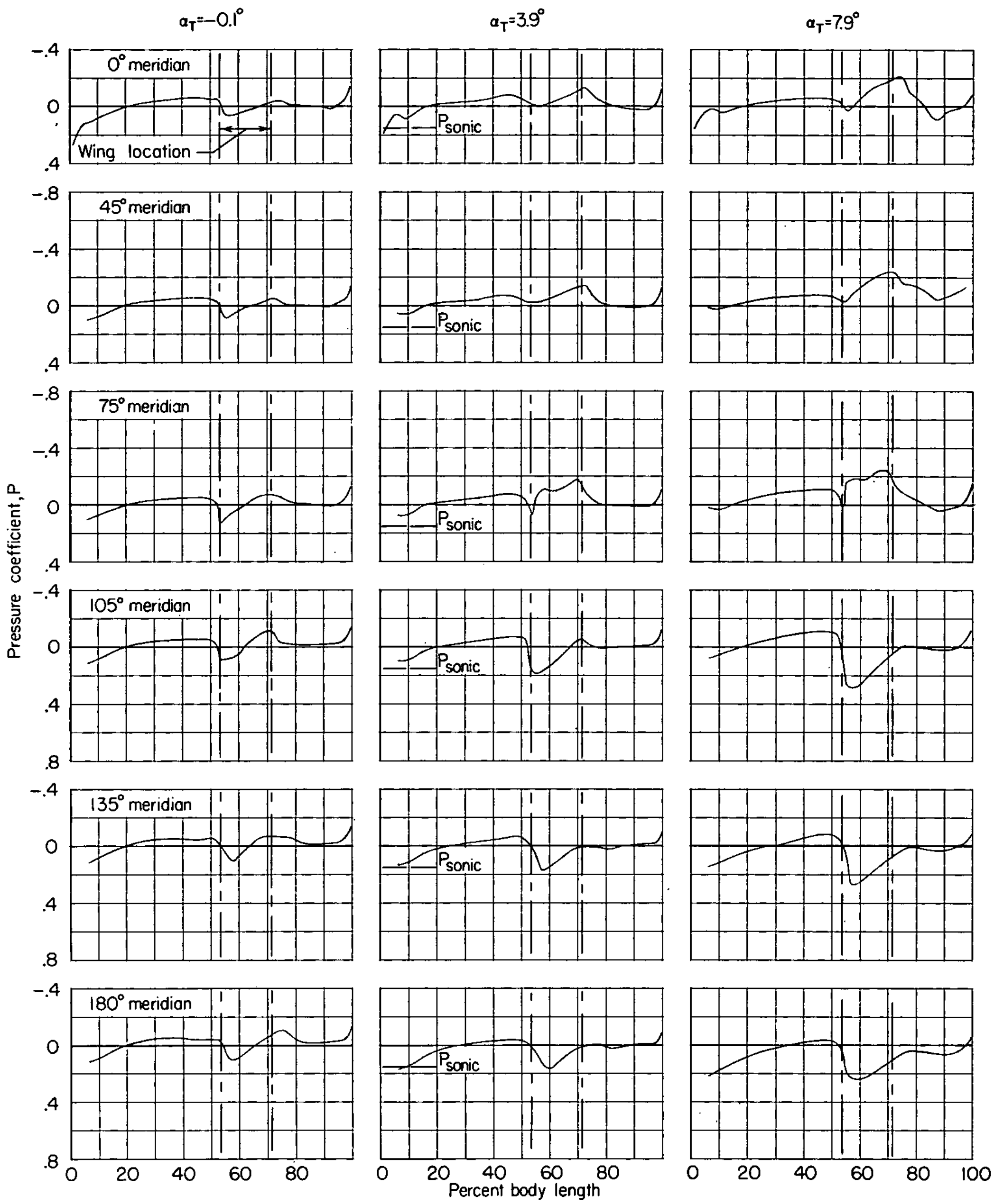

(j) M = 1.10.

Figure 7.- Continued.

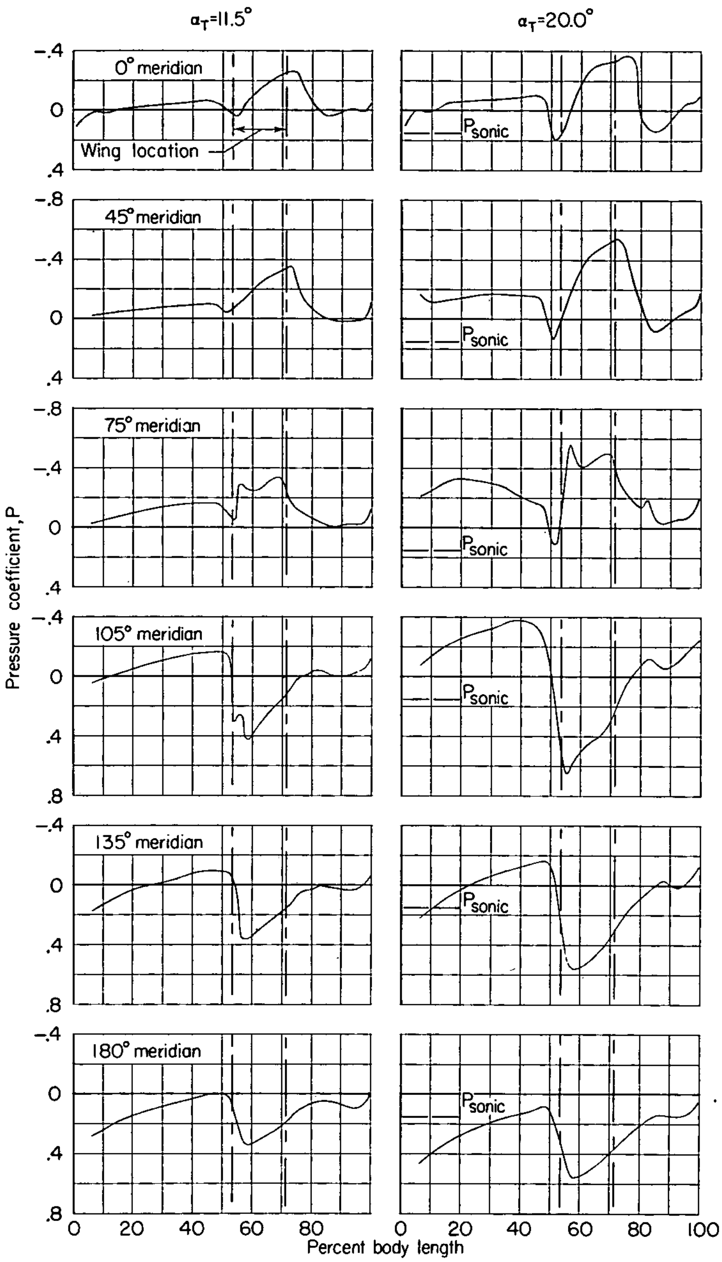

(j) M = 1.10. Concluded.

Figure 7.- Continued.

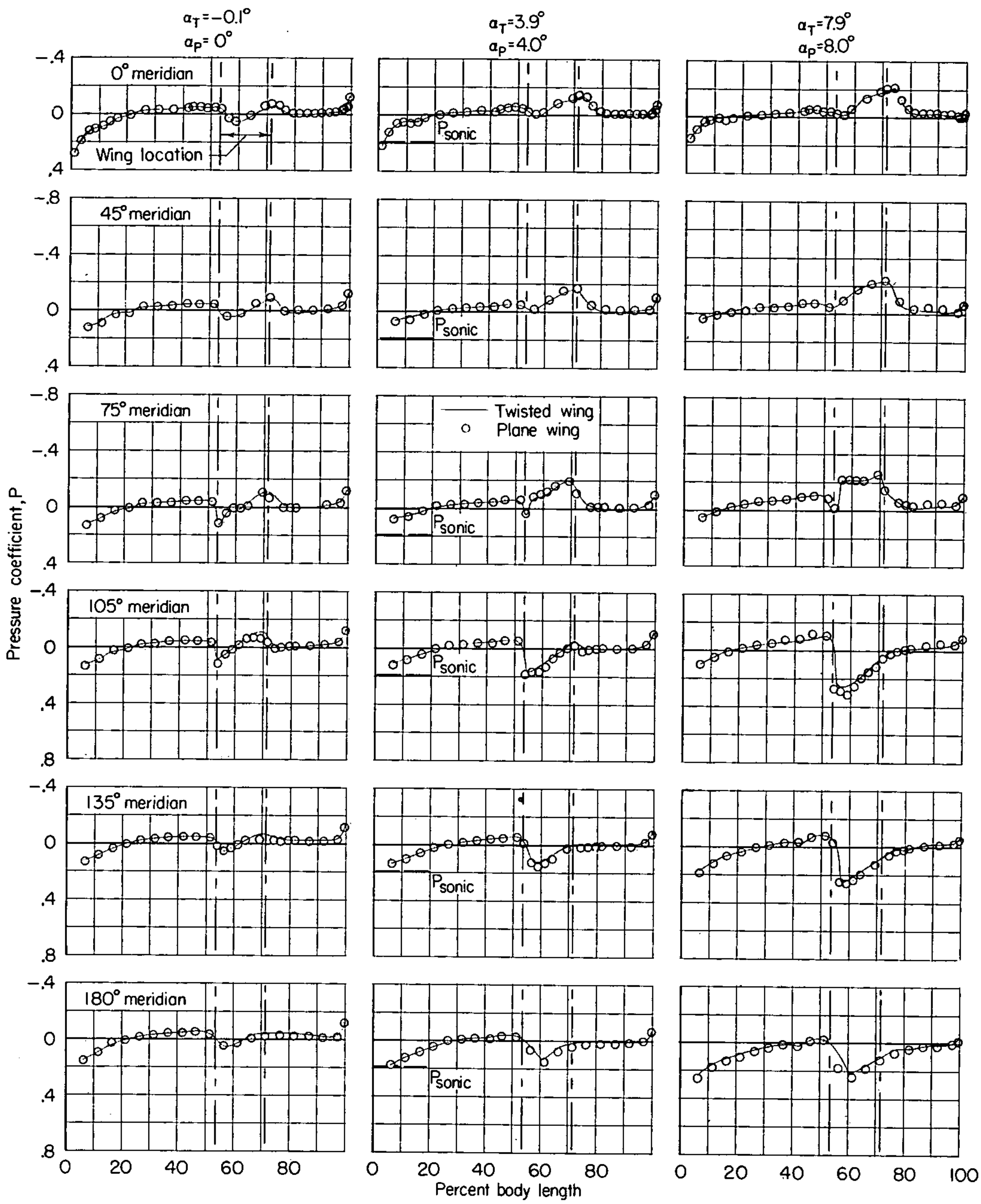

(k) M = 1.13.

Figure 7.- Continued.

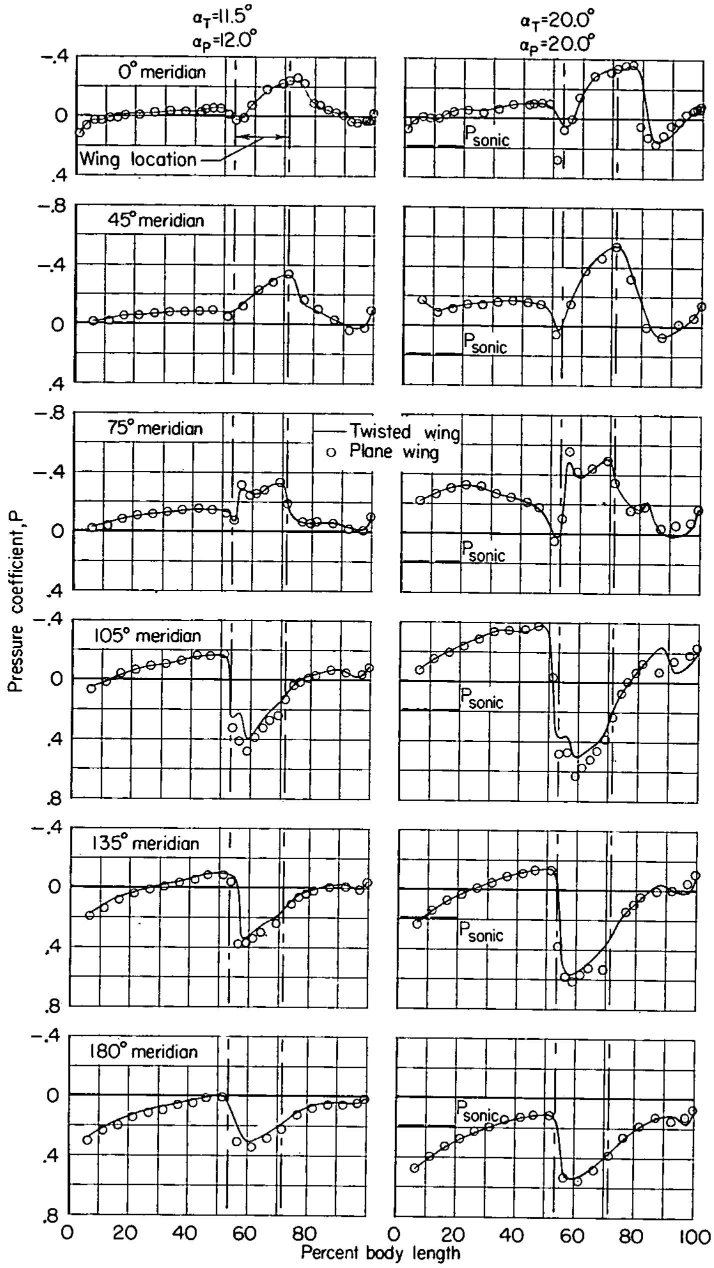

(k) M = 1.13. Concluded.

Figure 7.- Concluded.

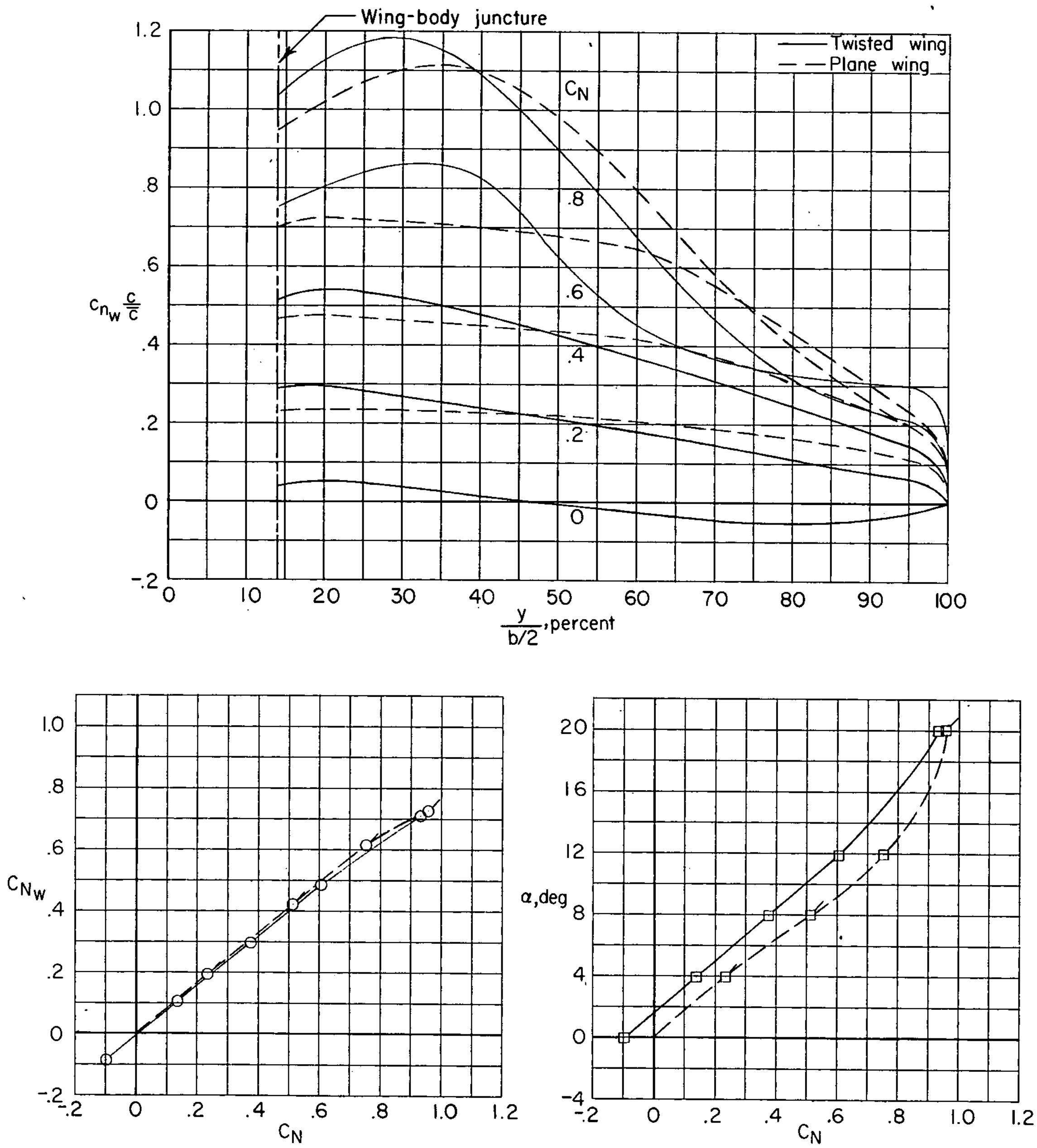

(a) M = 0.60.

Figure 8.- Normal-force characteristics for the twisted and plane wings.

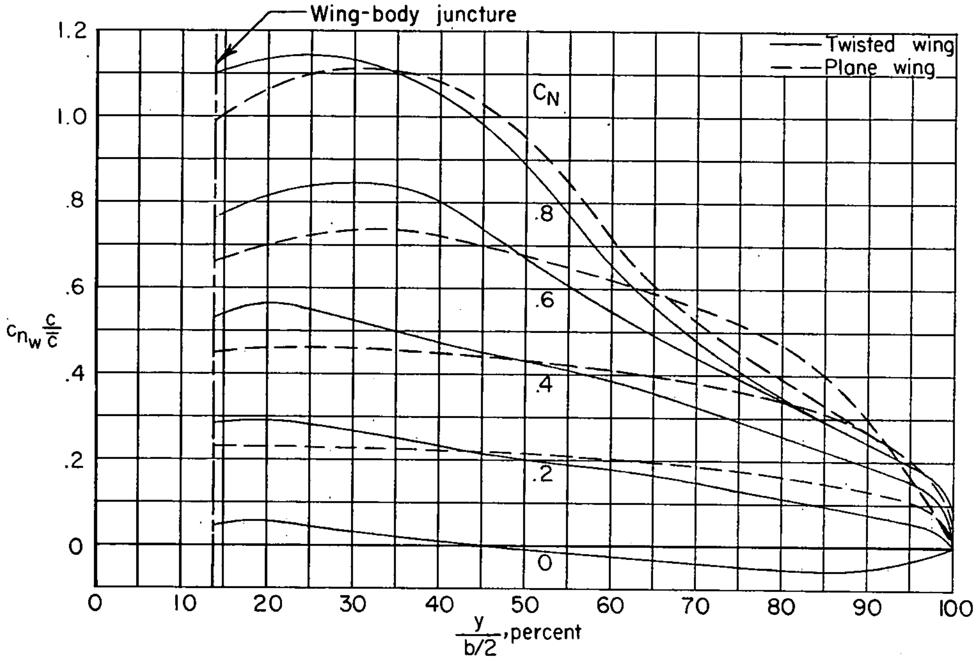

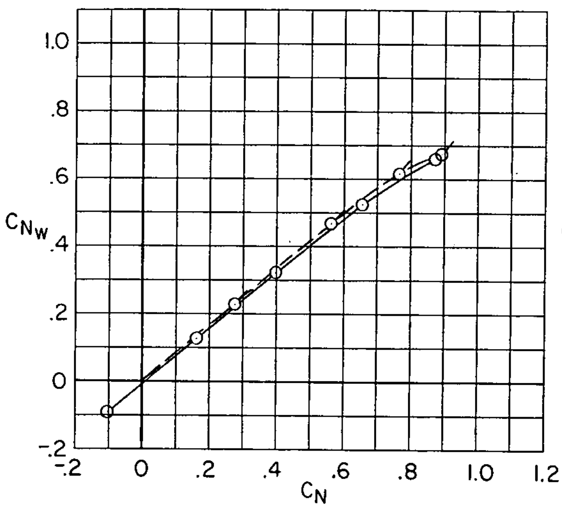

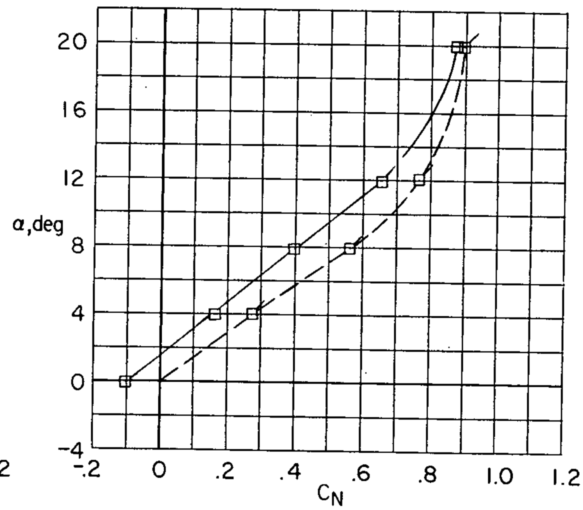

(b) M = 0.80.

Figure 8.- Continued.

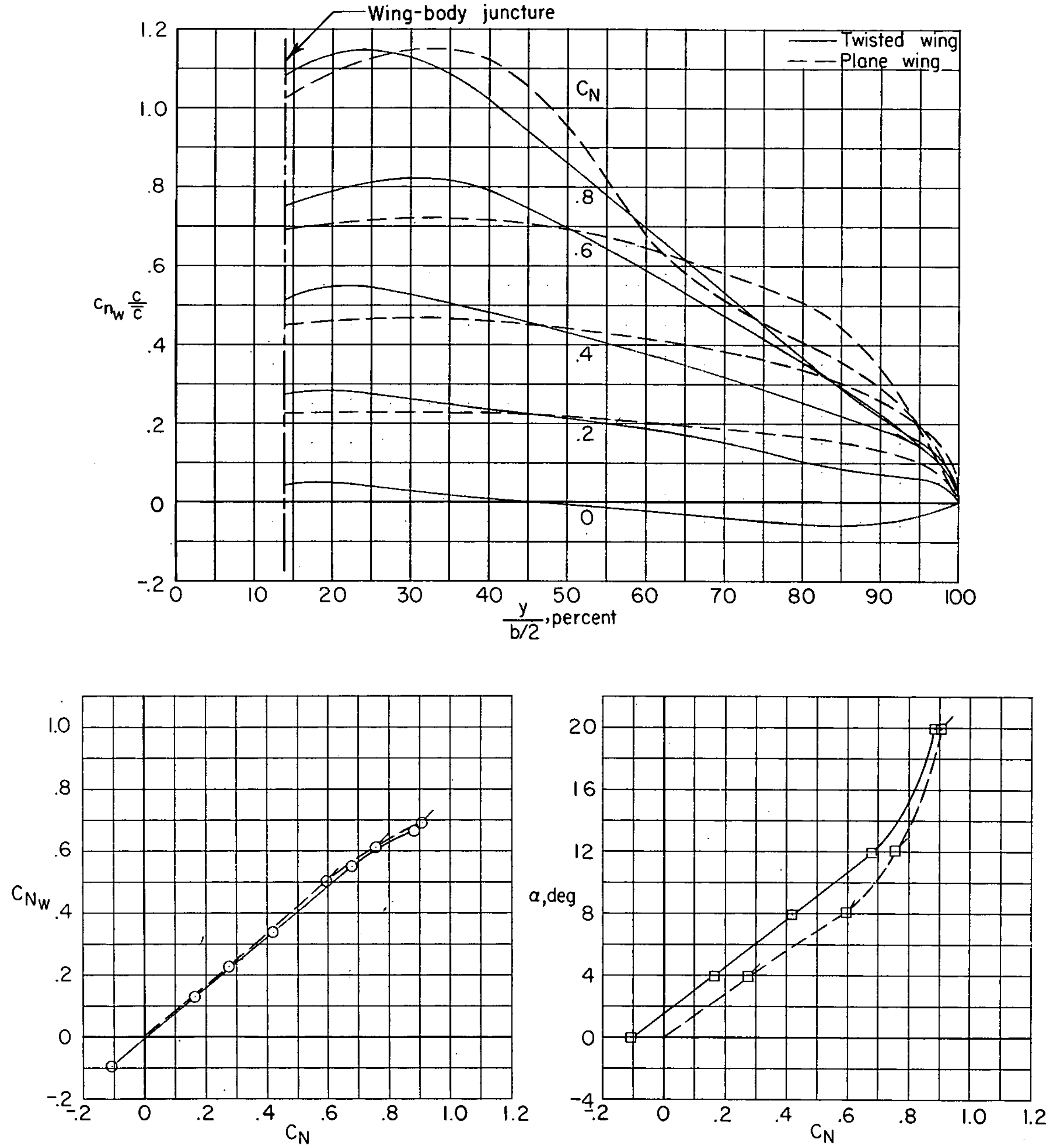

(c) M = 0.85.

Figure 8.- Continued.

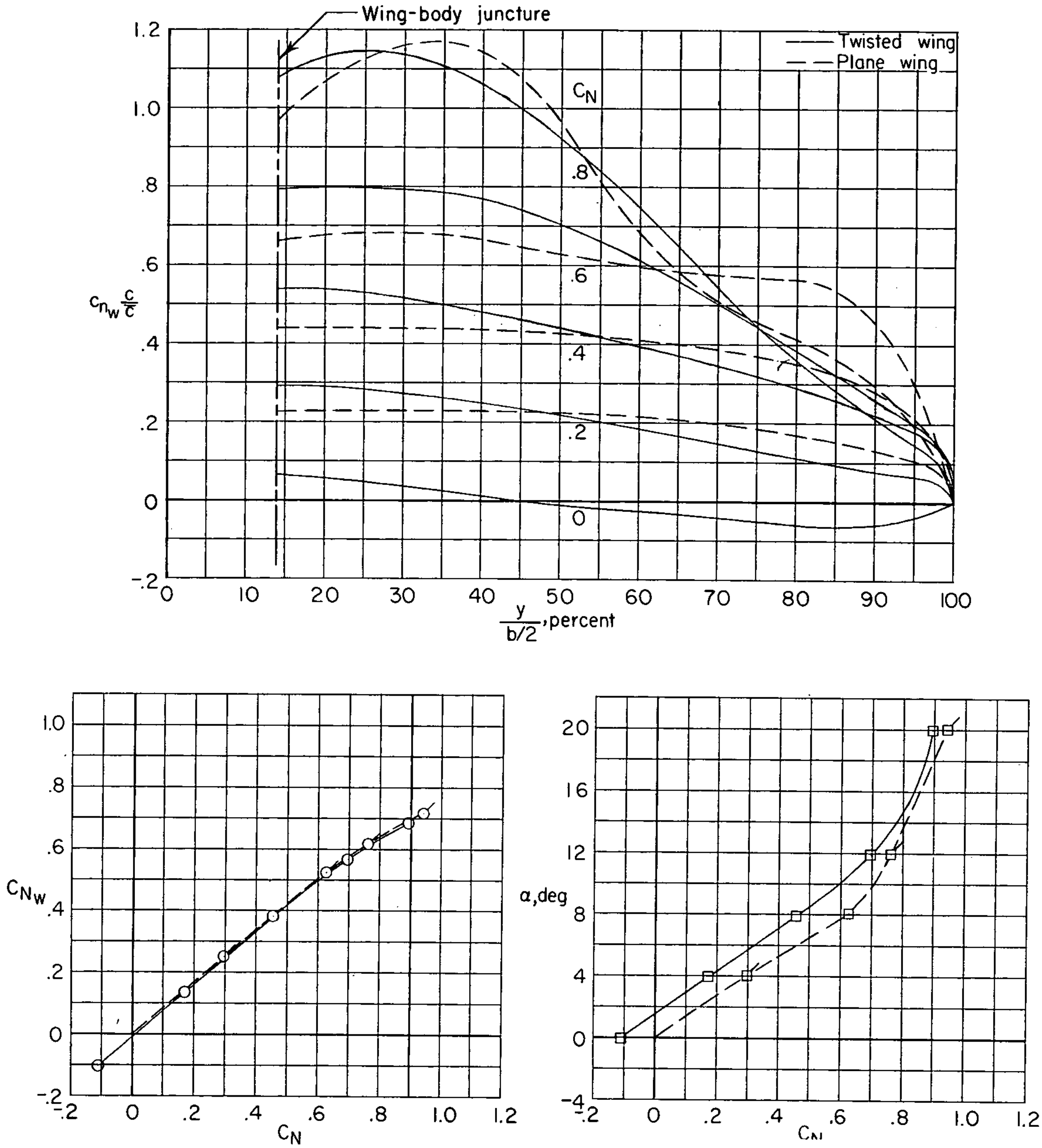

(d) M = 0.90.

Figure 8.- Continued.

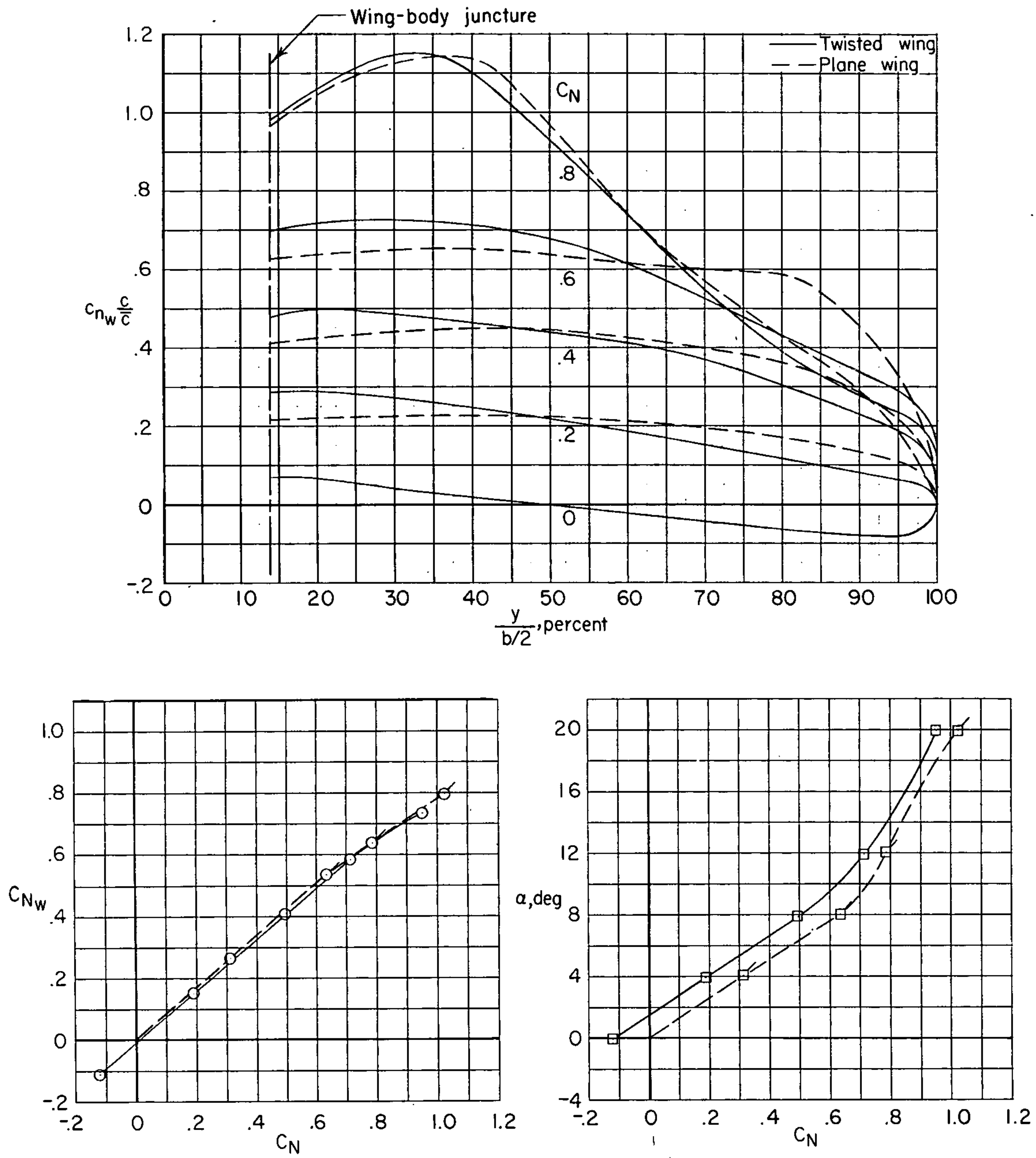

(e) M = 0.95.

Figure 8.- Continued.

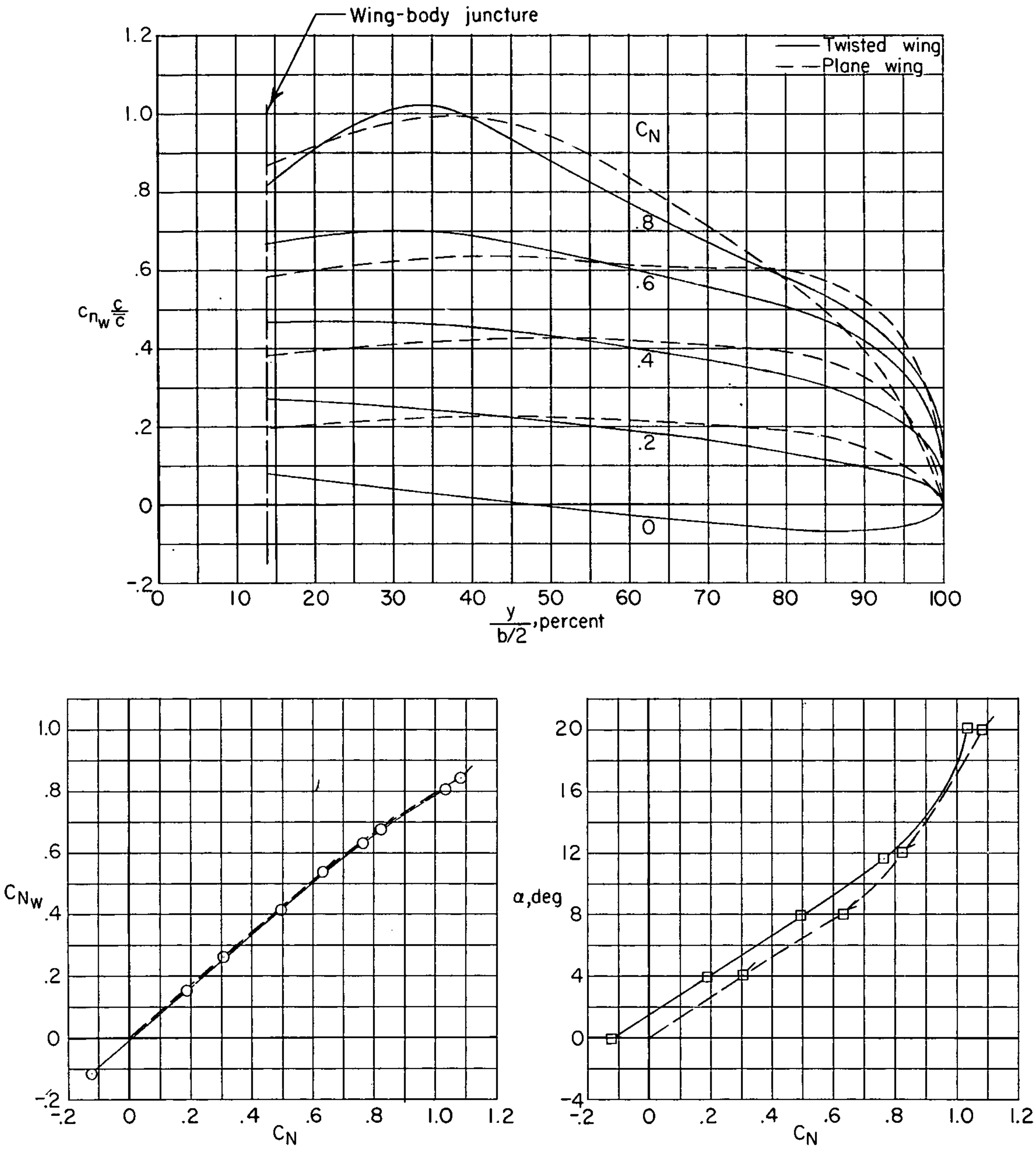

(f) M = 0.98.

Figure 8.- Continued.

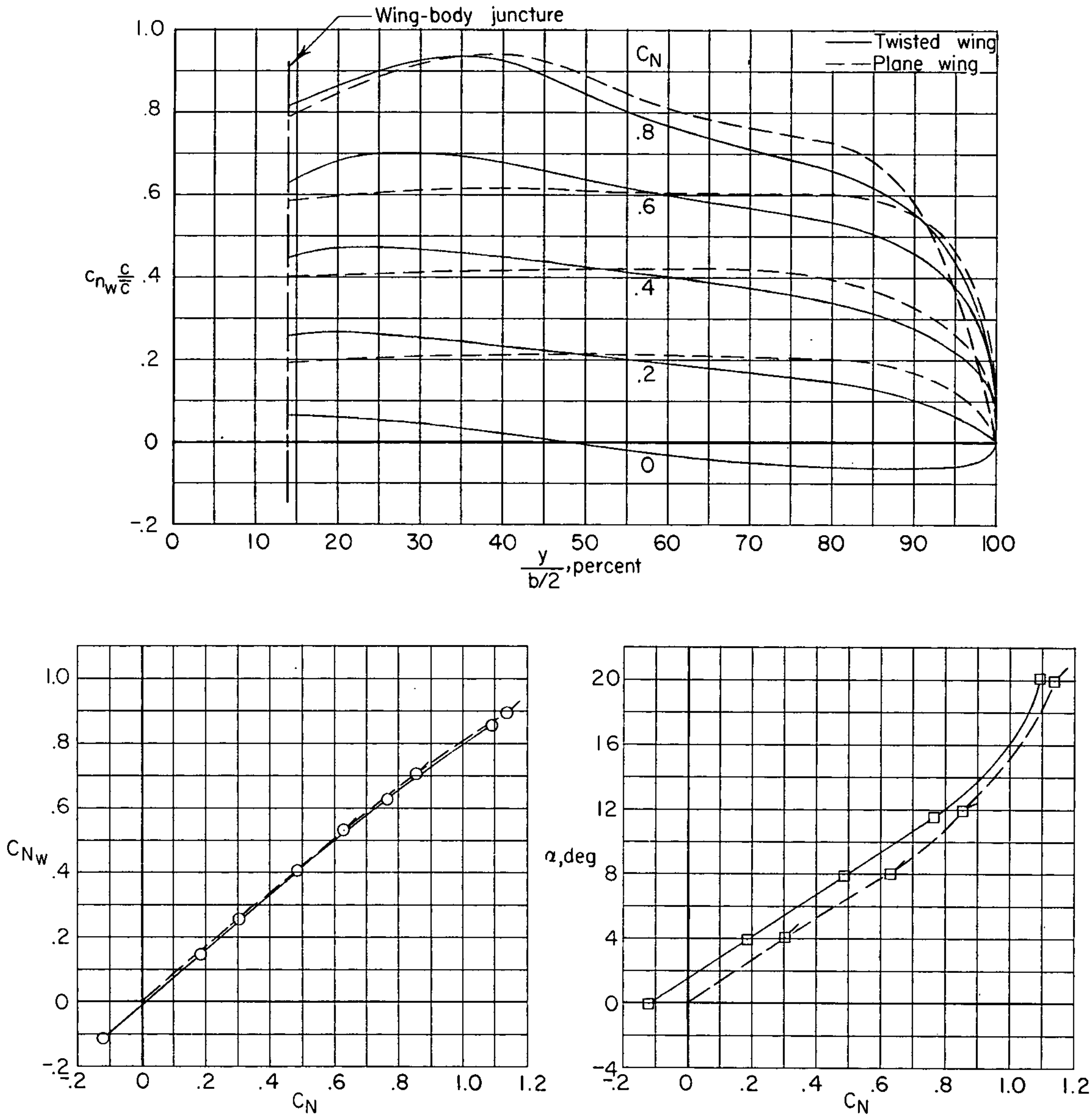

(g) M = 1.00.

Figure 8.- Continued.

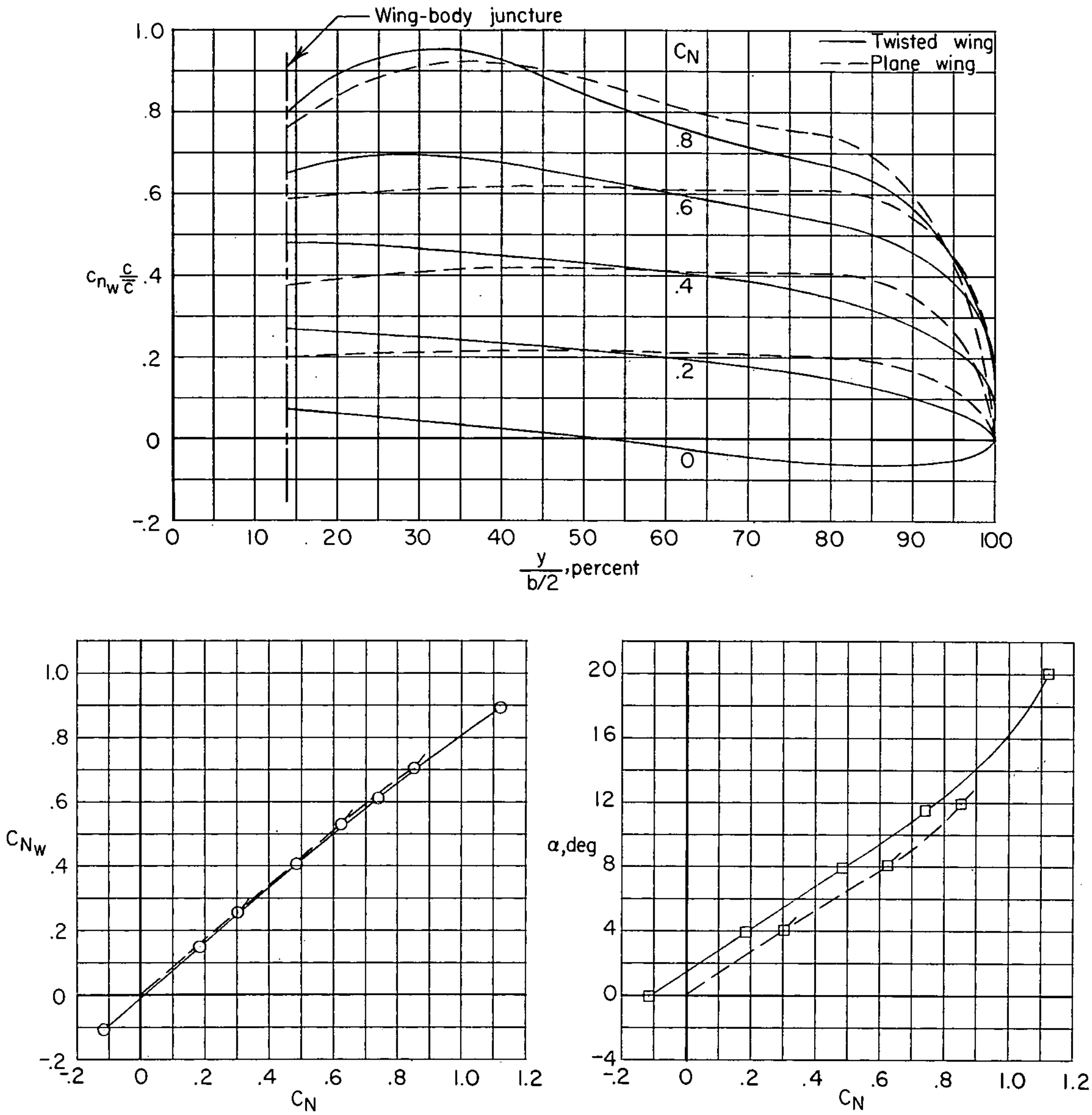

(h) M = 1.03.

Figure 8.- Continued.

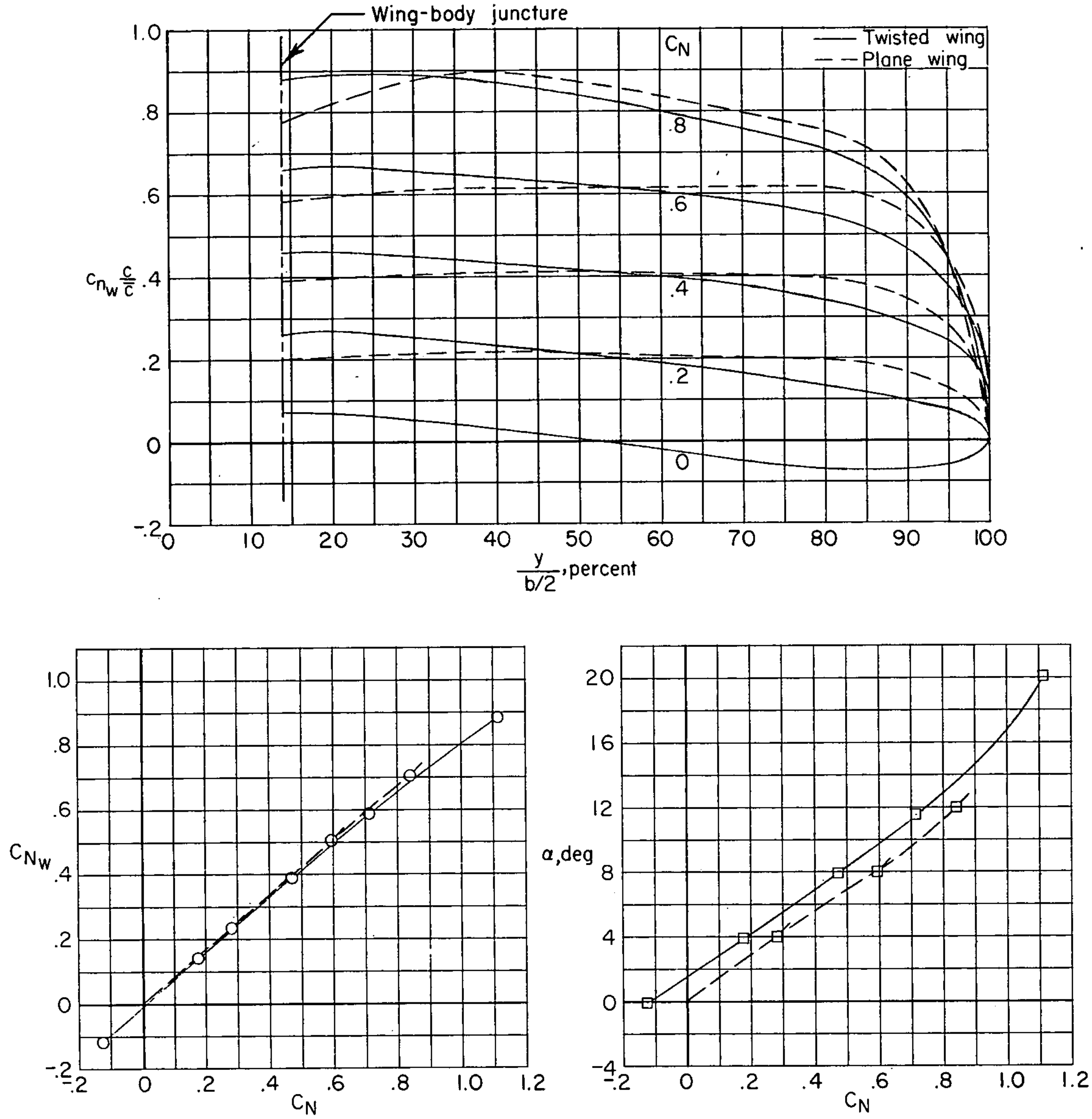

(i) M = 1.08.

Figure 8.- Continued.

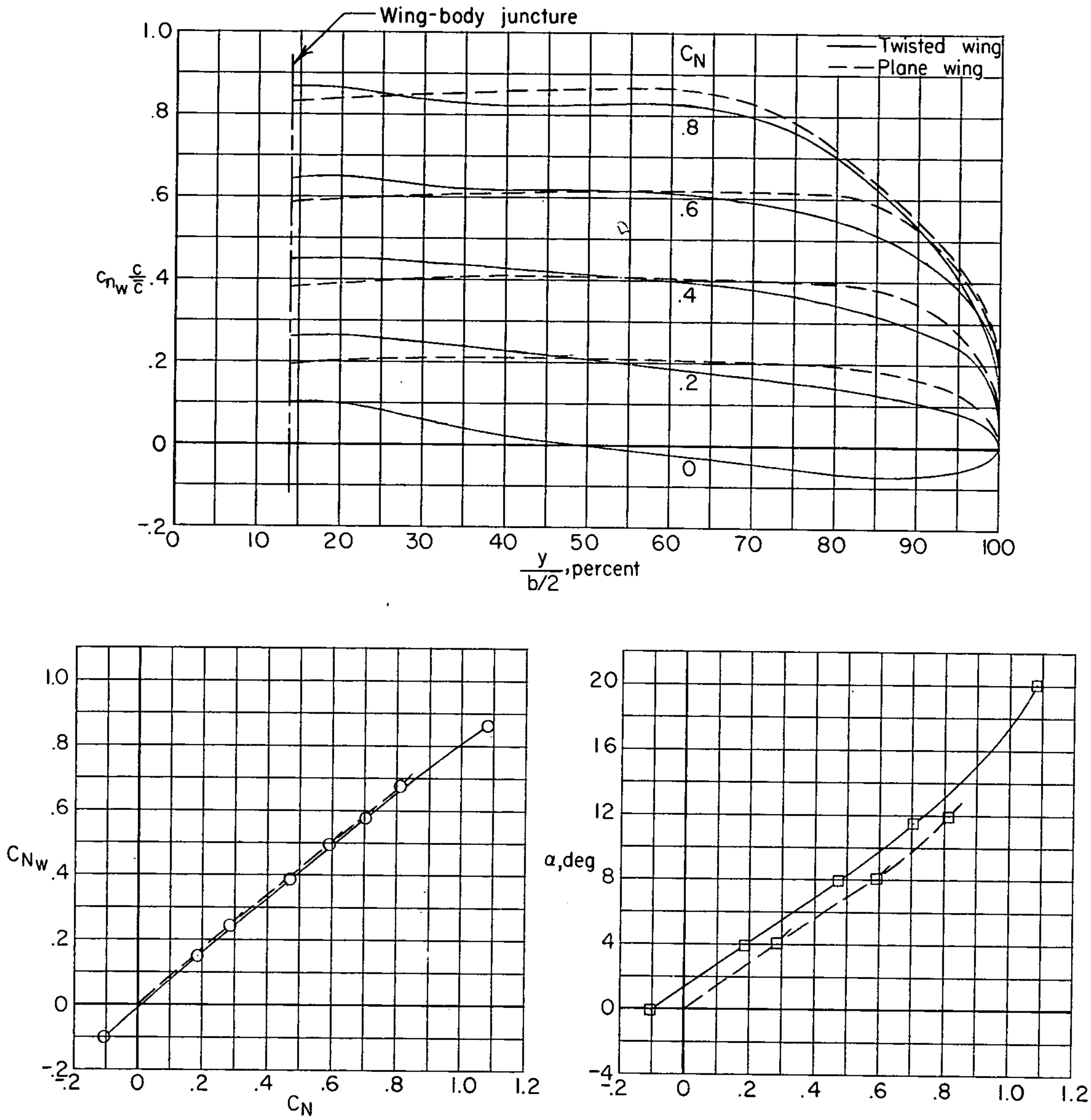

(j) M = 1.10.

Figure 8.- Continued.

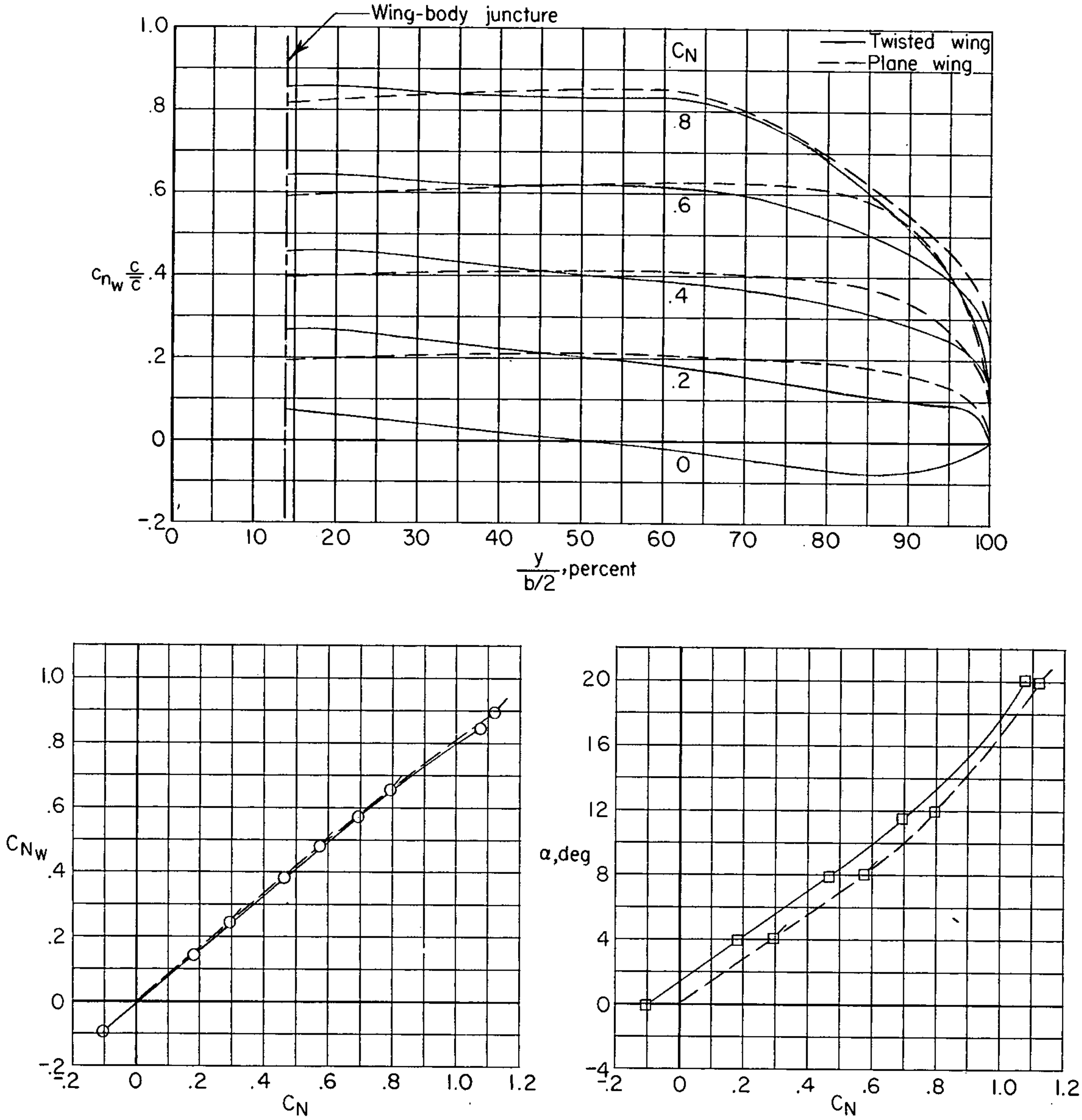

(k) M = 1.13.

Figure 8.- Concluded.

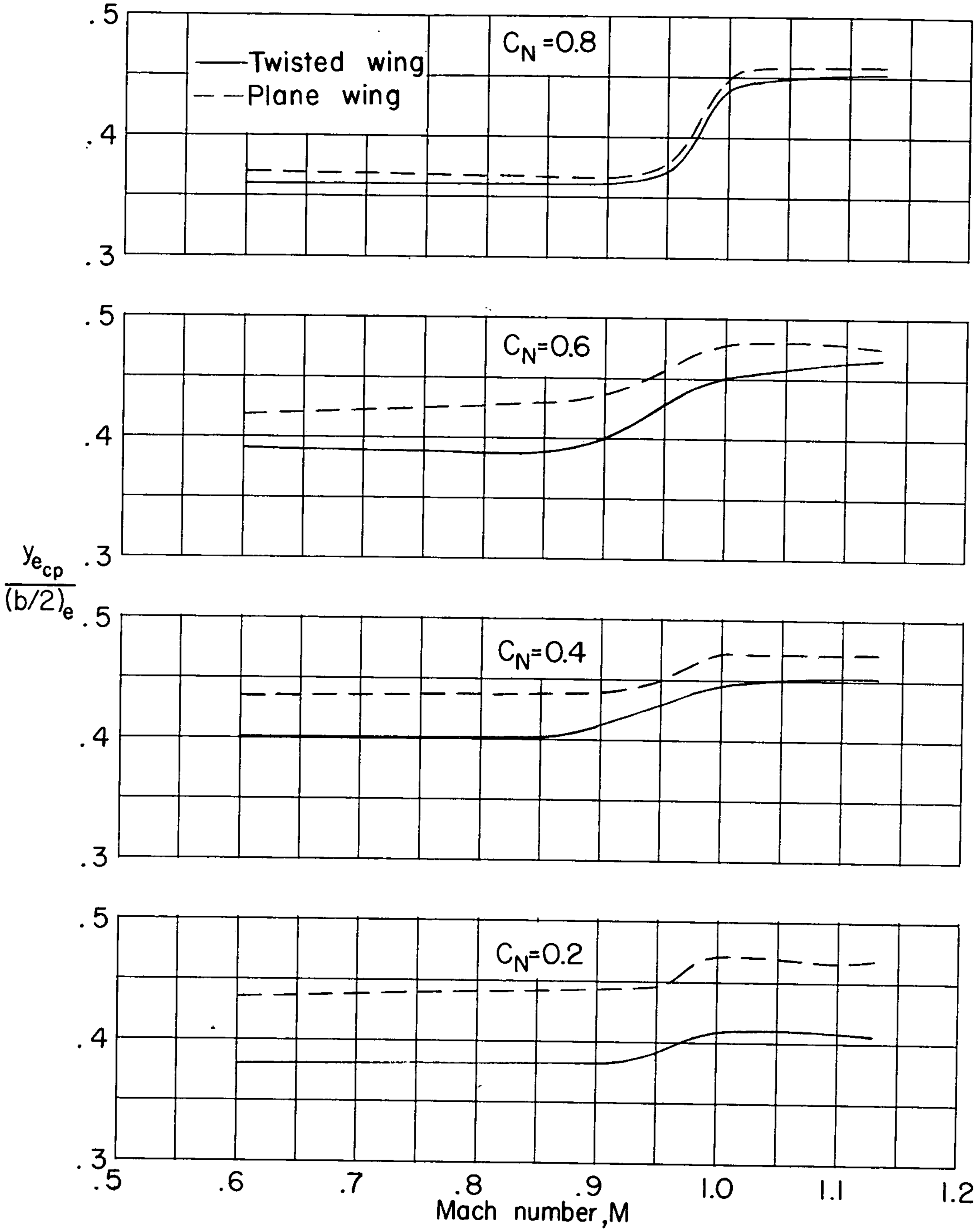

Figure 9.- Comparison of the spanwise center-of-pressure characteristics for the twisted and plane wings.

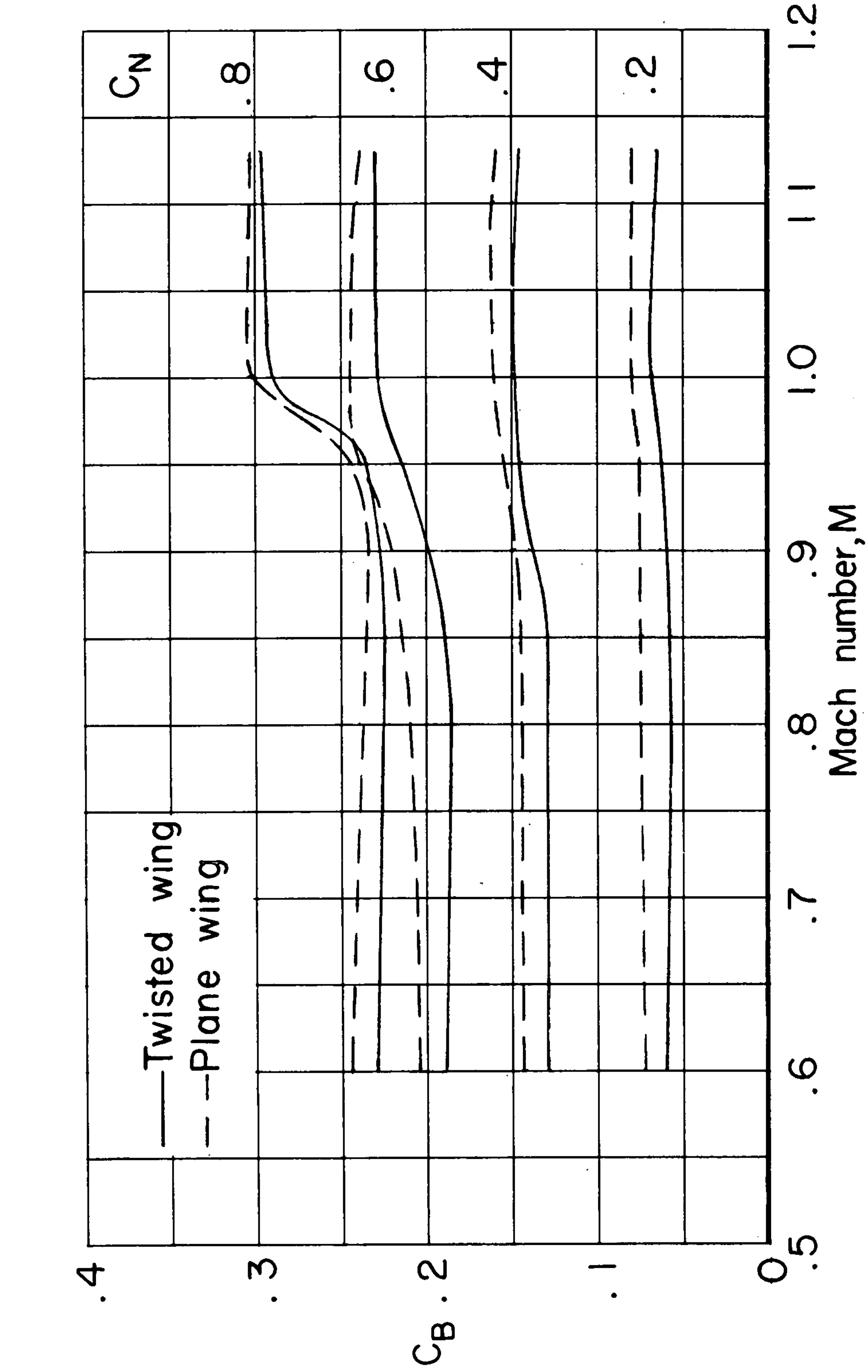

Figure 10.- Root-bending-coefficient characteristics at several normal-force coefficients for the twisted and plane wing-body configurations.

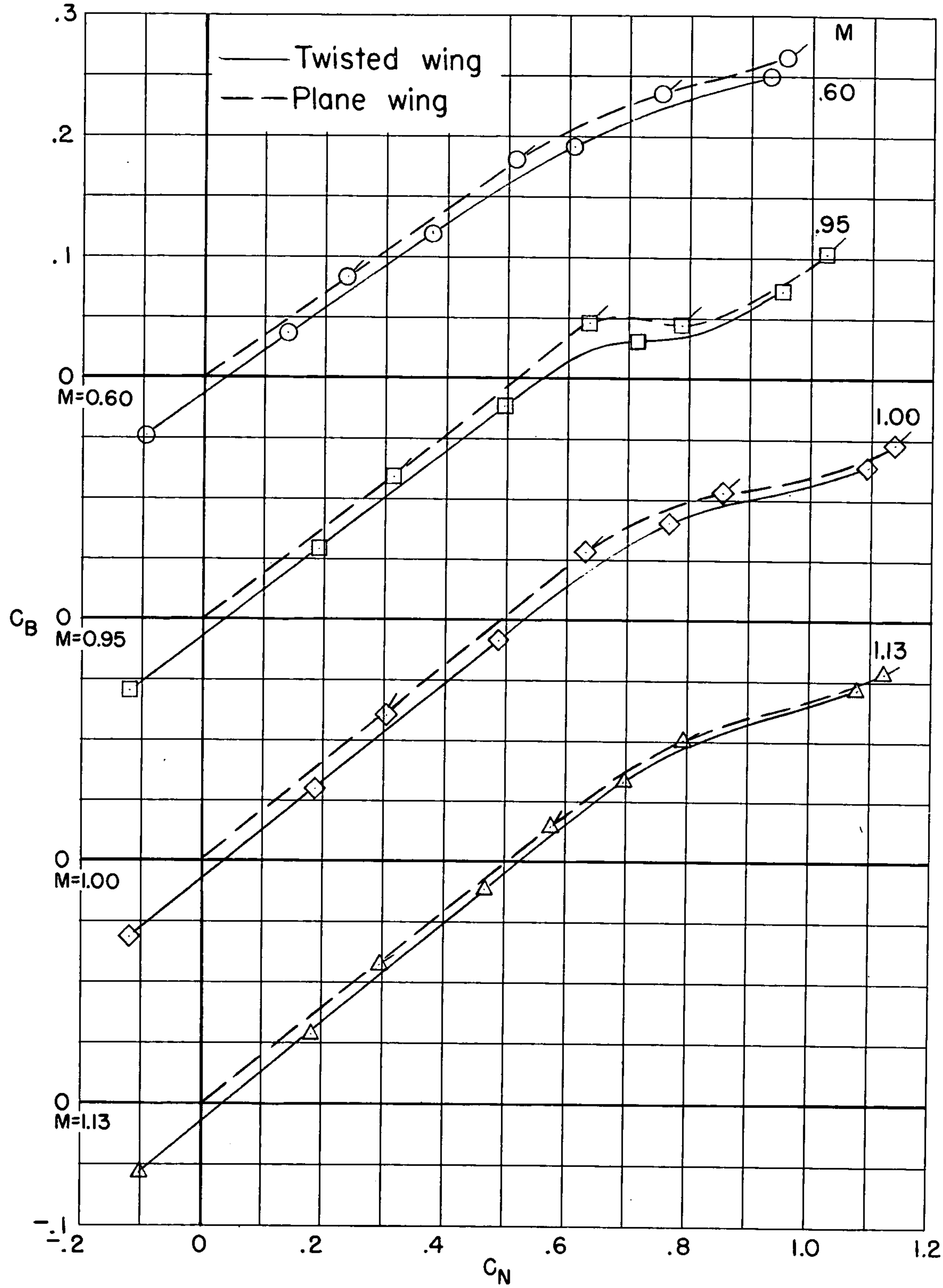

Figure 11.- Root-bending-moment-coefficient characteristics at several Mach numbers for the twisted and plane wing-body configurations.

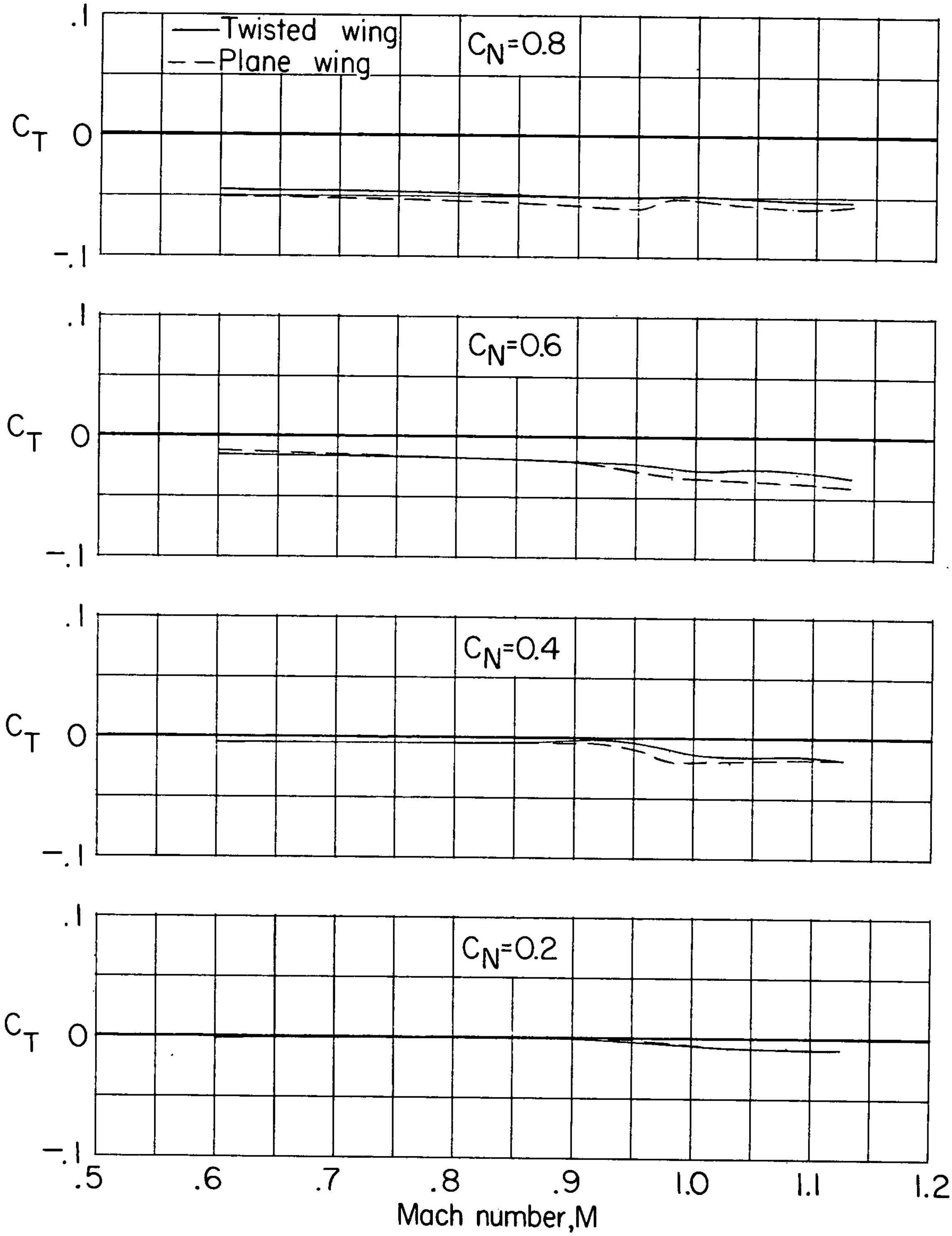

Figure 12.- Wing twisting-moment-coefficient characteristics for the twisted and plane wings.

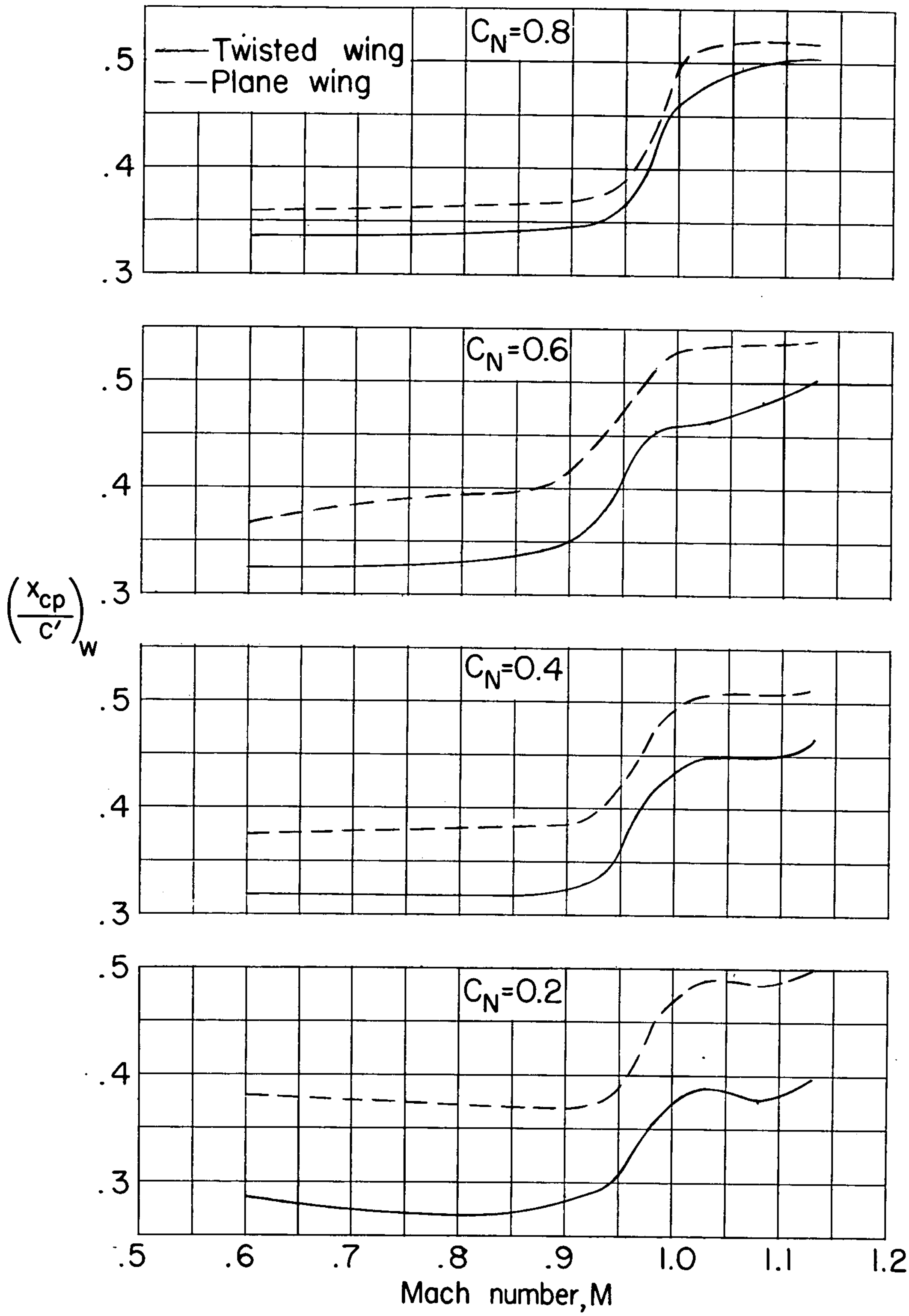

Figure 13.- Wing chordwise center-of-pressure characteristics for the twisted and plane wings.

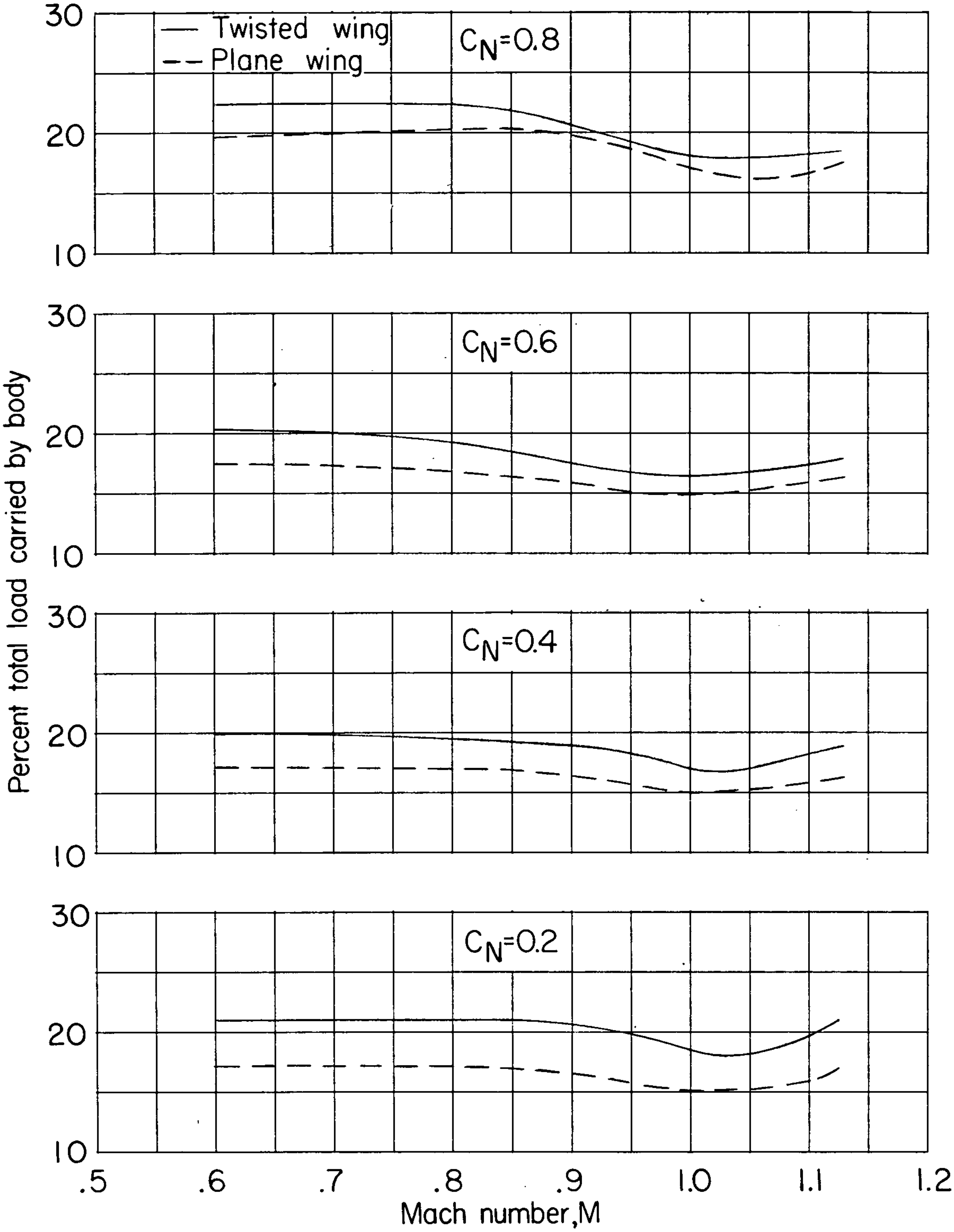

Figure 14.- Percent total load carried by the body for the twisted and plane wing-body configurations.

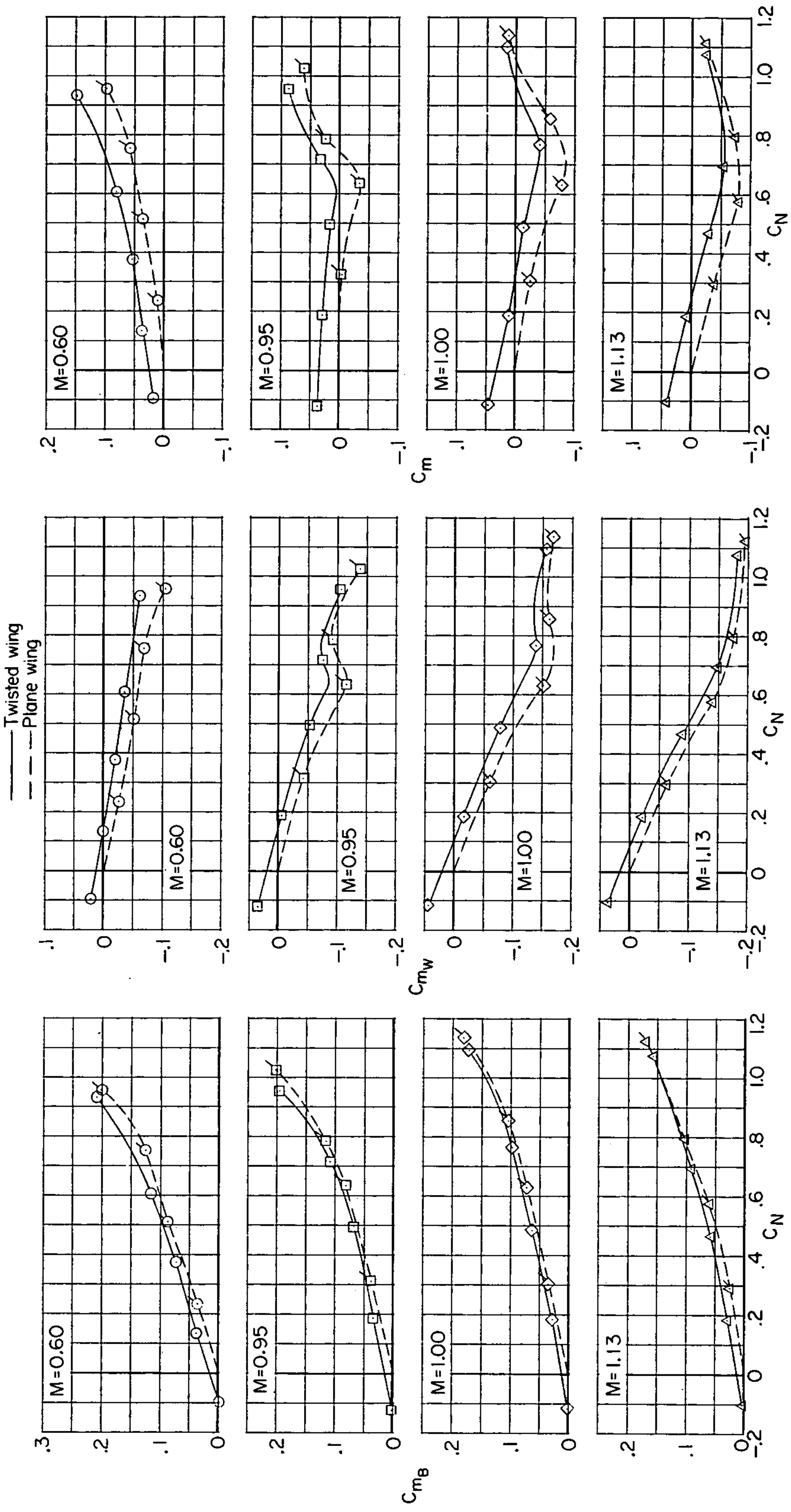

Figure 15.- Pitching-moment characteristics at several Mach numbers for the twisted and plane wing-body configuration. Flagged symbols indicate plane-wing configuration data.

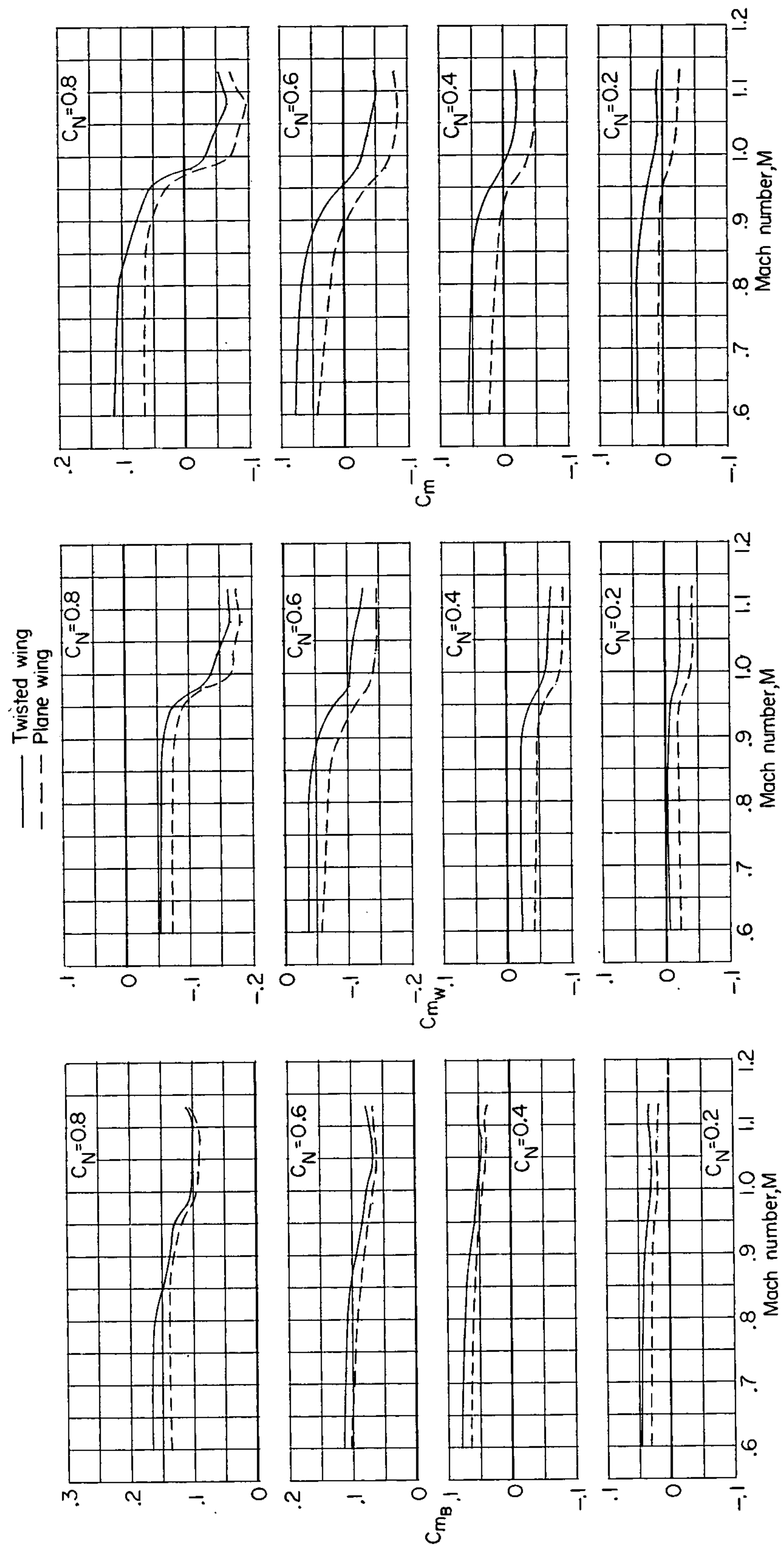

Figure 16.- Pitching-moment characteristics at several normal-force coefficients for the twisted and plane wing-body configurations.

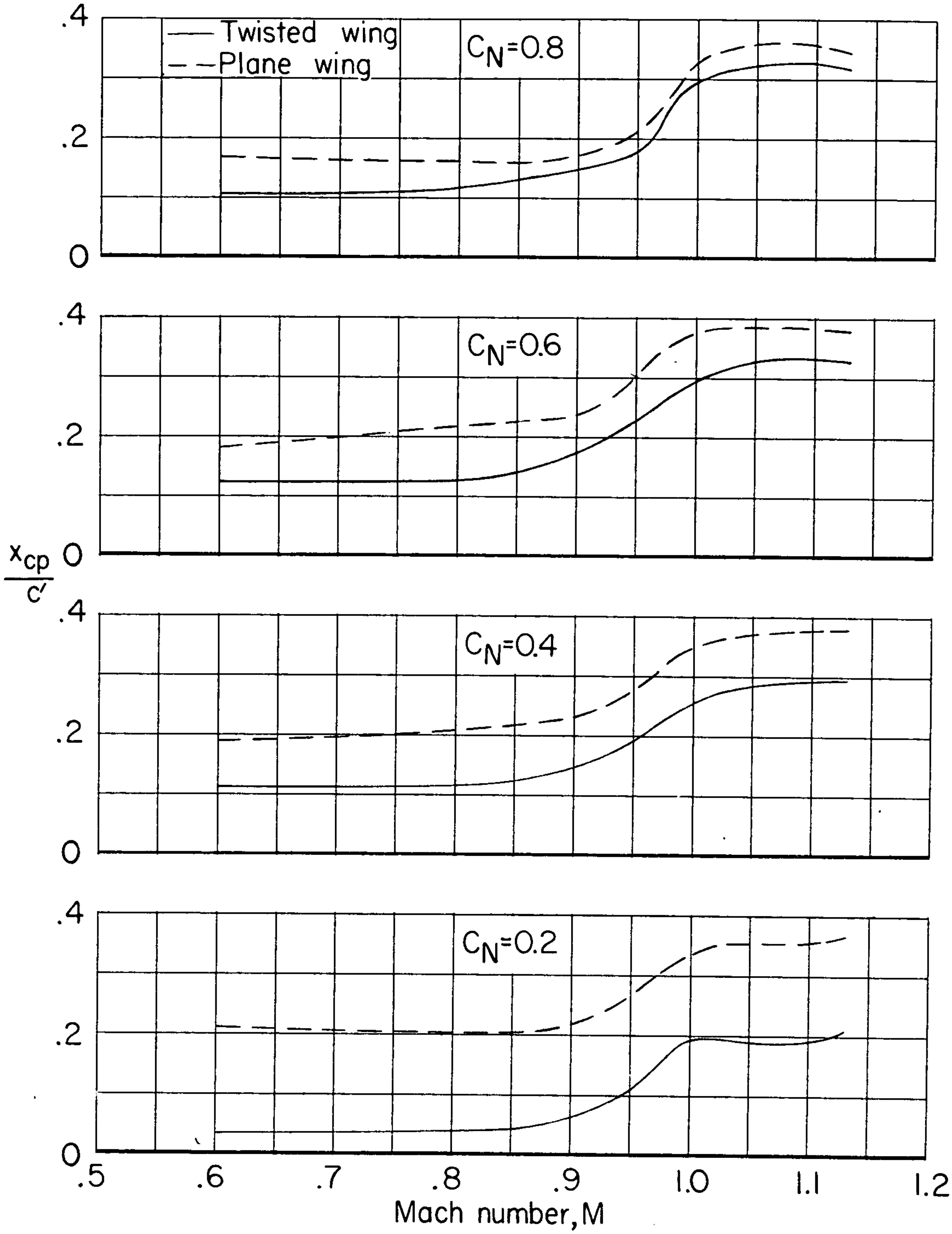

Figure 17.- Longitudinal center-of-pressure characteristics for the twisted and plane wing-body configurations.

NACA-Langley - 10-12-54 - 350